GPO PRICE $ _____

CFSTI PRICE(S) $ _____

Hard copy (HC) 3.00

Microfiche (MF) .75

ff 653 July 65

JET PROPULSION LABORATORY
CALIFORNIA INSTITUTE OF TECHNOLOGY
PASADENA, CALIFORNIA

FINAL REPORT

[illegible] CONTRIBUTION STUDY

JULY 20, 1964 TO APRIL 7, 1965

Contract No. 950919

Serial No. 6224

JET PROPULSION LABORATORY
PASADENA, CALIFORNIA

SPACE AND DEFENSE SCIENCES DEPT.
RESEARCH DIVISION
ALLIS-CHALMERS MFG. CO.
MILWAUKEE, WISCONSIN 53201

APRIL, 1965

FINAL REPORT

LUNAR SURFACE ROUGHNESS COMMINUTION STUDY

July 20, 1964 to April 7, 1965

Contract No. 950919
Serial No. 6224

Jet Propulsion Laboratory
Pasadena, California

This work was performed for the Jet Propulsion Laboratory, California Institute of Technology, sponsored by the National Aeronautics and Space Administration under Contract NAS7-100.

Space and Defense Sciences Dept.
Research Division
Allis-Chalmers Mfg. Co.
Milwaukee, Wisconsin 53201

April, 1965

Authors: Dr. T. P. Meloy and L. H. Faust

PREFACE

The work for this program was accomplished under Contract 950919, for the period from July 20, 1964 to April 7, 1965. The study was conducted by the Research Division, Allis-Chalmers, Milwaukee, Wisconsin. The program was under the direction of Dr. T. P. Meloy, Scientist-in-Charge, assisted by Mr. L. H. Faust, Scientific Systems Department. Management supervision was provided by Mr. Will Mitchell, Jr., Director of Research, Mr. C. L. Sollenberger, Assistant Director, and Dr. P. A. Joyner, General Manager, Space and Defense Sciences. Co-authors of this final report are Dr. Meloy and Mr. Faust.

TABLE OF CONTENTS

LIST OF FIGURES

SECTION I

Summary

This is the final report on a study of the roughness of the lunar surface, considering meteoric infall as the genesis of craters and the dust layers. By roughness is meant the likelihood of encountering large blocks of ejecta or debris thrown out of the crater. The size distribution and depth of the resulting dust or rubble layer has been calculated.

This study is divided into two main parts. The first part considers what happens during individual crater formation and computes the size distribution of the ejected material from individual craters. Also computed is the distance the material is thrown. In the second section, using a matrix method developed previously, an estimate is made of the size distribution and depth of the dust on the moon as a function of time. Only one set of infall data has been used.

There is nothing discovered in this study which indicates that the size distribution of the dust on the lunar surface is a hazard. Blocks a foot in size and larger are rare. They are so rare that they are not likely to be detected on any of the Ranger pictures. This is discussed in greater detail in Section VI. The depth of the dust, computed from using Hawkins[1] infall data, is estimated at 25 feet if a volume density of .4 is used. The dust itself is quite fine. Fifty percent of the mass of the material is finer than 40 microns; 80 percent of the mass is finer than 180 microns, and 99.9 percent of the mass is finer than 1 millimeter. The size distribution of the dust remains relatively constant while the depth is sensitive to the age of the moon and infall rate.

In our study of cratering several interesting conclusions have been reached. First, near the edge of a new, large crater a number of larger blocks can be expected. While these blocks are rare over most of the lunar surface, near the rims of large craters they are more frequent. Thus, landing in this region would be hazardous.

If one assumes the normal scaling laws used to estimate mass of ejecta in a crater as a function of energy it leads to a paradox. The law as it is usually stated says that the mass of ejecta is proportional to the energy of the infalling particle. If one assumes this energy law and that shattering or comminution

of the crater stops when the energy in the compressive elastic wave falls below a given density, then one can derive that there will be a lower limit beyond which craters cannot form. The latter assumption implies that there is a physical property of the rock - probably strength - which determines whether it will or will not break. This paradox has not been resolved.

Another scaling law which does not work is the distribution of the debris around the crater. Small craters are scoured clean of ejecta. It is thrown many diameters away. For large craters, however, the larger blocks are in the crater or near its rim. This means the new, smaller craters will be symmetrical in outline and will have little or no trace of ejecta near them. Larger craters will show ejecta patterns near their rims which give them a rough unsymmetrical appearance.

The authors would like to state unequivocally that all the estimates are the result of a theoretical study that led to a rather complex computer program. Though the results seem reasonable there is always the chance that logic or programming errors exist. This is more likely because the program in its totality may run but once. On the other hand, the authors see no "prima facie" reason to doubt the results.

SECTION II

Introduction and Fundamentals

The dominant features of a lunar surface are the craters. The majority of the visible craters are believed to have been caused by the infall of meteoric bodies. These bodies strike the lunar surface, build up very high pressures and explode. This process of cratering breaks up and throws out a quantity of debris. These rock fragments land, cause secondary craters and, over a period of time, are eroded by the infall of finer particles bombarding the lunar surface.

To estimate the lunar roughness it is necessary to consider this process of cratering caused by the infall. It is assumed in this study that the original lunar surface was hard, brittle rock similar to a fine grained basalt. It is furthermore assumed that the infall breaks this surface in a brittle manner. The brittle fracture of brittle rocks is known as comminution. Comminution is a widely used industrial process. Over the last hundred years a body of knowledge has grown up on comminution processes and recently some theoretical work has yielded a clearer understanding of the processes.

When a brittle solid - and glass is an excellent example - is compressed energy is stored in the solid. When the energy density reaches a given level catastrophic failure occurs. The solid breaks up into a size spectrum of daughter fragments. These daughter fragments range in size from that of the original particle down to molecular size. If the amount of energy stored in the crystal lattice is increased, then, the amount of shattering or comminution will increase. It has been found that for materials in slow compression that doubling the stored energy doubles the amount of comminution. This is known as the energy density law.

To better understand the comminution process Meloy[2] assumed that a ramulous network of random cracks passed through the specimen. It was assumed that the crack density was proportional to the energy stored in the lattice. From these assumptions came the equation

$$M(y,z) = 1 - (1-y)^z \qquad (2.1)$$

where $M(y,z)$ is the mass of material finer than particles of size x_y and r_z is the parameter that is proportional to the energy stored in the lattice. Karpinski[3], et. al. independently postulated this equation empirically by observing the size distribution of fragments broken by impact. Also independently Gilvarry[4] from a similar model derived an equation which behaves very similar to equation 1. Thus, recently, a theoretical equation which fits the experimental data has been developed to describe comminution events occurring in brittle solids with uniformly distributed energy densities. In the theoretical derivation of equation 1, it was assumed that the energy density throughout the specimen was uniform. Furthermore, it was assumed the crack density was a linear function of the energy stored at any given point. Many investigators working with a variety of materials have found that this is true. Amongst them are Charles[5], Bergstrom[6] and Hukki[7].

For cratering phenomenon a somewhat different assumption must be made. As the elastic compressive wave moves radially outward from the zero point of impact the strength of the wave decays. This means that the energy stored in the crystal lattice varies from point to point.

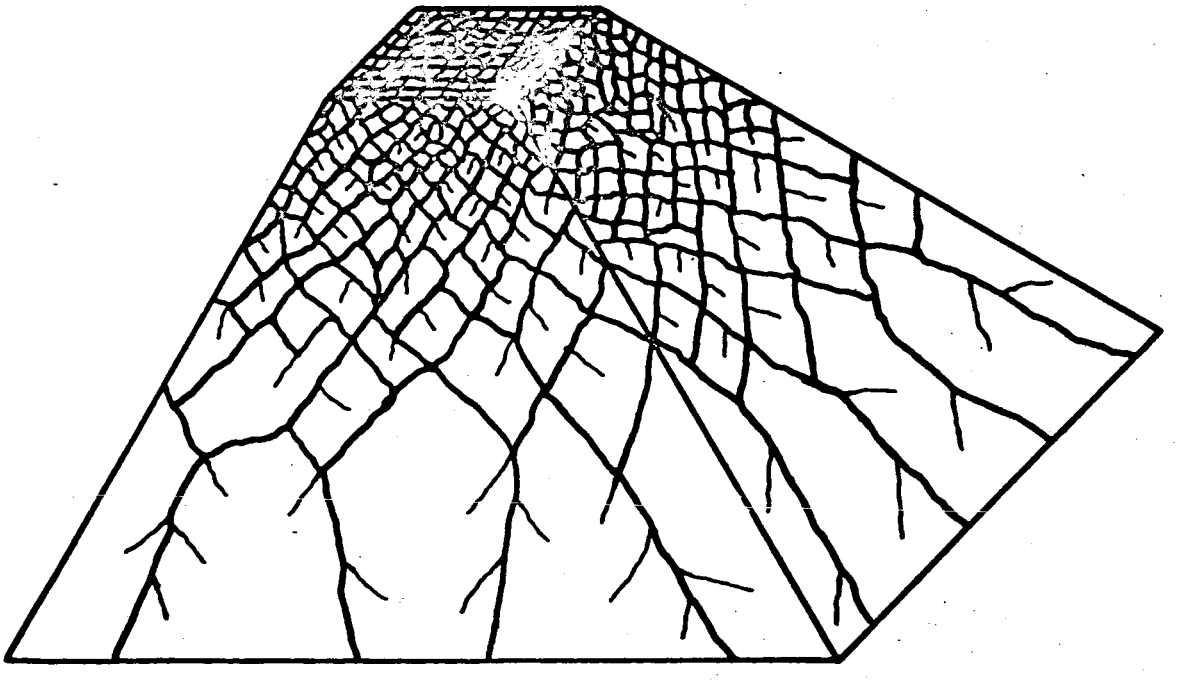

Figure 2.1

Figure 2.1 shows a section of a solid angle where at the top the energy density is higher than at the bottom. It is assumed that the crack density is a function of the energy density and, hence, more cracking takes place at the top than at the bottom.

To derive an equation which describes the size distribution of the fragment from a truncated pyramid where stored energy varies from position to position in the solid it is necessary to vary the classical approach. To describe this mathematically it is assumed the size distribution within any element of volume dV is directly proportional to the stored energy. By summing the size distribution for each incremental volume an overall size distribution equation can be derived. Thus one obtains

$$(2.2) \qquad M(y,z) = \frac{1}{V} \int_{V}^{z} \left\{1 - (1-y)^{z(r)}\right\} dV$$

In this equation V is the volume, dV is the differential volume and z(r) has replaced z in equation 2.1 and is the energy as a function of the distance, r, from the zero point of impact. Integrating this equation over the volume yields M(y,z), the cumulative mass of material finer than size of y, for a specimen in which the energy density varies from point to point in the specimen.

Therefore, in developing an adequate crater model it is important to know how the energy decays with position. In Section IV an energy decay law is derived. This energy decay law specifies the amount of energy available for comminution as a function of position in the specimen. Furthermore, since material leaves the crater it is important to know the amount of energy available for ejecting material from the crater. It also is important to know the fraction of the available energy that goes into kinetic energy of the particles. It is assumed that the kinetic energy of a fragment is directly proportional to the energy density and the surface area of the fragment. This energy partition is discussed in Section V on cratering.

When the material is comminuted and thrown out of the crater secondary craters are formed. Particles after traversing a specified distance land on the lunar surface and form their own crater. It was found, as discussed in Section VI, that the amount of secondary cratering was negligible as far as comminution is concerned.

It should be pointed out that only the solid particles are considered in this analysis. When a high speed particle collides with the target a small portion of the ejecta is melted and thrown out at very high speeds in a process called jetting. Because of this small amount of material involved and lack of an adequate available model, this mechanism was omitted from our analysis. When the particles land on the lunar surface, and speaking here of the larger particles, they may be traveling with sufficient speeds to break themselves up. Karpinski[3] has shown that equation 1, derived by Meloy[2], holds in this case and that r, the parameter directly proportional to energy, is equal to the kinetic energy of the particle. This effect was investigated and omitted. The discussion is in Section V.

In this "hard rock" model several negative assumptions were made; including the fact that no plastic deformation occurs in the rock. Basically the only importance of plastic deformation would be in the profile of the crater. Since an accurate crater profile was not germaine to the study, the assumption of no plastic deformation is not considered important. As mentioned previously, the liquid droplets in the jetting phase of the blast were not considered in our analysis. Much of the mass of these high speed particles leaves the lunar surface and does not affect the amount of secondary comminution. The amount of mass involved is small and the total effect on the analysis is to increase the estimate of the lunar surface roughness. It was assumed that the moon neither gained nor lost material. This assumption can very easily be changed in the program.

Whenever assumptions or choices were made during this analysis, the choice leading to a rougher lunar surface was chosen. All assumptions made in this study were made on the basis of their merit alone. No attempts at curve fitting or changing assumptions to fit the facts were made at any point, except as noted. In fact, the program was only run once and all data is from that single run.

SECTION III

The Hard Rock Model

The fundamental comminution process on the lunar surface is the formation of craters in the lunar surface material by meteoric bombardment. Published infall data indicates that the frequency[1] of such impacts increases rapidly with diminishing particle size. As a result, an exposed rock particle has a much higher probability of being struck by a particle much smaller than it, than by one of the same size or larger. As a result, most lunar impacts resemble a single projectile fired into a hard rock surface.

When a projectile strikes a hard surface, enormous pressures are built up in the vicinity of the impact. The material undergoes deformation and, at sufficiently high energy densities, melting and vaporization occurs. This molten and gaseous material is forced out of the crater at high velocities. Although the volume of material involved is very small compared to the total crater volume, this jetting process represents an important energy sink. The pressure wave is transmitted from the impact point into the substrate. It is assumed that this energy wave is transmitted equally in all directions into the substrate material. Thus the energy wave propagates with hemispherical symmetry. After the energy wave decays to the point where the material is no longer molten it is assumed that this energy wave is the sole cause of cracking, heating and motion of the crater material. Although little work was done on the wave form of the energy wave, it is assumed to be a compression rarifaction wave followed by other disturbances of smaller amplitudes.

Cracking can take place as a result of the hoop-stresses set up by the compression wave or as a direct result of the tension caused by the rarifaction wave. The hoop-stress cracking will be carried along by the crest of the compression wave, will thus occur along planes extending approximately radially from the point of impact, and will occur first. The tension cracks will tend to be in planes normal to the radial direction and will occur later in time. Particles can break free due to the coalescing of radial cracks or the creation of a tension crack.

Radial cracking will cause a displacement of material perpendicular to the polar radius vector centered at the point of impact. This displacement will tend to be cumulative and will be greatest near the surface. The compression and tension waves may displace material either outward or inward toward the impact

point. However, if a particle breaks free due to a tension crack it will spring back toward the impact poi t. If a particle breaks free due to coalescing of radial cracks it will have a velocity component directed outward and toward the surface. The magnitude of the particle velocity can be expected to increase with increasing energy density.

It is believed that near the surface of the crater, where hoop-stress forces are not balanced, most of the particles are freed as a result of radial cracking coalescing. Observation of hypervelocity impacts in high speed photographs[8,9] does in fact show large particles being "peeled" back from the advancing crater rim, at least, in the last stages of cratering. On the other hand, near the bottom of the crater symmetry considerations rule out any very large unbalanced forces except along the hemispherical radius. Hence, tension cracking is probably a major cause at the bottom. Other parts of the crater could be expected to exhibit some of both types of cracking.

As the energy wave advances through the substrate it will carry along with it the radial cracks and, if the energy density is sufficiently high, it will nucleate new cracks. The energy density required to propagate existing cracks will be relatively small compared to that required to nucleate new cracks. It is a fundamental assumption of this model that, for a given substrate material, the energy density required to nucleate cracks is fixed. Below a certain threshold value no new cracks are started. The existing cracks will continue to be propagated for a while, and, particularly near the rim, coalescing of cracks will continue to free particles.

As a consequence of these considerations, the crater can be expected to deviate from a strictly hemispherical shape to something more shallow. That is, cratering is cut off at the bottom by the nucleation threshold, but continues for a while near the rim as radial cracks coalesce.

Cracking in vertical planes will be essentially hoop-stress cracking. This will impart a "side-ways" velocity component to the ejected particles; that is, they will tend to spiral out from the crater. The net effect, however, will be to lower the angle at which the particles are ejected. In order to simplify the model these effects were compensated for by arbitrarily adjusting the departure angles to fit observation and thereafter neglecting these effects.

The model is essentially two-dimensional. A polar coordinate system is used with the origin at the point of impact. The energy density function is assumed to be a function of the impacting

energy, the substrate material, and the polar radius only. The limits of cratering are assumed to be an ellipse. Various eccentricities were tried, but one giving a crater diameter to depth ratio of 4 to 1 was settled on as being in reasonable agreement with observation. Cratering is assumed to stop when the energy density at the rim reaches a fixed threshold value.

SECTION IV

The Energy Decay Law

Energy is assumed to be propagated from the point of impact with hemispherical symmetry. If a hemispherical surface is constructed about the origin with radius R then a certain amount of energy will propagate out through the surface as a result of the impact. If this quantity is divided by the surface area of the hemisphere a figure is obtained representing the flux density of the energy, or the energy per unit area.

Let $p(r)$ = energy flux density function

Consider a hemispherical shell in the substrate material of inner radius r and thickness Δr. (See Figure 4.1)

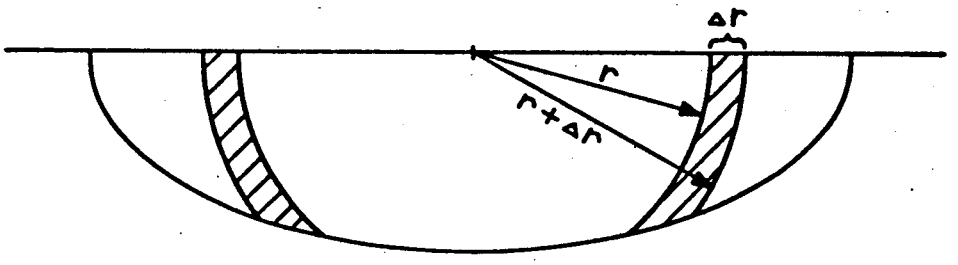

Figure 4.1

Such a shell will have a volume:

$$(4.1) \qquad \Delta V = \frac{2\pi}{3} \left\{ (r + \Delta r)^3 - r^3 \right\} .$$

The total energy passing through the inside surface into the shell is, by the definition of the function $p(r)$:

$$(4.2) \qquad 2\pi\, r^2 \cdot p(r)$$

The total energy passing out of the shell through the outer surface is:

$$(4.3) \qquad 2\pi(r + \Delta r)^2 \cdot p(r + \Delta r)$$

Hence, the net energy per unit volume remaining with the processed substrate material in the shell is:

$$(4.4) \qquad \frac{2\pi r^2 \cdot p(r) - 2\pi(r + \Delta r)^2 \cdot p(r + \Delta r)}{\Delta V}$$

We assume that the net energy per unit volume retained in the processed material is directly proportional to the energy flux density function, $p(r)$. Let α be the constant of proportionality. Then, equating this quantity to the expression (4.4) above and using relation (4.1), we obtain:

$$(4.5) \qquad \frac{2\pi r^2 \cdot p(r) - 2\pi(r + \Delta r)^2 \cdot p(r + \Delta r)}{2/3\ \pi\left\{(r + \Delta r)^3 - \cdot r^3\right\}} = \alpha \cdot p(r)$$

Expanding and rewriting, we obtain:

$$r^2 \cdot p(r) - (r+ \Delta r)^2 \cdot p(r+ \Delta r) = \alpha p(r) \cdot 1/3\left\{(r+ \Delta r)^3 - r^3\right\},$$

or

$$r^2 \cdot p(r) - r^2 \cdot p(r+\Delta r)^2 - (2r\Delta r + \Delta r^2) \cdot p(r+\Delta r) = \alpha \cdot p(r) \cdot \left\{r^2 \Delta r + r\Delta r^2 + \frac{\Delta r^3}{3}\right\},$$

or

$$-r^2 \left[p(r+\Delta r) - p(r)\right] = (2r\Delta r + \Delta r^2) \cdot p(r+\Delta r) + \alpha \cdot p(r) \left\{r^2 \Delta r + r\Delta r^2 + \frac{\Delta r^3}{3}\right\}$$

Dividing through by Δr,

$$-r^2 \left[\frac{p(r+\Delta r) - p(r)}{\Delta r}\right] = (2r+\Delta r) \cdot p(r+\Delta r) + \alpha \cdot p(r) \left\{r^2 + r\Delta r + \frac{\Delta r^2}{3}\right\}$$

Passing to the limit as $\Delta r \to 0$, we obtain the differential equation of the energy function;

$$(4.6) \qquad -r^2 \frac{dp}{dr} = 2\, r \cdot p + \alpha\, r^2\, p$$

Rewriting, we get;

(4.7) $$\frac{1}{p}\frac{dp}{dr} = -2/r - \alpha$$

This can readily be integrated. If log β is the arbitrary constant, then

$$\log p = \log 1/r^2 + (-\alpha r) + \log \beta,$$

or

$$\log p = \log 1/r^2 + \log (e^{-\alpha r}) + \log \beta$$

or

$$\log p = \log (\beta/r^2\, e^{-\alpha r})$$

or

(4.8) $$p(r) = \beta/r^2\, e^{-\alpha r}$$

This equation is the fundamental energy relation. A little further analysis helps to clarify the role of the parameter β. Resorting again to the definition of p(r), if we multiply p(r) by the surface area of a hemisphere of radius r,

(4.9) $$p(r)\cdot 2\pi r^2$$

We have the total energy passing through the surface. Expanding and simplifying the above, we obtain:

(4.10) $$(2\pi\beta)e^{-\alpha r}$$

An upper bound on (4.10) is certainly given by the total energy of the impacting particle. Hence, writing Ep for the projectile energy,

(4.11) $$(2\pi\beta)\, e^{-\alpha r} \leq Ep$$

Since (4.11) holds for all r,

(4.12) $$\beta \leq \frac{Ep}{2\pi}$$

This would be an equality if the elastic model were valid for the very center of the crater. Since it is not, it is more realistic to write

$$(4.13) \quad R = \frac{\nu}{2\pi} Ep$$

for some suitable ν.

Experimental evidence indicates that the mass of ejected material is approximately proportional to the energy of the projectile. The relation:

$$(4.14) \quad M_e = Ep/8 \times 10^3$$

is suggested by Gault, et al.[8] If the density of the lunar substrate is ρ, then the ejected volume is approximated by

$$(4.15) \quad V_e = M_e/p = Ep/p \times 8 \times 10^8$$

The volume of one half an ellipsiod of eccentricity e_c and major semi-axis R_{max} is given by:

$$(4.16) \quad V_e = \frac{2\pi}{3} \frac{R^3_{max}}{e_c}$$

Equating (4.15) and (4.16) gives a means of predicting the crater radius, assuming elliptical boundaries:

$$(4.17) \quad R^3_{max} = \frac{3e_c}{2\pi} \frac{Ep}{8x10^8\rho}$$

Recalling that cratering is assumed to be stopped by a threshold value of the energy function, $p(r)$, then, independent of the nature of the impact

$$(4.18) \quad p(R_{max}) = C = \text{constant}$$

Hence, using relation (4.8) and assuming R to be known from (4.13) and R_{max} to be known from (4.17), we may write:

(4.19) $$\frac{A}{R^2_{max}} e^{-\alpha \cdot R_{max}} = C$$

or

(4.20) $$e^{-\alpha \cdot R_{max}} = C \cdot R^2_{max} / A$$

or

(4.21) $$\alpha = -\frac{1}{R_{max}} \log (C \cdot R^2_{max} / A) \quad .$$

Hence, taken collectively, 4.8), 4.13), 4.17), and 4.21) define the energy decay law inside the crater.

The energy per unit volume left behind by the wave in the processed ejecta is given by

(4.22) $$E_{rem} = \alpha \cdot p(r) = \frac{\alpha \cdot A}{r^2} e^{-\alpha r} \quad .$$

This remaining energy is assumed to be partitioned into thermal energy, kinetic energy required to move the centers of gravity of the particles, energy required to generate new surface (comminution energy) and various other possible energy sinks not used by this model. Thus the increase in thermal energy per unit volume at a point will be:

(4.23) $$E_{th} \cdot \alpha \cdot p(r)$$

The kinetic energy required to move centers of gravity will be:

(4.24) $$E_k \cdot \alpha \cdot p(r)$$

where $E_{th} + E_k < 1$.

SECTION V

Cratering

In this section, the events that occur during cratering are investigated and then described mathematically, During the cratering process, the substrate is shattered, material is ejected, the ejecta lands, shatters and creates new craters. A method is set up to calculate the size distribution of the fragments ejected, their radial distribution about the crater, and the effect of secondary cratering.

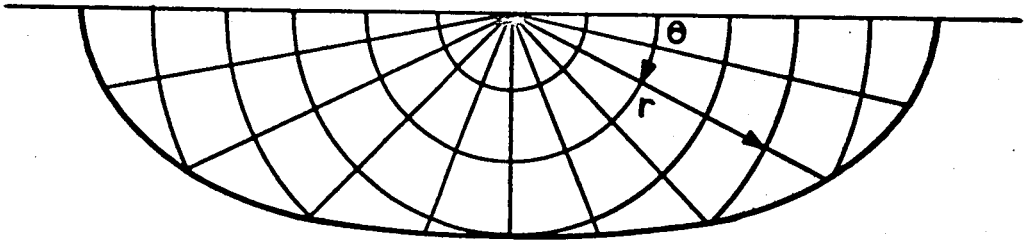

Figure 5.1

The region around a point of impact is addressed by means of polar coordinates. The third (spherical) coordinate is ignored except for volume calculations, making the model essentially two dimensional. The outer boundary of the crater is chosen to be an ellipsoid. After a little experimentation a depth to diameter ratio of 1 to 4 was picked and all computations were based on this. The crater radius is obtained from the postulated input energy by using equation (4.17).

In the immediate vicinity of the impact point, the ejecta material will be molten and probably even vaporized. This material is forced out at extremely high pressures and velocities.

It is likely that most of this material is lost to outer space. In any event, it constitutes only a very small percentage of the total mass of ejecta. It is assumed in this model that this material is lost, i.e., does not play any further role in the character of the lunar surface. However, in the program mass is conserved.

To obtain the boundary between molten and solid material, the energy function is used to find the melting point. Thus, let H be the energy required to raise one unit volume of substrate to its melting point. Then, at the plastic-elastic interface; using expression (4.23)

$$(5.1) \qquad H = E_{th} \cdot \alpha \cdot p(R_{min}) \ .$$

This equation serves to define R_{min}, the radius of the interface of melting E_{th} the thermal energy fraction had to be estimated. Values ranging from 0.1 to 0.9 were tried along with various values of E_k, the kinetic energy fraction. Values of 0.5 for E_{th} and 0.2 for E_k yielded a mean particle velocity of 2.95 km./sec. at the interface and these values were used for the remainder of the computations; α is the constant of proportionality in equation (4.5) and p(r) is the energy flux density of equation (4.2).

Size distributions of fragments within the crater are obtained by using the comminution formula discussed in Section II, equation 2.1,

$$(5.2) \qquad M(y,z) = 1 - (1-y)^z \ ,$$

where y is the ratio of fragment size to the largest possible rock diameter, and z is directly proportional to the energy density in the rock.

To apply this to the crater model, consider a spherical rock of diameter D. If this rock is subjected by some means to a stress resulting in a uniform energy density, then:

$$(5.3) \qquad M(x/D,z) = 1-(1-X/D)^z$$

will be the cumulative fraction of material breaking into size x or smaller. This will be on a per unit volume basis. If it

is assumed that the crack structure is random, then this size distribution will be valid for any portion of the rock. Now consider a thin hemispherical shell of radius r and volume dv inside the crater, possibly cut off by the elliptic boundary. The symmetry assumption gives a uniform stressing of this rock. Hence, the amount of material in this shell breaking into diameter x or less is;

$$(5.4) \qquad dS(x,r) = dv \cdot \left\{1-(1-x/2r)^{z(r)}\right\} \text{ for } x \leq 2r.$$

The exponent $z(r)$ is simply $k \cdot p(r)$; k was evaluated experimentally in the Allis-Chalmers laboratories by dropping steel balls of known weight onto uniformly sized rock specimens. By comparing the resulting fragmentation with the known input energies a value of 10^{-6} was obtained for the cgs system of units.

Equation (5.4) serves to define the size distributions in all parts of the crater. In actual computations the crater is divided up into a finite set of hemispherical shells. For each shell a mean value of $p(r)$ is computed and (5.4) is evaluated for fifty values of x, ranging from 10^{-7} cm. to 10^{3} cm. The results are stored in a large table.

The actual evaluation of (5.4) proved to be unexpectedly difficult. In practice, $z(r)$ takes values ranging from 1 up to more than 10^{8}. For very large values of the exponent and very small (10^{-5} or so) values of $x/2r$, computer programs for logs and exponentials prove unreliable. An infinite series was programmed to handle cases where $x/2r$ is very small and the expression $z(r) \cdot (x/2r)$ is less than one. There remains a region of interest for which neither method yields satisfactory results. This has limited our crater studies to impacts of 10^{20} ergs or less.

The computer program for the crater model is presented in flow chart form in Figure 5.2. It consists of a main program which reads input data, sets up various fixed tables, computes a table of the energy function, finds volumes of the hemispherical crater shells, and computes the size distribution table already mentioned. Various output subprograms can be attached to the main program. These will be discussed separately. As can be seen from Figure 5.2 the program is set up to study impacts of various energies, keeping the other parameters fixed.

The first output subprogram of interest computes the overall size distribution of ejecta from a single crater. This is done by summing the values computed in equation (5.4) over the entire volume. This is permissible since (5.4) is on a volume

MAIN CRATER PROGRAM

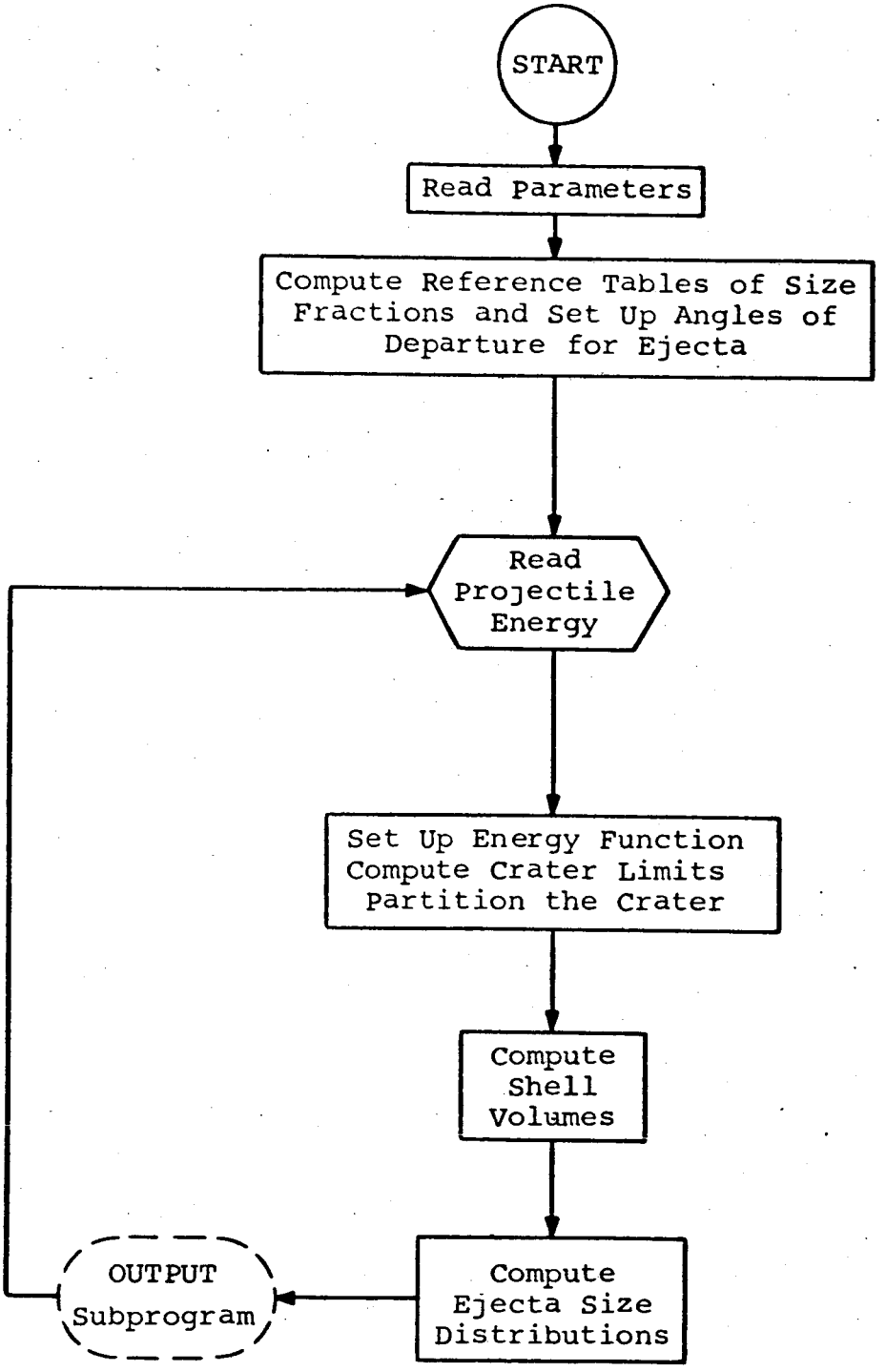

Figure 5.2

basis, i.e., is not normalized. The totals for each size x are then divided by the total elastic crater volume. The results are printed out and also punched into cards for later reference.

This program was run for a wide range of impact energies and gives plausible output for energies between 10^5 and 10^{20} ergs. Outside this range computational problems arise. The results for the above mentioned energy range are shown in Figure 5.3.

Figure 5.3 is a plot of the cumulative fraction of material finer than size x vs. fragment size x. These size distribution plots have been made for energies ranging from 10^5 ergs to 10^{20} ergs. It should be noted that in the upper size ranges the curves have a flatter appearance than in the smaller size range where the curves steepen to uniform slope. The pinching of the curves seen at points A and B is believed to be due to computational difficulties mentioned above. At points A and B is believed to be due to computational difficulties mentioned above. At points A and B there are logic changes. At point C the curves are wavy and are reminiscent of those obtained by Gault[8], et. al. Specifically they are quite similar to the shape of the eight curves in Figure 2[8]. Since the computed curves of Figure 5.3 are similar to those shown by Gault and since the model is a logical one it was felt that this was a validation of our model of cratering. Both the experimental curves of Gault and the computed curves of 5.3 are unlike the classical size distribution curves found in normal comminution.

In order to obtain the radial distribution of ejecta about a crater it is necessary to have an estimate of the vector velocities of the ejected particles.

The problem of assigning a direction to departing particles is complex and was treated only superficially in this project. The problems of determining how a particle breaks free were discussed in Section III. Once the particle is free the problem of collisions arises. We disposed of the latter problem by ignoring it. That is, it is assumed that once a particle is free, it has an unobstructed orbit to its final resting place.

Let a particle be freed at point P. (See Figure 5.4). Let V be a unit vector in the direction of the particle's initial motion. Let ϕ be the angle of departure, i.e., the angle between V and the horizon. We resolve V into radial and tangential components R and T. We assume that R and T are functions of the polar angle θ only.

Let α be the angle between V and the tangent at P. Then

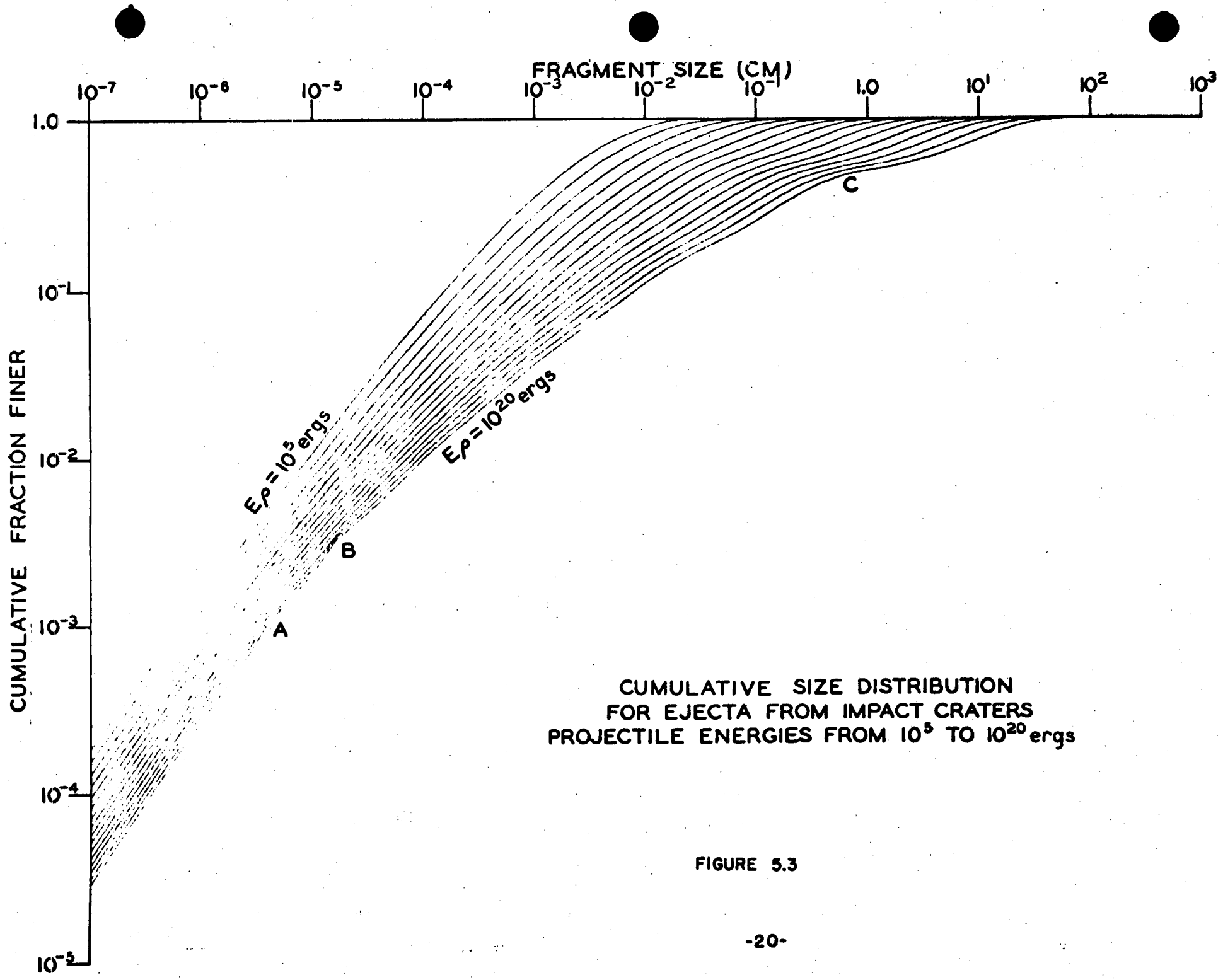

CUMULATIVE SIZE DISTRIBUTION
FOR EJECTA FROM IMPACT CRATERS
PROJECTILE ENERGIES FROM 10^{5} TO 10^{20} ergs

FIGURE 5.3

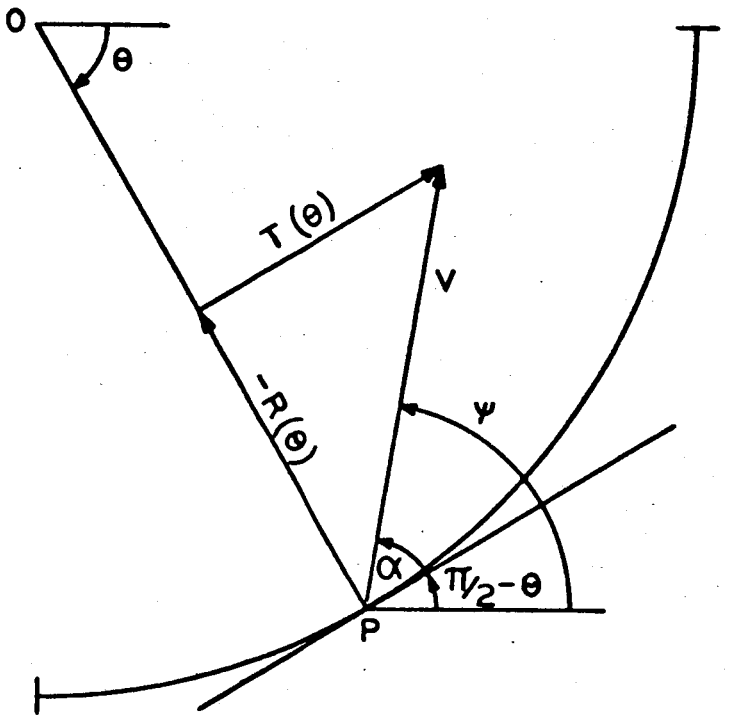

Figure 5.4

(5.5) $$\varphi = (\pi/2 - \theta) + \alpha.$$

But

(5.6) $$\alpha = \tan^{-1}\left(-\frac{R(\theta)}{T(\theta)}\right) .$$

Hence

(5.7) $$\varphi = (\pi/2 - \theta) - \tan^{-1}\left(\frac{R(\theta)}{T(\theta)}\right) .$$

$R(\theta)$ and $T(\theta)$ were approximated using linear functions and the considerations set forth in Section III. High speed photographs of hypervelocity impacts gives the impression of a high concentration of material leaving at 45° to 60°[8,9]. The particular

functions picked

(5.8) $R(\theta) = -4\theta + 2.5$ and $T(\theta) = -1.5\theta + \pi$

were selected to give this concentration. Figure 5.5 gives a tabulation of (5.7) and (5.8) for 18 values of θ. Degrees are shown.

θ	φ
2.5	50.41
7.5	48.64
12.5	47.46
17.5	47.03
22.5	47.50
27.5	49.03
32.5	51.74
37.5	55.63
42.5	60.46
47.5	65.77
52.5	70.90
57.5	75.28
62.5	78.57
67.5	80.65
72.5	81.60
77.5	81.58
82.5	80.74
87.5	79.23

Polar Angle vs.
Angle of Departure

Figure 5.5

This table does not change from one crater to another. For economy of computing it is set up in the initial part of the main program.

Estimates of the magnitude of the particle velocities are obtained from the energy laws. Recall from (4.24) that the kinetic energy per unit volume is: $E_k \cdot \alpha \cdot p(r)$.

Let $Q(x,r)$ = amount of material of diameter x or less per unit volume at radius r.

Let $\{0 = x_0 < x_1 < x_2 < \cdots < x_n = 2r\}$ be a partition of the possible rock diameters at radius r.

Let ΔV be a small volume element at radius r. Then,

(5.9) $E_k \cdot \alpha \cdot p(r) \cdot \Delta V$ = total kinetic energy available in the volume element.

Also,

(5.10) $\{Q(x_i,r)-Q(x_{i-1},r)\} \cdot \Delta V$ = total amount of material in the size (x_{i-1} to x_i) in the volume element ΔV.

We assume that the available kinetic energy partitions itself over particles of various diameters in some manner which is dependent on the characteristic diameter x. Thus, for some partition function, w(x), and some constant of proportionality c(r), the total kinetic energy in the volume element ΔV devoted to the size fraction (x_{i-1} to x_i) will be:

$$(5.11) \quad C(r)\cdot E_k\cdot\alpha\cdot p(r)\cdot\Delta V\left[Q(x_i,r) - Q(x_{i-1},r)\right]\cdot w(\hat{x}_i)$$

where the mean value theorem is used to obtain a suitable $\hat{x}_i$. If (5.11) is summed over the entire size range, we obtain an expression for the total kinetic energy in the volume element, ΔV.

$$(5.12) \quad C(r)\cdot E_k\cdot\alpha\cdot p(r)\cdot\Delta V \sum_{i=1}^{n} w(\hat{x}_i)\left[Q(x_i,r)-Q(x_{i-1},r)\right]$$

Passing to the limit as $n \to \infty$ and $|x_i - x_{i-1}| \to 0$,

we obtain for the total kinetic energy in ΔV :

$$(5.13) \quad C(r)\cdot E_{th}\cdot\alpha\cdot p(r)\cdot\Delta V \int_0^{2r} w(x)\cdot\frac{\partial Q(x,r)}{\partial x}\,dx$$

Equating (5.9) to (5.13) and simplifying, we obtain:

$$(5.14) \qquad 1 = C(r) \int_0^{2r} w(x) \frac{\partial Q(x,r)}{\partial x} dx$$

or, solving for the constant of proportionality,

$$(5.15) \qquad C(r) = \left[\int_0^{2r} w(x) \cdot \frac{\partial Q(x,r)}{\partial x} dx \right]^{-1}$$

Returning to (5.11), if $w(x)$ is identically 1, then equal volumes of material will get equal amounts of energy regardless of the size of particles they contain. That is, energy is partitioned by the volume of the particles. If $w(x) = 1/x$ the partition is on surface area, and if $w(x) = 1/x^2$, the partition is on characteristic diameter.

With some choice made for $w(x)$, equation (5.15) defines the constant, $C(r)$.

Let the size range be partitioned as before and suppose the rock has density ρ. Then, using (5.10),

$$(5.16) \qquad \rho \left\{ Q(x_i,r) - Q(x_{i-1},r) \right\} \cdot \Delta V = \text{total mass of material in size range } (x_{i-1} \text{ to } x_i) \text{ in a small volume element } \Delta V.$$

Suppose that these particles have a mean speed of $v(\hat{x}_i,r)$. Then, the kinetic energy of this material may be written;

$$(5.17) \qquad \tfrac{1}{2} \rho \left\{ Q(x_i,r) - Q(x_{i-1},r) \right\} \cdot \Delta V \cdot v^2(\hat{x}_i,r)$$

If (5.17) is equated to (5.11), then after simplification we obtain:

$$(5.18) \qquad C(r) \cdot E_k \cdot \alpha \cdot p(r)\, w(\hat{x}_2) = \tfrac{1}{2} \rho \cdot v^2(\hat{x}_i,r)$$

Passing to the limit on the x- partition as before and solving for the speed we obtain:

$$(5.19) \qquad v(x,r) = \sqrt{\frac{2}{\rho} \cdot C(r) \cdot E_k \cdot \alpha \cdot p(r) \cdot w(x)}$$

With velocity direction known from (5.7) and magnitude known from (5.19), the trajectory of a particle can be computed.
Let R = lunar radius = 1.74×10^8 cm
Let g = lunar gravitational acceleration = $1.62 \times 10^2 \text{cm/sec}^2$.

Then the circumferential distance $\bar{D}$ from the point of departure to the point of secondary impact is given by: (8)

$$(5.20) \qquad \bar{D} = 2R \tan^{-1}\left(\frac{\frac{v^2(x,r)}{Rg} \sin\omega \cos\omega}{1 - \frac{v^2(x,r)}{Rg}\cos^2\omega}\right)$$

Equation (5.20) serves to define the distance from point of departure to point of secondary impact. Correcting for the displacement of a particle within the crater before it is ejected, the total distance from the point of primary impact to the point fo secondary impact is given by:

$$(5.21) \qquad D = \bar{D} + r\cos\theta$$

The expression for $\bar{D}$ in (5.20) is mathematically sound, but computationally intractable for small values of $\bar{D}$. Fortunately, the power series for arc tangent is rapidly convergent for small $\bar{D}$, i.e., small v(x,r). Thus for $\Phi < 10^{-5}$, we replace $\tan^{-1}(\Phi)$ with Φ itself.

The flow chart of the radial distribution output routine is shown in Figure 5.6. The region around the crater is divided up into 35 ring-like regions. The first 30 are proportional to the crater radius, the last five are fixed at 1 km, 10 km, 100 km, 1000 km and 1740 π km, the last figure being the lunar semi-circumference. For each of these rings there is a burden table with entries for the amount in each size fraction.

The program initially sets these burden entries to zero, computes the ring radii, and computes the constant of proportionality, C(r), (see 5.15), for each hemispherical shell. Then, integrating over the entire crater, for each size fraction at each location, the trajectory, hence landing point is computed. Then the volume of material in that size fraction is added to the current entry in the burden table. When the table is complete it is printed

RADIAL DISTRIBUTION OUTPUT SUBPROGRAM

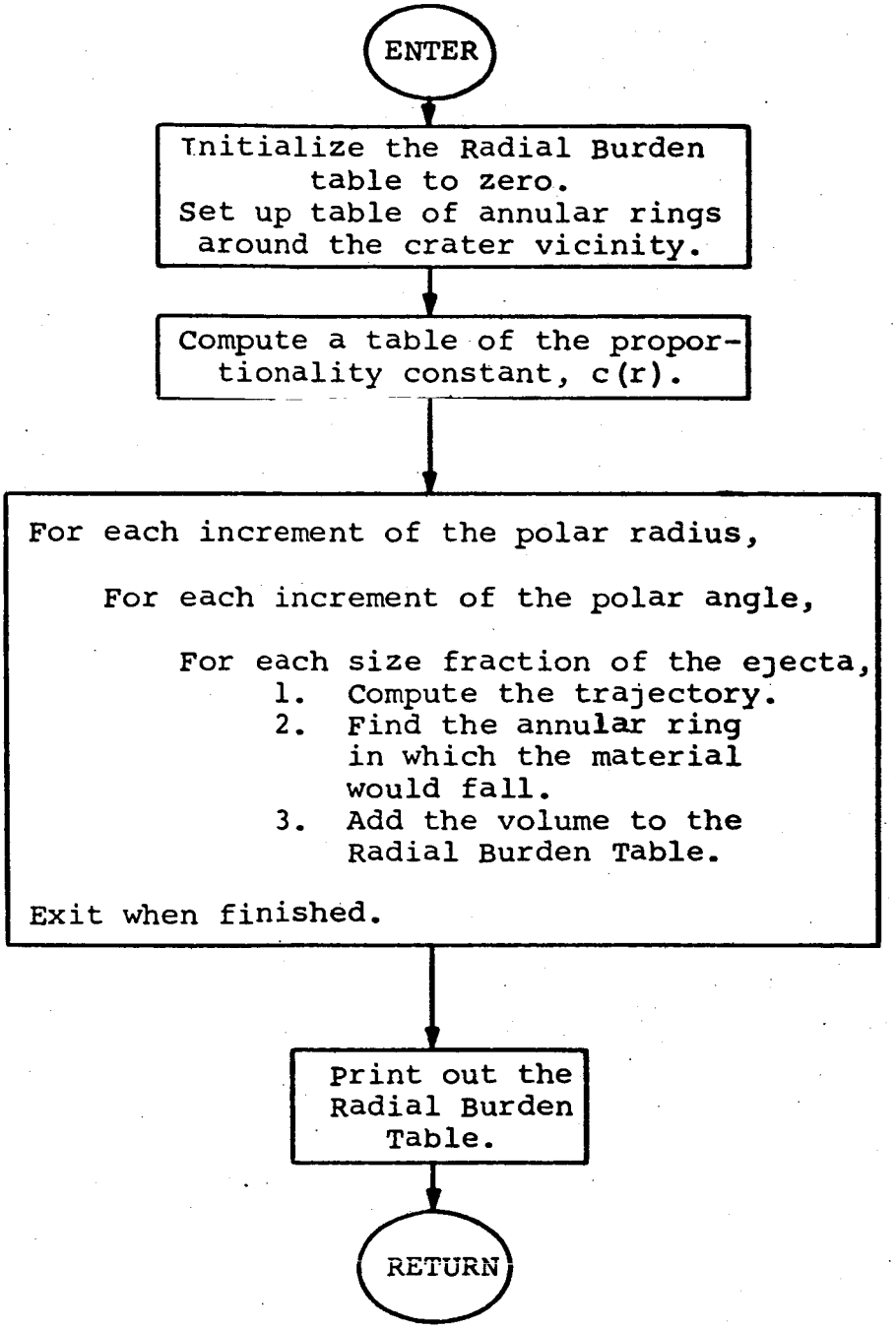

Figure 5.6

out, along with volume totals for each ring and estimated depths, based on a packing density of 50 percent solids, 50 percent voids.

The program was run for impact energies from 10^5 to 10^{20} ergs with some experimentation with the parameters. The partition function, w(x), was set equal to 1 (partition on volumes) and to 1/x (partition on surface area). The surface area partition seemed more plausible, and all later computations were performed with that function.

The output for four typical impacts, 10^{12}, 10^{14}, 10^{16}, and 10^{18} ergs is reproduced in Appendix A. There is a column for each ring. In every case ring No. 1 is the crater itself. For reference, the left hand column on each page tabulates the characteristic diameters, in cm. The values shown in the table are volumes of material in cm^3.

The results show that smaller craters are simply scoured out, all of the ejecta falling at least 130 crater radii away from the point of impact. The fines travel large distances. In a 10^{10} erg shot, for example, the crater radius is 1.6515 cm. and 4.88 percent of the ejecta travels more than 10 km. All of this material is finer than 4×10^{-4} cm. In the larger craters material in the largest size fractions begins to appear close in, and in the largest craters, there would be blocks of material inside the crater.

Our study indicates that craters cannot be scaled. Small craters will have a clean profile. Around and inside the large craters there will be large blocks of material. Of course, in time the large blocks will become eroded.

Computation of the number of particles ejected at the various energy levels is made by another "OUTPUT" subprogram similar to the one just described for radial distributions. In this case, the angle of departure plays no role, only the kinetic energy of each particle is needed. Hence, it is unnecessary to sum the calculations numerically over the polar angle.

From equation (5.18), the kinetic energy per unit volume of material of diameter $\hat{x}$ is:

$$C(r) \cdot E_k \cdot \alpha \cdot p(r) \cdot w(\hat{x}_i) \tag{5.22}$$

Hence, for one such particle, having a volume $\hat{x}_i^3$, the ejected particle will have an energy of:

$$(5.23) \qquad ES(x_i,r) = C(r)\cdot E_k\cdot\alpha\cdot p(r)\cdot w(\hat{x}_i)\cdot x_i^3$$

The number of such particles in the hemispherical shell of radius r will be

$$(5.24) \qquad NS(\hat{x}_i,r) = \left\{Q(x_i,r) - Q(x_{i-1},r)\right\} V_s(r)/\hat{x}_i^3$$

where $V_s(r)$ is the total volume of the hemispherical shell at radius r . If (5.24) is summed over the entire crater for those particles for which (5.23) yield approximately the same energy level, the result is a count of the number of particles ejected at that energy level.

Computationally a table is set up for energy classes of 1 erg, 10 ergs, 10^2 ergs, $\cdots$, 10^{23} ergs. For each hemispherical shell and each size class, (5.23) and (5.24) are evaluated. (5.23) is used to add the figure given in (5.24) to the appropriate table entry. The result is a table giving the number of secondary particles in each energy class arising from one primary impact of energy E_p.

This table is printed out and also punched into cards for later use in studying secondary cratering. The program was run for primary impacts of 10^5 to 10^{20} ergs. As was pointed out earlier, computational difficulties arise outside the range.

The results of this computation are shown graphically in Figure 5.7.

To obtain information on secondary cratering, the results shown in Figure 5.7 were extrapolated to form a 24 by 24 matrix $A = (a_{ij})$ where a_{ij} = number of particles of energy class i resulting from an impact of energy class j, where energy class i is nominally 10^{i-1} ergs.

Let $V_o = (v_{oj})$ be a 24 element vector where v_{oj} is the number of primary impacts of energy class j per unit time. Then,

$$(5.25) \qquad v_{1i} = \sum_{j=1}^{24} a_{ij}\cdot v_{oj}$$

is the total number of secondary particles of class i per unit time. Rewriting in vector-matrix notation,

$$(5.26) \qquad V_1 = A\ V_o$$

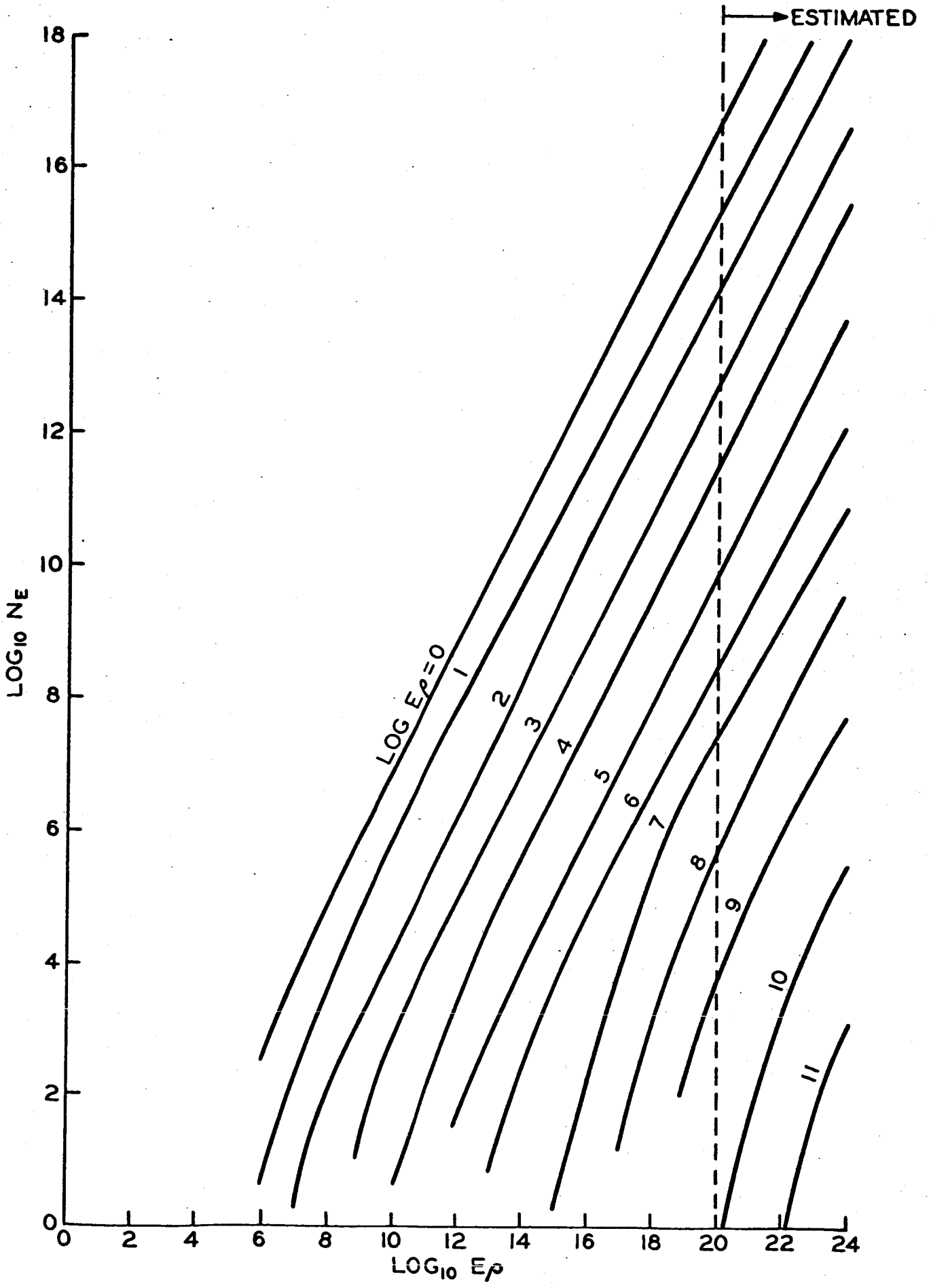
ESTIMATED
LOG Eρ=0
1
2
3
4
5
6
7
8
9
10
11
LOG10 NE
LOG10 Eρ
0
2
4
6
8
10
12
14
16
18
20
22
24

Figure 5.7

gives the total secondary infall rate. Combining primary and secondary infall gives

$$(5.27) \qquad V_o + V_1 = A\,V_o + V_o$$

Tertiary infall will be given by:

$$(5.28) \qquad V_2 = A\,V_1 = A^2\,V_o$$

Extending this, it is clear that the total infall per unit time will be:

$$(5.29) \qquad V_\infty = V_o + A\,V_o + A^2\,V_o + A^3 V_o + \text{-----}$$

Conservation of energy dictates that the matrix A will be nilpotent. Hence (5.29) cannot have more than 24 terms and there is no question of convergence. To solve for V_∞,

$$(5.30) \qquad V_\infty = (I + A + A^2 + A^3 + \text{-----})\,V$$

But

$$(5.31) \qquad (I-A)^{-1} = (I + A + A^2 + A^3 + \text{---})$$

Hence

$$(5.32) \qquad V_\infty = (I-A)^{-1}\,V_o$$

(I-A) is a triangular matrix of determinant = 1. Hence $(I-A)^{-1}$ exists.

A small program was written to read in the matrix A from cards punched by the previously discussed program, compute $(I-A)^{-1}$, read in a vector V_o for primary infall, compute V_∞ and print it out. This was done for two sources of primary infall (I, II). Primary particle velocities were assigned a nominal velocity of 20 km/sec. to obtain these rates.

The result in both cases was that $v \geq v_o$. That is, primary infall constitutes at least $(1-10^{-6})$ of the total infall. As a consequence of this, the only infall considered after this is the primary infall.

The process of secondary comminution was considered. By the term secondary comminution is meant the breakup of rocks upon landing. The primary event is the comminution that takes place in the primary crater. From this crater rock fragments are thrown out at various speeds and land on the lunar surface. Upon landing these rocks may break up into smaller particles.

It has been shown by Karpinski[3], et. al., that solid particles impacting on a solid surface break up according to the equation derived by Meloy[2]. The parameter z is directly proportional to the kinetic energy of the particle. Furthermore, it has been estimated by Meloy and Bergstrom[10] that z varies as the one-fourth power of the size of the particle for a given energy density. Thus, to compute the amount of comminution that occurs for a particle one need only know its kinetic energy and its size to compute the amount of break up.

In the cratering model the size distribution and velocity distribution of particles is computed such that the degree of secondary comminution could readily be computed. However, the hardness of the lunar surface varies with time and an adjustment must continually be made. Since preliminary estimates indicated that the effect of the secondary comminution would be small this process was not incorporated in the final program because the amount of computation needed would increase the program running time due to the changing thickness of the lunar dust layer. The effect of this assumption was to increase the roughness estimate of the lunar surface in the larger particle sizes.

In the cratering model there is an inherent contradiction that our cratering scaling law has turned up. If one assumes the comminution stops at a given energy level and that the amount of ejecta from a crater is directly proportional to the energy of the impacting body then one is faced with the following paradox. There is a lower size limit beyond which the energy density at the edge of the crater will not be sufficient to comminute material. In other words, at a radius less than that of the crater size predicted by energy-scaling-law comminution will stop because the energy in the compressive wave is less than that required to break the material. This paradox occurs because the energy in the wave falls off as the square of the radius while the ejecta is proportional to the cube of the radius.

We have no explanation for this paradox. It seems physically sound to assume comminution stops when the energy density in the compressive elastic wave reaches a given value. This is true experimentally and has a sound theoretical basis. The crater-size-law has been established over a wide variety of sizes empirically. This is one area which bears further investigation.

Our study also shows the pattern of ejecta distribution around craters cannot be scaled. Small craters will be swept clean and the ejecta will land many diameters away. Large craters will have much of the larger fragments on or near the crater rim. This means the landing near the edge of a relatively young large crater would be more dangerous. In older craters the debris would be eroded away and would not be as rough. Landing near small craters, new or old, would not be dangerous for the material would be thrown too far to appreciably increase the surface roughness.

SECTION VI

The Roughness Estimate

This section describes a computation, based upon the preceding hard rock crater work, designed to estimate the depth and composition of the lunar dust layer. It is assumed throughout this computation that a given current infall estimate is valid throughout the entire lunar lifetime and that impacting is the only mechanism affecting the lunar surface. The method to be described could be altered to handle variable infall rates if they were slow, long term changes. It would also be possible to include vulcanism if estimates of the degree of volcanic activity were available. Tectonic action must be ignored for the present.

The method is based upon a matrix whose elements are the transitional probabilities that lunar material in one classification at time will end up in some other classification at the end of some time interval Δt. By multiplying a vector giving the amount of material in each class at time t by this matrix, the resulting vector is the amount of material in each class at time $t + \Delta t$. If the conditions affecting the transitional probabilities do not change, a computational advantage may be gained by raising the matrix to a power, enabling the computer to take many time increments in a single step.

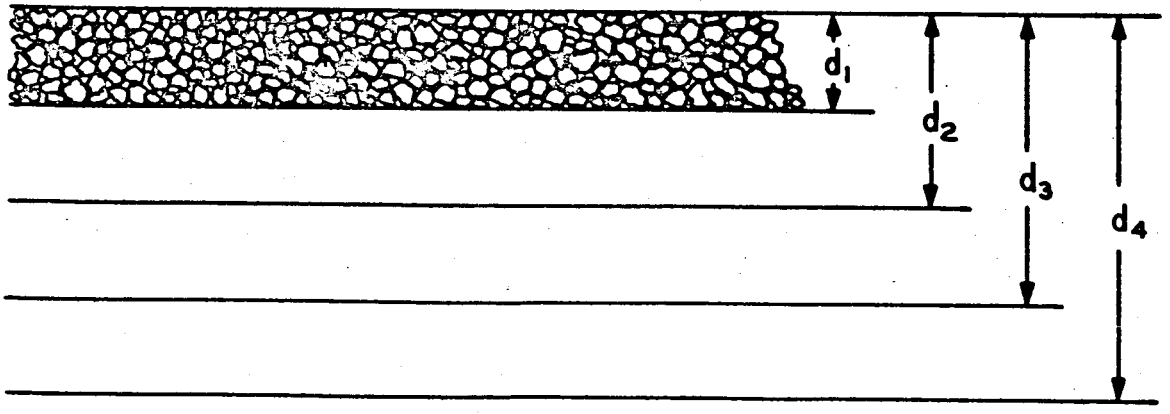

Figure 6.1

The lunar surface is divided into four layers. The first is the layer of dust and debris on the surface. Let it have a depth = d_1. The hard rock substrate is divided at three depths, d_2, d_3, and d_4. (See Figure 6.1). Within the dust layer the material is broken down into 17 size classes; 10^{-5} cm, $\sqrt{10}\times10^{-5}$ cm, 10^{-4} cm, ... , 10^{3} cm. Material can enter any of these size classes from any larger size classes or the substrate layers. Material can leave a class to any smaller class.

Consider one square meter of lunar surface. Let V_{oj}, $j = 1,2$ be the amount of material in each of the classes. Let a_{ij} be the transitional probability of material leaving class j and entering class i per unit time. Then at the end of one time unit there will be:

$$(6.1) \qquad V_{1j} = \sum_{j=1}^{20} a_{ij}\, v_{oj}$$

cm^3 of material in class.

It remains only to calculate the matrix (a_{ij}).

We start with the rubble in the top layer. Let this layer have depth d_1. Consider a particle of diameter x_j. Let x_j/d_1 be the probability that this particle is at the top of the layer so that it has an exposed surface. (We realize that for thin layers this quantity could be greater than 1, but in such a case the patticle will be exposing much more than a single face greatly increasing its rate of erosion). Let x_j^2 be the exposed surface area. Then if an impact takes place inside the given square meter, the probability that the given particle is struck will be:

$$(6.2) \qquad \frac{x_j}{d_1} \cdot \frac{x_j^2}{10^4} \quad \text{, assuming } x_j \text{ and } d_1 \text{ in cm.}$$

For convenience and because of difficulties with the crater program, all impacts are assumed to take place at one of the 16 discreet energies: 10^5, 10^6, ... , 10^{20} ergs. Let n_{ℓ}, $\ell = 1, 10$ be the number of impacts of energy class 1 per square meter per unit time. Then, the number of impacts of energy class ℓ per unit time which a given x_j particle will undergo will be:

$$(6.3) \qquad P_{j\ell} = n_{\ell} \cdot \frac{x_j^3}{d_1 \cdot 10^4}$$

Suppose there are V_{oj} cm^3 of material of sixe x_j in the layer. Then the number of such particles is V_{oj}/x_j^3. Multiplying the particle counts by the probability that each is struck by a class ℓ projectile, the expected number of craters is:

$$(6.4) \qquad \frac{P_{j\ell}}{x_o^3} \cdot V_{oj} = \frac{n_\ell}{d_1 \cdot 10^4} \cdot v_{oj}$$

Let VC_ℓ be the volume of ejecta from a crater of energy class ℓ.

Let $DM(x_i,\ell)$ be the relative amount of material breaking into size class x_i from an impact of energy class ℓ. Then, if a class ℓ impact occurs, it will generate:

$$(6.5) \qquad VC_\ell \cdot DM(x_i,\ell) \quad cm^3 \text{ of new material in size class } x_i.$$

Combining (6.5) with (6.4), we get the expected amount of material breaking out of size j and into size i due to impacts of class ℓ:

$$(6.6) \qquad VC_\ell \; DM(x_i,\ell) \cdot \frac{n_\ell}{d_1 \cdot 10^4} \cdot v_{oj}$$

We make the assumption at this point that particles are eroded only by involvement in craters smaller than the particle itself. Of course this is not true, but, except in the finest sizes, the probability of a particle being involved in a crater larger than it is much less than the probability of its being eroded by smaller craters. This assumption makes the hard rock crater model applicable. The magnitude of the error due to this assumption is small for all but the smallest size ranges. In any event, it will cause an apparently rougher size distribution than actually exists.

On this basis, we sum expression (6.6) over those energy classes for which the assumption above holds obtaining:

$$(6.7) \qquad \sum_\ell \left[VC_\ell, DM(x_i,\ell) \frac{n_\ell}{10^4 \cdot d_1} \right] V_{oj} = a_{ij} \cdot V_{oj}$$

a_{ij} is the sought-after transitional probability for material in size j breaking into size i.

Relation (6.7) makes sense only for rocks in the upper layer. Some account must be made of the material breaking out of the substrate layers. The upper layers will tend to protect the lower layers. (See Figure 6.2). Only an impact larger than a certain threshold value will have sufficient energy to penetrate the protective dust layers. If such an impact does take

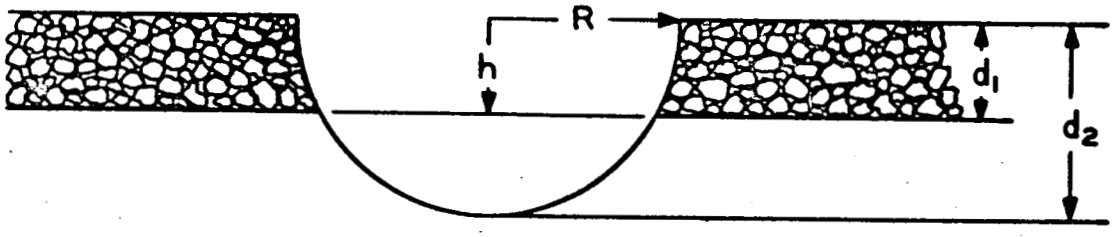

Figure 6.2

place, the volume of material knocked out will be that part of the crater which is not deeper than the depth of the bottom of the layer, diminished by the volume already accounted for in preceding layers. Let

(6.8) $VC_{\ell}(k)$ = volume of material involved from substrate layer k in a crater of class ℓ, assuming that layer k is hit.

Suppose, as before, that there are n_{ℓ} impacts per unit time per square meter of energy class ℓ. Then, these impacts will process:

(6.9) $n_\ell \cdot VC_\ell(k)$ $\quad k = 2,3,4$

cm^3 of material from the k layer. The uneroded volume of the k layer will be:

(6.10) $10^4 \cdot (d_k - d_{k-1})$ $\quad k = 2,3,4$

Hence, the fraction of k-layer material that is involved in class ℓ impacts is:

(6.11) $$\frac{n_\ell \cdot VC_\ell(k)}{10^4 (dk - d_{k-1})}$$

In time, the k-layer will become eroded. Nevertheless, we assume that (6.11) is still the probability that one cm^3 of k-layer material will be struck by an ℓ-impact.

If some k-layer material is impacted at class ℓ, then the fraction of the material breaking into size x_i will be $DM(x_i,\ell)$ as before. (See 6.5). Then, summing over the energy classes large enough to strike the k-layer, we obtain:

(6.12) $$b_{ik} = \sum DM(x_i,\ell) \frac{n_\ell \cdot VC_\ell(k)}{10^4 (dx - d_{k-1})} \quad , \quad k - 2,3,4$$

which is the transitional probability of material in layer k entering size class x_i.

Combining (6.12) and (6.7), a square matrix $A = (a_{ij})$ can be constructed giving all the required probabilities. The diagonal elements are just:

(6.13) $$a_{ij} = 1 - \sum_{i=1}^{j-1} a_{ij} \qquad j=1, 2 \text{ ---- } 20$$

The computation is as follows:

If $V_o = (v_{oj})$ is the amount of material in each class at time t, then the amounts after time Δ t will be:

$$(6.14) \qquad V_1 = A\, V_o = \left(\sum a_{ij}\, v_{oj} \right)$$

After n time intervals, the amounts will be:

$$(6.15) \qquad V_n = A\, V_{n-1} = A^n\, V_o$$

assuming A is independent of time. Since A is dependent on the depth of the last layer d, (6.15) cannot be used with impunity unless A is periodically recalculated.

When this was programmed, we had very little idea of what to expect in the behavior of A with time. As a result, a program was written which permitted inspection of the dust layer depth while the problem was on the computer. By manipulating switches it was possible to recompute A at any point, or square the current matrix being used, or simply let the program keep iterating on equation (6.15).

The program was run using Hawkins[1] infall data, a nominal projectile velocity of 20 km/sec., and a basic time increment of 1000 years. The initial vector of material assumed a bare surface, no broken material, the substrate layers being assumed full. The program sets transitional probabilities to zero if the layer has zero thickness.

After 1 iteration there were 1.058 cms of dust. The matrix was then recomputed. This time, at the end of the second iteration we had 1.078 cms of dust. This matrix was kept for a while. Generally speaking, we tried to compute a new matrix before the dust layer grew to more than 125 percent of the depth at which the first matrix was computed.

The depth grew rapidly at first, slowing its growth with time as may be seen in Figure 6.3. At first the matrix had to be recomputed every 10-15 iterations. Later it was possible to take advantage of matrix powers and move in larger time steps. Toward the end of the calculation, we were using the 8192th power of the matrix.

Because the matrix was recomputed periodically due to increasing dust layer thickness there is a scatter in the data. Two calculations made for the same length of time, one using a matrix

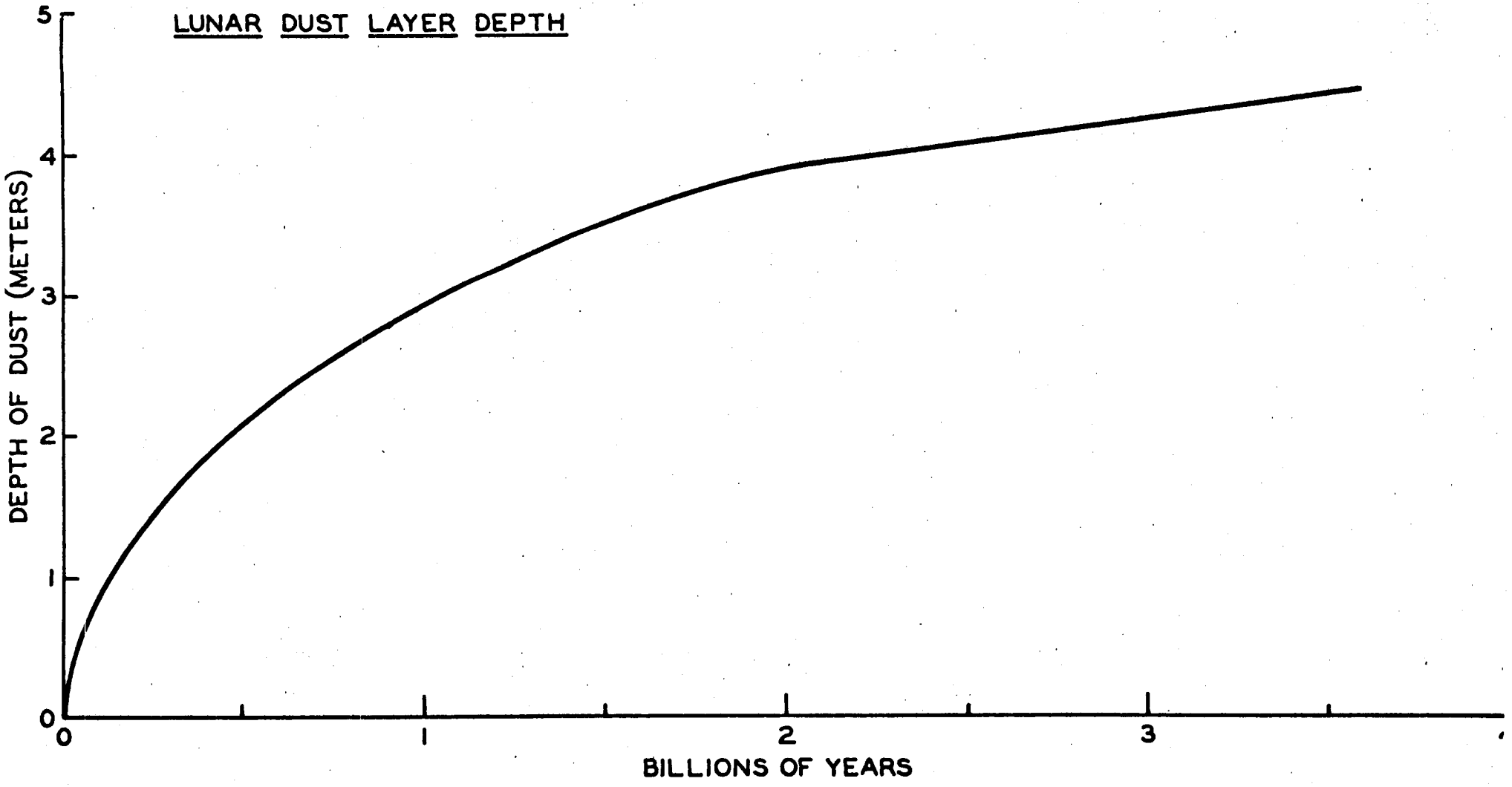
LUNAR DUST LAYER DEPTH
DEPTH OF DUST (METERS)
0
1
2
3
4
5
0
1
2
3
BILLIONS OF YEARS

Figure 6.3

based on dust layer depth of 1.0M and another on a dust layer depth of 1.25 M will yield different answers for mass of material in each size range. These variations are minor but when one is used to smooth curves from computational data these variations at first appear as errors.

Figure 6.4 is a log-log plot of the data that appears in Figure 6.3. The middle curve, labeled Hawkins' data, is a plot of the depth of the lunar dust layer vs. time using the latest available meteoric infall data specified by Hawkins[1]. The one-fifth Hawkins data and five Hawkins data are, respectively, in depths of lunar dust based on one-fifth Hawkins infall data and five times his data. Our estimate of three meters deep is different from Orrok's[12] estimate of 0.12 to 0.7 meter depth. However, using one-fifth Hawkins data brings the depth down to one meter thickness. We believe this variation is due primarily to differences in the infall rate and to a lesser extent on a computational method.

Our method, using transitional matrices, which are re-evaluated for increasing dust depths, giving a running account of the status of not only the dust but the substrate and the size distribution of material. Consequently, a ten meter block created in one period is kept track of until it erodes away to nothing throughout the rest of the history of the lunar surface. This dynamic bookkeeping approach for the accounting of every block formed should give the reasonably close approximation of the lunar surface if the infall data and crater behavior mechanics are correct.

Figure 6.5 is a plot of the cumulative mass fraction of material finer than size x vs. size x. This plot shows that 80 percent of the material is less than 180 microns, 50 percent of the material is less than 40 microns and 10 percent of the material is smaller than 1.6 microns; 99.9 percent of the material is smaller than 1 millimeter. This means that the surface of the moon is covered with a fine powder. If it is assumed that the powder packs to 40 percent solids then the depth of the layer would be approximately 25 feet. All estimates of depth appearing in Figures 6.4 and 6.5 and in the computation are depths in terms of solid rock. Thus, one divides the depth of the solid rock by the density of the powder to obtain the depth of the dust layer.

The actual size distribution or fineness of the powder does not change appreciably with time. Figure 6.6 is a plot of the fraction of mass finer than the indicated size vs. time in years. Looking now at the 0.001 centimeter curve, one can see that the percent of material finer than this falls from about 37 percent down to about 31 percent and stays constant for the rest of the lunar history. The other curves are similar. Thus, the fineness

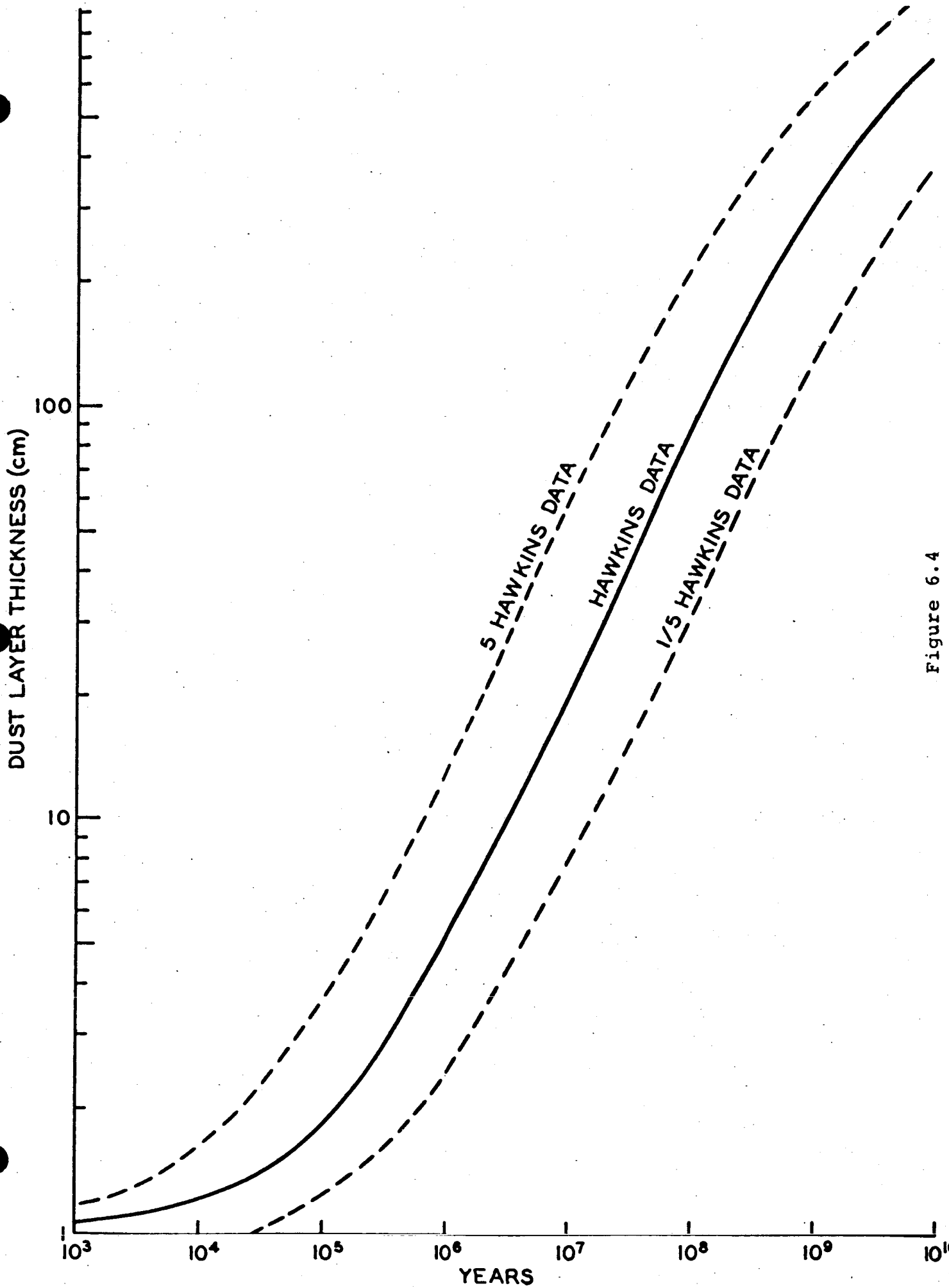
DUST LAYER THICKNESS (cm)
100
10
1
5 HAWKINS DATA
HAWKINS DATA
1/5 HAWKINS DATA
10^3
10^4
10^5
10^6
10^7
10^8
10^9
10^{10}
YEARS

Figure 6.4

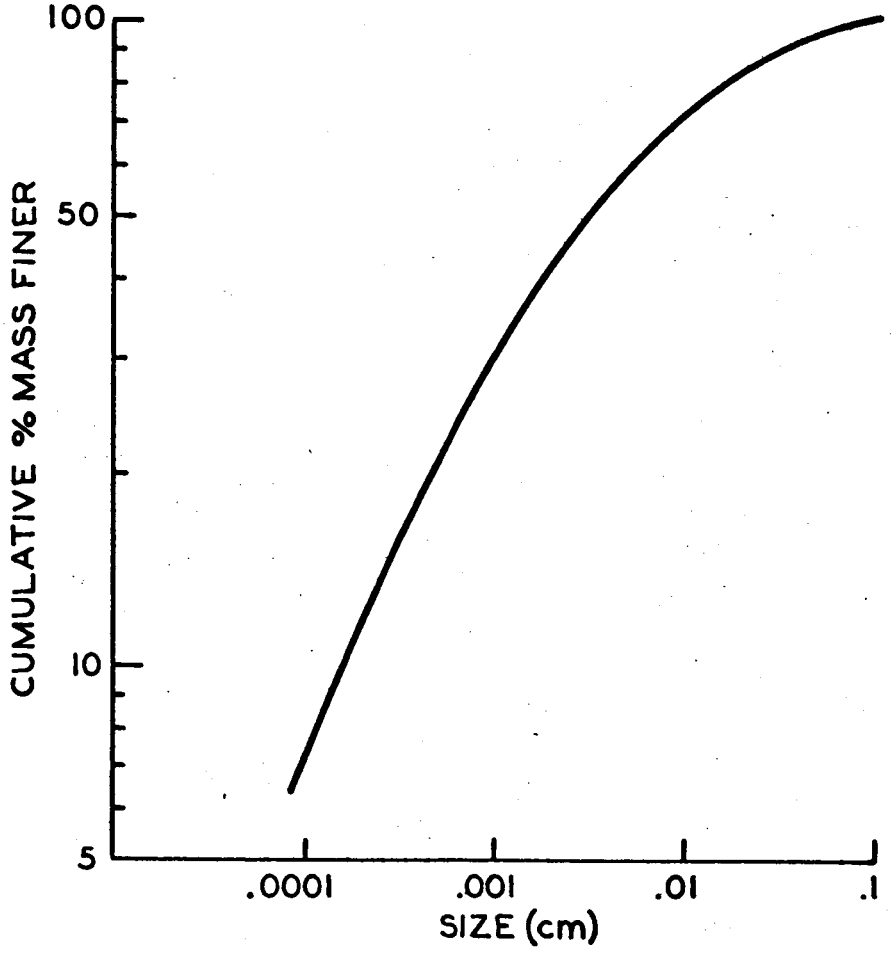

Figure 6.5

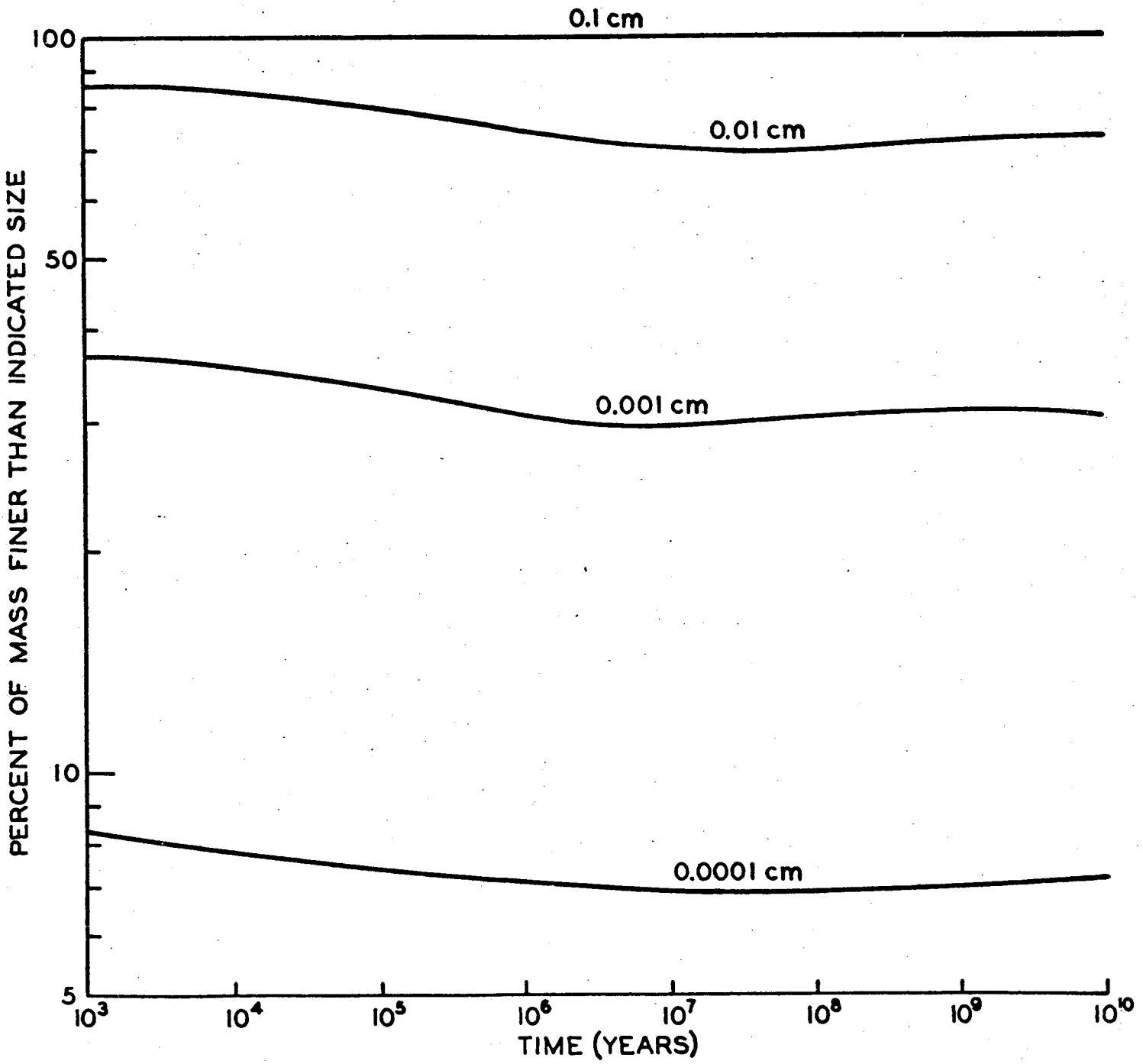
0.1 cm
0.01 cm
0.001 cm
0.0001 cm
100
50
10
5
PERCENT OF MASS FINER THAN INDICATED SIZE
10^3
10^4
10^5
10^6
10^7
10^8
10^9
10^{10}
TIME (YEARS)

Figure 6.6

of the powder is not affected by the age assumed for the feature or the meteoric bombardment rate. The depth on the other hand is sensitive to both the infall rate and the age.

The probability of being bothered by or seeing large blocks of material is relatively low. At the end of a billion years there are 3.2 times 10^{-8} ten meter blocks per square kilometer. In the one meter block size range there is one per square kilometer. In the one foot size range (32 centimeters), there are 40 square kilometers. These blocks would be badly eroded and would appear as gentle mounds. It should be pointed out that the blocks will not stand straight up and cast sharp shadows. There will be a process whereby dust particles drift over the block blurring its outline. Therefore, any block should be looked for as an unexplained mound. At the resolution of the Ranger shots it is very unlikely that any material in it will be due to solid rock chunks. There are a number of particles in the 3 and 1 centimeter size range. However, these constitute a very small fraction of the surface.

SECTION VII

Discussion

The work in this study falls into three parts: energy decay law, cratering and the lunar surface roughness. In each part the analysis was done and then the results were programmed. The individual programs were assembled into an overall program which could compute the lunar surface roughness, given the initial surface roughness, the infall curve and the size distribution data from the crater studies. The overall program was run once. It was assumed that the initial surface was composed of solid rock and that Hawkins[1] infall data was the best estimate of the meteoric bombardment rate. The results of this single run are the data presented.

Hawkins[1] infall data was used because it was the best available[13]. The authors are not experts on infall and thus they felt that it would be best to accept the data of experts in the field. Furthermore, the program was written so that at object time the infall data is fed to the program. Thus, a wide variety of infall curves may be used by running the program for each infall curve.

Energy Decay

The energy decay law is central to this analysis. To predict the size distribution of the ejecta in a crater the strength of the energy wave must be known as a function of position in the crater. In classical comminution, the amount of shattering has been found, theoretically and experimentally, to be directly proportional to the energy stored in the crystal lattice just before fragmentation. As the energy wave moves out from the center of impact, the strength of the wave is attenuated by the increasing area that it passes through as well as by the work that it does in comminuting the material that it passes through. Thus a fraction of the energy of the wave as it passes through a volume of material is left behind as new surface area, kinetic energy and thermal energy. The law that was finally used said in essence that the amount of energy left in the incremental volume was directly proportional to the energy in the wave. Prior to accepting the law a number of empirical laws were tried and found unsatisfactory.

The law as now derived assumes that the material is homogeneous or contains homogeneous heterogeneities. By the latter is meant that cracks or grains are sufficiently numerous and evenly

distributed that the rock may be treated as a homogeneous substance. For larger craters one would have to assume that the material contained major cracks which were not randomly distributed.

When medium size meteorites collide with the dust layer there is a discontinutiy at the interface between the dust layer and the underlying rock. This shows up in different material strength, density and propagation characteristics. This problem was not considered in our analysis.

Once a reasonable energy decay law was established, the analysis of the cratering process began. Craters historically, whether they be chemical or meteoric, have a diameter to depth ratio of four to one. No simple explanation of this ratio was found. The ratio was accepted fact.

Cratering

Having assumed the shape and derived an energy decay law, it was possible then to compute the size distribution of the ejecta fragments from the crater. This was done in a straightforward manner as described in Section V.

The shape of the size distribution of the ejecta fragments is similar to those that Gault[8] found experimentally. It was assumed in the analysis that the kinetic energy of each fragment was found to be directly proportional to the crater fragment interface area and the strength of the energy wave. In other words, the kinetic energy of a fragment was proportional to its area as well as strength of the energy wave. This assumption is sound theoretically and yields a velocity profile which is realistic for the fragments.

To compute the radial distribution of the ejecta around the crater, one has to know both the velocity and the angle of departure. The model assumed is based on empirical observations and yields relatively good ejecta patterns. It is, nevertheless, an assumption which is not based on a physical model. More work must be done in this area.

In the early stages of cratering the intensity of the shock is sufficient to melt material and jet it out at very high speeds. There is no satisfactory model to predict how much of the energy in the compressive wave is lost in this process. For want of a better figure, it was assumed that 50 percent of the energy was lost. It is hoped that this problem will be solved soon. It was also assumed that the amount of material gained or lost by the moon was zero. It is a very simple matter to change the program

to take into account accretion or loss of material from the surface due to high speed jetting.

The analysis shows secondary and tertiary cratering of solid fragments contain very little energy and hence the effect of of the ejecta on roughening the lunar surface is negligible. In other words, the only real crater creation comes from meteoric bombardment. It should be remembered that the study considered only the solid fragments ejected and did not consider the liquid fragments jetted in the early stage of the cratering process.

The crater scaling law that states that the mass of the ejecta is directly proportional to the energy of the incoming body, was assumed. This assumption, along with an energy decay law, leads to a paradox. The paradox says that there is a lower limit in the size of crater that can be formed. (See Section VI.) There is a way out of the paradox and that is to assume that the energy decay law is essentially the scaling law. This means that:

$$(7.1) \qquad Me = Kr^2 e^{\alpha r}$$

In this equation, Me is the mass of the ejecta, r the radius of the crater and α the partition of energy in the decay wave into the substrate. This postulated scaling law indicates that the energy required to form the larger craters goes up faster than the ejecta mass. Since this is not true experimentally it means that for larger craters α is smaller. This in turn may mean that in larger craters the presence of cracks or other inhomogeneities cause α to behave differently. The implications of the scaling law were only thought of after the study was completed.

If the larger ejecta fragments were to land on the hard surface one would expect them to comminute further. This process was considered and omitted because it would have added to the complexity of the computation and appears to have a relatively small effect on the size distribution of the fragments.

Computing difficulties were encountered with the Fortran routine. These routines were not set up to handle the comminution equation. In computing the expression $1-(1-\epsilon)^{\omega}$ difficulty was encountered when ϵ was small and ω large. This seemingly trivial problem prevented the computation of the size distribution of ejecta from craters formed by explosions with energies over 10^{20} ergs. A power series evaluation gives only temporary relief. For a more accurate crater model, further work must be done in finding wasy to compute this simple expression.

The study shows that the distribution pattern around small craters varies significantly from that around large craters. For large craters there is a significant amount of material near their rims. This means that it would be hazardous to land near such a crater. For small craters the ejecta is thrown many diameters away. Therefore a fresh, small crater would appear to be perfectly formed with no ejecta near its rim. This result may explain why a number of almost perfectly formed small craters appear in both telescope and Ranger VII pictures.

Lunar Surface Roughness

In Section VI the logic for describing the method of computing the depth and size distribution of the lunar surface is described in detail. Basically, the method is to sum over all the individual cratering events. At object time, the infall data is read in. Energies in each size range is computed. The size distribution of ejecta from craters at each energy level is computed. A roughness is then computed by a transitional matrix. The depth of the debris or dust layer is computed and printed out. Then, if the depth of the dust layer is 25 percent greater than at the last recomputation a new transitional matrix is computed. In computing the new transitional matrix it is assumed that a meteor which cannot dig a crater deep enough to penetrate the dust layer cannot comminute the substrate. If the meteor has enough energy to penetrate the dust layer it will comminute the substrate. In the transitional matrix, comminuted material in each substrate is tabulated so that the percent of each substrate comminuted is known. Therefore, as the dust layer gets deeper the amount of new material thrown up is decreased.

For a larger crater which penetrates the dust layer, the volume of new material comminuted and thrown out as ejecta is the fraction of the crater's volume that lies below the dust layer (see Figure 6.2). The matrix process yields an accurate method of accounting for all layers of the lunar surface, including its substrate. Erosion is automatically computed in the transitional matrix because the exposed particles are considered to be bombarded by the finer particles. In a way this computational method obscures the role of erosion, but it makes the computation possible in a reasonable length of time. Thus, to test the effect of erosion on the roughness it is necessary to change the shape of the infall data.

Our estimate of the depth of the dust or rubble layer are higher than other people's for several reasons. First, we used Hawkins' data which is of greater magnitude than that used by Orrok. If

we cut Hawkins'[1] infall rate arbitrarily by one-fifth, then we get a one meter depth which is closer to Orrok's 70 centimeter upper limit. In our program we considered that the debris from the very large meteors was uniformly distributed over the surface. In later stages of the moon's history virtually all new material going into the dust layer is from the large craters. Orrok[12] cut off size distribution of the larger meteors and computed equilibrium depth. Cutting off the large meteors has two effects. First, after a dust layer of a given thickness is reached, only the very large craters penetrate the dust layer and dig out new material to increase its thickness. Second, most of the debris from the larger craters falls near their rims and does not contribute to the general thickness of the dust layer. Thus, we strongly urge that the program be run with a cut off size for the larger meteors. It is believed that by using Orrok's[12] infall data, rather than Hawkins[1], we will have a thickness closer to Orrok's.

Another reason for differing with other estimates of the depth of the dust layer is the so-called comminution law. Those used by Gault, Orrok and others is, though widely used, empirical. For exponents less than one it implies that the surface area created is infinite. Thus, it is physically unsound. In this study a more sophisticated comminution law was derived specifically for cratering which fits the experimental data reasonably well and yields finite surface area. The size distribution or fineness of the dust layer is not appreciably changed with time. It started off at 37 percent below 40 microns and dropped to 31 percent after a billion years. This indicates a slight roughening of the dust layer which is due, undoubtedly, to the burying of the larger particles. When the particles are buried they are not eroded. It was assumed that the dust layer was not comminuted by the larger particles because no valid model for determining the amount of comminution that would take place was available. The effect of this assumption is rather small in the larger size ranges because there are so few large particles. The shape of the size distribution curve of the dust layer is independent of time and the intensity of infall. It may, however, be sensitive to the shape of the infall curve. Thus, if less cometary material relative to the stones and irons is assumed for the infall curve, then a rougher surface may accrue due to the slower erosional rate. It should be pointed out that the erosional rate of the particles is directly incorporated into the matrix method.

It was assumed that all material hit the lunar surface at 20 kilometers a second. A suggested change in the program would read in the velocity profile of the incoming particle as a function of particle size. This would enhance the programs flexibility and accuracy. The change is relatively small both in the work to be done and the increase in computational time.

The program was run with only one infall size distribution and for one initial boundary condition. However, with the present program it is possible to compute the size distribution or roughness near a larger crater when it is formed and how this roughness varies with time. The size distribution and depth of the dust layers in regions free from large craters can also be computed.

Since the shape and intensity of the infall curve is object time input to the program, it is easy to compute the size distribution and depth of the dust layer as a function of a wide variety of infall curves. It is recommended that this work be done because it would take relatively little time and much information would be gained.

The program, as now written, cannot be used by others or on other computers. Information is printed out "on line" and on tapes. This is controlled by the machine operator. Furthermore, the operator decides when the transitional matrix should be recomputed by reading the "on line" data. This was done because the authors did not know what to expect from the program, and object time control gave great flexibility. This may be seen in Figure 7.1. Since writing and running the program, criteria for decision has been arrived at which can readily be included in the program. The basic language of the program is Fortran II with freely adjoined pseuds SAP instruction as binary patches. It is suggested that the program be revised so that it may be compiled on the average scientific computer and run without operator intervention. In this way, the program could be used as a research tool by JPL and others.

LUNAR ROUGHNESS PROGRAM
SENSE SWITCH LOGIC

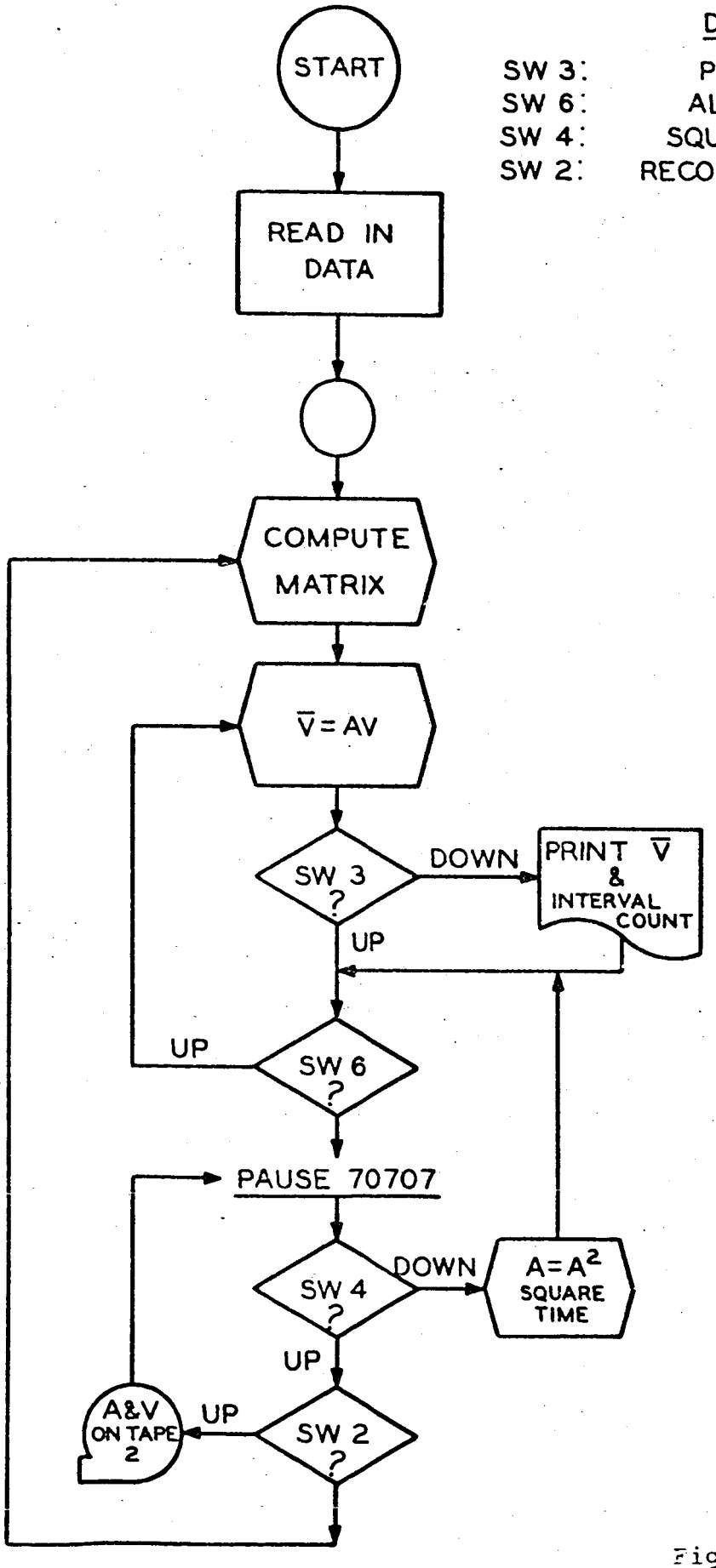

Figure 7.1

SECTION VIII

Recommendations for Further Work

The purpose of this study was to make an estimate of the roughness of the lunar surface based on the size distribution of material in the dust layer covering the moon. To finish the program in the allotted time certain problems were treated less thoroughly than was desired. Furthermore the roughness estimate did not consider roughness due to the pocking of the lunar surface with craters. These craters blasted out by the infall are softened or blurred with time. It is recommended that for future work (1) the program used to compute the roughness be strengthened technically and run for a variety of infalls, and (2) an estimate be made of the roughness due to craters.

More specifically, the program used to compute the roughness of the lunar surface contains certain mathematical models which we feel require further development for a more sophisticated model. Furthermore the program, while it may be run by us on our machine, cannot be run on other machines. Also, in utilizing the program we used only the latest published data of Hawkins[1] to make our roughness estimate.

I. We propose, therefore, the following additional work:

(a) This work would include studying the departure angles of the debris as they leave the crater, the velocity profile of the infalling meteorites, and such things as the partition of energy in the compressive wave between heat, vibration and kinetic energy of the fragments. It would also attempt to resolve the paradox of the scaling laws.

(b) The program be revised so that it could be compiled on any computer and run at any installation. The current program has considerable "on line" decision making requirements associated with it. By revision it could be used as a research tool by JPL and others.

(c) The program be run with a variety of infall data as well as variation in other input parameters. It is known that the shape of the infall data is significant in the creation and erosion of

blocks. Since we were able to run the program only once, the effect of various infall rates and shapes could not be tested.

II. Our study showed that there was little likelihood of roughness due to the presence of larger blocks. However, the roughness contribution due to craters was not studied. We propose that we use the same techniques to estimate the creation and disappearance of craters.

We propose, therefore, the following new work:

(a) Develop a method of estimating the birthrate of new craters.

(b) Develop a method of estimating the catastrophic disappearance of old craters.

(c) Develop a method of estimating crater rim erosion or deterioration.

(d) Develop a method of estimating crater fill-in rate.

(e) Using (a) through (d), develop a method to simulate the behavior of the lunar surface as a function of time and in-fall rate.

(f) From (e) develop a method for estimating the roughness of the moon.

(g) Make an estimate of the roughness of the surface due to craters.

We believe that we can use the matrix approach used in this study on the crater problem. The output would probably be in the form of the number of craters of a given size per square kilometer. For a given crater size the number of a given diameter to depth ratio would be computed. Thus, the output would be a two dimensional array with diameter on one side and diameter to depth ratios on the other side.

REFERENCES

1. Hawkins, G. S., Annual Review of Astronomy and Astrophysics, Goldberg, L., editor, Chapt., Meteors Annual Reviews, Inc., Palo Alto, preprint (1964).

2. Meloy, T. P., Ph.D. Thesis, Mass. Inst. of Tech., (1960).

3. Karpinski, J. M., and R. O. Tervo, Trans. A.I.M.E., Vol. 229, p. 126 (1964).

4. Gilvarry, J. J., Jnl. Applied Physics, Vol. 32, p. 391 (1961).

5. Charles, R. J., Trans. A.I.M.E., Vol. 208, p. 80 (1957).

6. Bergstrom, B. H., C. L. Sollenberger and W. Mitchell, Jr., Trans. A.I.M.E., Vol. 220, p. 367 (1961).

7. Hukki, R. T., Sc. D. Thesis, Mass. Inst. of Tech. (1943).

8. Gault, D. E., Shoemaker, E. M., and Moore, H. J., NASA TN D-1767 (1963).

9. Gault, D. E., Heitowit, E. D., Moore, H. J., NASA TM X-54,009 (1963).

10. Meloy, T. P., Bergstrom, B. H., Preprints of VIIth International Mineral Processing Congress, Gordon & Beach, N.Y. (1964).

11. Moore, H. J., Astrogeological Studies, Annual Progress Report, Part D, page 34, (1964).

12. Orook, G. T., Meteoric Infall and Lunar Surface Roughness, Bellcomm, Inc., Washington, D. C., (1964).

13. Whipple, F., Private communication.

APPENDIX A

LUNAR CRATER MODEL

$E_p = 10^{12}$ ergs

CRATER EJECTA SIZE DISTRIBUTIONS

SCREEN SIZE	RING NO. 1 RAD. = 7.6656E 00	RING NO. 2 RAD. = 1.5331E 01	RING NO. 3 RAD. = 2.2997E 01	RING NO. 4 RAD. = 3.0662E 01	RING NO. 5 RAD. = 3.8328E 01
10.0000E-08	0.	0.	0.	0.	0.
1.5849E-07	0.	0.	0.	0.	0.
2.5119E-07	0.	0.	0.	0.	0.
3.9811E-07	0.	0.	0.	0.	0.
6.3096E-07	0.	0.	0.	0.	0.
10.0000E-07	0.	0.	0.	0.	0.
1.5849E-06	0.	0.	0.	0.	0.
2.5119E-06	0.	0.	0.	0.	0.
3.9811E-06	0.	0.	0.	0.	0.
6.3096E-06	0.	0.	0.	0.	0.
10.0000E-06	0.	0.	0.	0.	0.
1.5849E-05	0.	0.	0.	0.	0.
2.5119E-05	0.	0.	0.	0.	0.
3.9811E-05	0.	0.	0.	0.	0.
6.3096E-05	0.	0.	0.	0.	0.
10.0000E-05	0.	0.	0.	0.	0.
1.5849E-04	0.	0.	0.	0.	0.
2.5119E-04	0.	0.	0.	0.	0.
3.9811E-04	0.	0.	0.	0.	0.
6.3096E-04	0.	0.	0.	0.	0.
10.0000E-04	0.	0.	0.	0.	0.
1.5849E-03	0.	0.	0.	0.	0.
2.5119E-03	0.	0.	0.	0.	0.
3.9811E-03	0.	0.	0.	0.	0.
6.3096E-03	0.	0.	0.	0.	0.
10.0000E-03	0.	0.	0.	0.	0.
1.5849E-02	0.	0.	0.	0.	0.
2.5119E-02	0.	0.	0.	0.	0.
3.9811E-02	0.	0.	0.	0.	0.
6.3096E-02	0.	0.	0.	0.	0.
10.0000E-02	0.	0.	0.	0.	0.
1.5849E-01	0.	0.	0.	0.	0.
2.5119E-01	0.	0.	0.	0.	0.
3.9811E-01	0.	0.	0.	0.	0.
6.3096E-01	0.	0.	0.	0.	0.
10.0000E-01	0.	0.	0.	0.	0.
1.5849E 00	0.	0.	0.	0.	0.
2.5119E 00	0.	0.	0.	0.	0.
3.9811E 00	0.	0.	0.	0.	0.
6.3096E 00	0.	0.	0.	0.	0.
10.0000E 00	0.	0.	0.	0.	0.
1.5849E 01	0.	0.	0.	0.	0.
2.5119E 01	0.	0.	0.	0.	0.
3.9811E 01	0.	0.	0.	0.	0.
6.3096E 01	0.	0.	0.	0.	0.
10.0000E 01	0.	0.	0.	0.	0.
1.5849E 02	0.	0.	0.	0.	0.
2.5119E 02	0.	0.	0.	0.	0.
3.9811E 02	0.	0.	0.	0.	0.
6.3096E 02	0.	0.	0.	0.	0.
EJECTA VOLUME	0.	0.	0.	0.	0.
EJECTA DEPTH	0.	0.	0.	0.	0.

$E_p = 10^{12}$ ergs

LUNAR CRATER MODEL

CRATER EJECTA SIZE DISTRIBUTIONS

SCREEN SIZE	RING NO. 6 RAD. = 4.5993E 01	RING NO. 7 RAD. = 5.3659E 01	RING NO. 8 RAD. = 6.1325E 01	RING NO. 9 RAD. = 6.8990E 01	RING NO. 10 RAD. = 7.6656E 01
10.0000E-08	0.	0.	0.	0.	0.
1.5849E-07	0.	0.	0.	0.	0.
2.5119E-07	0.	0.	0.	0.	0.
3.9811E-07	0.	0.	0.	0.	0.
6.3096E-07	0.	0.	0.	0.	0.
10.0000E-07	0.	0.	0.	0.	0.
1.5849E-06	0.	0.	0.	0.	0.
2.5119E-06	0.	0.	0.	0.	0.
3.9811E-06	0.	0.	0.	0.	0.
6.3096E-06	0.	0.	0.	0.	0.
10.0000E-06	0.	0.	0.	0.	0.
1.5849E-05	0.	0.	0.	0.	0.
2.5119E-05	0.	0.	0.	0.	0.
3.9811E-05	0.	0.	0.	0.	0.
6.3096E-05	0.	0.	0.	0.	0.
10.0000E-05	0.	0.	0.	0.	0.
1.5849E-04	0.	0.	0.	0.	0.
2.5119E-04	0.	0.	0.	0.	0.
3.9811E-04	0.	0.	0.	0.	0.
6.3096E-04	0.	0.	0.	0.	0.
10.0000E-04	0.	0.	0.	0.	0.
1.5849E-03	0.	0.	0.	0.	0.
2.5119E-03	0.	0.	0.	0.	0.
3.9811E-03	0.	0.	0.	0.	0.
6.3096E-03	0.	0.	0.	0.	0.
10.0000E-03	0.	0.	0.	0.	0.
1.5849E-02	0.	0.	0.	0.	0.
2.5119E-02	0.	0.	0.	0.	0.
3.9811E-02	0.	0.	0.	0.	0.
6.3096E-02	0.	0.	0.	0.	0.
10.0000E-02	0.	0.	0.	0.	0.
1.5849E-01	0.	0.	0.	0.	0.
2.5119E-01	0.	0.	0.	0.	0.
3.9811E-01	0.	0.	0.	0.	0.
6.3096E-01	0.	0.	0.	0.	0.
10.0000E-01	0.	0.	0.	0.	0.
1.5849E 00	0.	0.	0.	0.	0.
2.5119E 00	0.	0.	0.	0.	0.
3.9811E 00	0.	0.	0.	0.	0.
6.3096E 00	0.	0.	0.	0.	0.
10.0000E 00	0.	0.	0.	0.	0.
1.5849E 01	0.	0.	0.	0.	0.
2.5119E 01	0.	0.	0.	0.	0.
3.9811E 01	0.	0.	0.	0.	0.
6.3096E 01	0.	0.	0.	0.	0.
10.0000E 01	0.	0.	0.	0.	0.
1.5849E 02	0.	0.	0.	0.	0.
2.5119E 02	0.	0.	0.	0.	0.
3.9811E 02	0.	0.	0.	0.	0.
6.3096E 02	0.	0.	0.	0.	0.
EJECTA VOLUME	0.	0.	0.	0.	0.
EJECTA DEPTH	0.	0.	0.	0.	0.

$E_p = 10^{12}$ ergs

LUNAR CRATER MODEL

CRATER EJECTA SIZE DISTRIBUTIONS

SCREEN SIZE	RING NO. 11 RAD. = 9.1987E 01	RING NO. 12 RAD. = 1.0732E 02	RING NO. 13 RAD. = 1.2265E 02	RING NO. 14 RAD. = 1.3798E 02	RING NO. 15 RAD. = 1.5331E 02
10.0000E-08	0.	0.	0.	0.	0.
1.5849E-07	0.	0.	0.	0.	0.
2.5119E-07	0.	0.	0.	0.	0.
3.9811E-07	0.	0.	0.	0.	0.
6.3096E-07	0.	0.	0.	0.	0.
10.0000E-07	0.	0.	0.	0.	0.
1.5849E-06	0.	0.	0.	0.	0.
2.5119E-06	0.	0.	0.	0.	0.
3.9811E-06	0.	0.	0.	0.	0.
6.3096E-06	0.	0.	0.	0.	0.
10.0000E-06	0.	0.	0.	0.	0.
1.5849E-05	0.	0.	0.	0.	0.
2.5119E-05	0.	0.	0.	0.	0.
3.9811E-05	0.	0.	0.	0.	0.
6.3096E-05	0.	0.	0.	0.	0.
10.0000E-05	0.	0.	0.	0.	0.
1.5849E-04	0.	0.	0.	0.	0.
2.5119E-04	0.	0.	0.	0.	0.
3.9811E-04	0.	0.	0.	0.	0.
6.3096E-04	0.	0.	0.	0.	0.
10.0000E-04	0.	0.	0.	0.	0.
1.5849E-03	0.	0.	0.	0.	0.
2.5119E-03	0.	0.	0.	0.	0.
3.9811E-03	0.	0.	0.	0.	0.
6.3096E-03	0.	0.	0.	0.	0.
10.0000E-03	0.	0.	0.	0.	0.
1.5849E-02	0.	0.	0.	0.	0.
2.5119E-02	0.	0.	0.	0.	0.
3.9811E-02	0.	0.	0.	0.	0.
6.3096E-02	0.	0.	0.	0.	0.
10.0000E-02	0.	0.	0.	0.	0.
1.5849E-01	0.	0.	0.	0.	0.
2.5119E-01	0.	0.	0.	0.	0.
3.9811E-01	0.	0.	0.	0.	0.
6.3096E-01	0.	0.	0.	0.	0.
10.0000E-01	0.	0.	0.	0.	0.
1.5849E 00	0.	0.	0.	0.	0.
2.5119E 00	0.	0.	0.	0.	0.
3.9811E 00	0.	0.	0.	0.	0.
6.3096E 00	0.	0.	0.	3.7899E-06	0.
10.0000E 00	0.	0.	0.	0.	0.
1.5849E 01	0.	0.	0.	0.	0.
2.5119E 01	0.	0.	0.	0.	0.
3.9811E 01	0.	0.	0.	0.	0.
6.3096E 01	0.	0.	0.	0.	0.
10.0000E 01	0.	0.	0.	0.	0.
1.5849E 02	0.	0.	0.	0.	0.
2.5119E 02	0.	0.	0.	0.	0.
3.9811E 02	0.	0.	0.	0.	0.
6.3096E 02	0.	0.	0.	0.	0.
EJECTA VOLUME	0.	0.	0.	3.7899E-06	0.
EJECTA DEPTH	0.	0.	0.	6.0383E-10	0.

LUNAR CRATER MODEL

$E_p = 10^{12}$ ergs

CRATER EJECTA SIZE DISTRIBUTIONS

SCREEN SIZE	RING NO. 16 RAD. = 1.6864E 02	RING NO. 17 RAD. = 1.8397E 02	RING NO. 18 RAD. = 1.9931E 02	RING NO. 19 RAD. = 2.1464E 02	RING NO. 20 RAD. = 2.2997E 02
10.0000E-08	0.	0.	0.	0.	0.
1.5849E-07	0.	0.	0.	0.	0.
2.5119E-07	0.	0.	0.	0.	0.
3.9811E-07	0.	0.	0.	0.	0.
6.3096E-07	0.	0.	0.	0.	0.
10.0000E-07	0.	0.	0.	0.	0.
1.5849E-06	0.	0.	0.	0.	0.
2.5119E-06	0.	0.	0.	0.	0.
3.9811E-06	0.	0.	0.	0.	0.
6.3096E-06	0.	0.	0.	0.	0.
10.0000E-06	0.	0.	0.	0.	0.
1.5849E-05	0.	0.	0.	0.	0.
2.5119E-05	0.	0.	0.	0.	0.
3.9811E-05	0.	0.	0.	0.	0.
6.3096E-05	0.	0.	0.	0.	0.
10.0000E-05	0.	0.	0.	0.	0.
1.5849E-04	0.	0.	0.	0.	0.
2.5119E-04	0.	0.	0.	0.	0.
3.9811E-04	0.	0.	0.	0.	0.
6.3096E-04	0.	0.	0.	0.	0.
10.0000E-04	0.	0.	0.	0.	0.
1.5849E-03	0.	0.	0.	0.	0.
2.5119E-03	0.	0.	0.	0.	0.
3.9811E-03	0.	0.	0.	0.	0.
6.3096E-03	0.	0.	0.	0.	0.
10.0000E-03	0.	0.	0.	0.	0.
1.5849E-02	0.	0.	0.	0.	0.
2.5119E-02	0.	0.	0.	0.	0.
3.9811E-02	0.	0.	0.	0.	0.
6.3096E-02	0.	0.	0.	0.	0.
10.0000E-02	0.	0.	0.	0.	0.
1.5849E-01	0.	0.	0.	0.	0.
2.5119E-01	0.	0.	0.	0.	0.
3.9811E-01	0.	0.	0.	0.	0.
6.3096E-01	0.	0.	0.	0.	0.
10.0000E-01	0.	0.	0.	0.	0.
1.5849E 00	0.	0.	0.	0.	0.
2.5119E 00	0.	0.	0.	0.	0.
3.9811E 00	0.	0.	1.6950E-03	5.3069E-03	0.
6.3096E 00	0.	0.	0.	0.	0.
10.0000E 00	0.	0.	0.	0.	0.
1.5849E 01	0.	0.	0.	0.	0.
2.5119E 01	0.	0.	0.	0.	0.
3.9811E 01	0.	0.	0.	0.	0.
6.3096E 01	0.	0.	0.	0.	0.
10.0000E 01	0.	0.	0.	0.	0.
1.5849E 02	0.	0.	0.	0.	0.
2.5119E 02	0.	0.	0.	0.	0.
3.9811E 02	0.	0.	0.	0.	0.
6.3096E 02	0.	0.	0.	0.	0.
EJECTA VOLUME	0.	0.	1.6950E-03	5.3069E-03	0.
EJECTA DEPTH	0.	0.	1.8364E-07	5.3236E-07	0.

$E_p = 10^{12}$ ergs

LUNAR CRATER MODEL

CRATER EJECTA SIZE DISTRIBUTIONS

SCREEN SIZE	RING NO. 21 RAD. = 3.0662E 02	RING NO. 22 RAD. = 3.3328E 02	RING NO. 23 RAD. = 4.5993E 02	RING NO. 24 RAD. = 5.3659E 02	RING NO. 25 RAD. = 6.1325E 02
10.0000E-08	0.	0.	0.	0.	0.
1.5849E-07	0.	0.	0.	0.	0.
2.5119E-07	0.	0.	0.	0.	0.
3.9811E-07	0.	0.	0.	0.	0.
6.3096E-07	0.	0.	0.	0.	0.
10.0000E-07	0.	0.	0.	0.	0.
1.5849E-06	0.	0.	0.	0.	0.
2.5119E-06	0.	0.	0.	0.	0.
3.9811E-06	0.	0.	0.	0.	0.
6.3096E-06	0.	0.	0.	0.	0.
10.0000E-06	0.	0.	0.	0.	0.
1.5849E-05	0.	0.	0.	0.	0.
2.5119E-05	0.	0.	0.	0.	0.
3.9811E-05	0.	0.	0.	0.	0.
6.3096E-05	0.	0.	0.	0.	0.
10.0000E-05	0.	0.	0.	0.	0.
1.5849E-04	0.	0.	0.	0.	0.
2.5119E-04	0.	0.	0.	0.	0.
3.9811E-04	0.	0.	0.	0.	0.
6.3096E-04	0.	0.	0.	0.	0.
10.0000E-04	0.	0.	0.	0.	0.
1.5849E-03	0.	0.	0.	0.	0.
2.5119E-03	0.	0.	0.	0.	0.
3.9811E-03	0.	0.	0.	0.	0.
6.3096E-03	0.	0.	0.	0.	0.
10.0000E-03	0.	0.	0.	0.	0.
1.5849E-02	0.	0.	0.	0.	0.
2.5119E-02	0.	0.	0.	0.	0.
3.9811E-02	0.	0.	0.	0.	0.
6.3096E-02	0.	0.	0.	0.	0.
10.0000E-02	0.	0.	0.	0.	0.
1.5849E-01	0.	0.	0.	0.	0.
2.5119E-01	0.	0.	0.	0.	2.1700E-06
3.9811E-01	0.	0.	0.	0.	0.
6.3096E-01	0.	0.	0.	0.	0.
10.0000E-01	0.	0.	0.	4.4374E 00	0.
1.5849E 00	0.	0.	0.	0.	0.
2.5119E 00	0.	4.1436E-01	0.	0.	0.
3.9811E 00	0.	0.	0.	0.	0.
6.3096E 00	0.	0.	0.	0.	0.
10.0000E 00	0.	0.	0.	0.	0.
1.5849E 01	0.	0.	0.	0.	0.
2.5119E 01	0.	0.	0.	0.	0.
3.9811E 01	0.	0.	0.	0.	0.
6.3096E 01	0.	0.	0.	0.	0.
10.0000E 01	0.	0.	0.	0.	0.
1.5849E 02	0.	0.	0.	0.	0.
2.5119E 02	0.	0.	0.	0.	0.
3.9811E 02	0.	0.	0.	0.	0.
6.3096E 02	0.	0.	0.	0.	0.
EJECTA VOLUME	0.	4.1436E-01	0.	4.4374E 00	2.1700E-06
EJECTA DEPTH	0.	4.2480E-06	0.	4.6481E-05	1.9527E-11

LUNAR CRATER MODEL

$E_p = 10^{12}$ ergs

CRATER EJECTA SIZE DISTRIBUTIONS

SCREEN SIZE	RING NO. 26 RAD. = 6.8990E 02	RING NO. 27 RAD. = 7.6656E 02	RING NO. 28 RAD. = 8.4321E 02	RING NO. 29 RAD. = 9.1987E 02	RING NO. 30 RAD. = 9.9653E 02
10.0000E-08	0.	0.	0.	0.	0.
1.5849E-07	0.	0.	0.	0.	0.
2.5119E-07	0.	0.	0.	0.	0.
3.9811E-07	0.	0.	0.	0.	0.
6.3096E-07	0.	0.	0.	0.	0.
10.0000E-07	0.	0.	0.	0.	0.
1.5849E-06	0.	0.	0.	0.	0.
2.5119E-06	0.	0.	0.	0.	0.
3.9811E-06	0.	0.	0.	0.	0.
6.3096E-06	0.	0.	0.	0.	0.
10.0000E-06	0.	0.	0.	0.	0.
1.5849E-05	0.	0.	0.	0.	0.
2.5119E-05	0.	0.	0.	0.	0.
3.9811E-05	0.	0.	0.	0.	0.
6.3096E-05	0.	0.	0.	0.	0.
10.0000E-05	0.	0.	0.	0.	0.
1.5849E-04	0.	0.	0.	0.	0.
2.5119E-04	0.	0.	0.	0.	0.
3.9811E-04	0.	0.	0.	0.	0.
6.3096E-04	0.	0.	0.	0.	0.
10.0000E-04	0.	0.	0.	0.	0.
1.5849E-03	0.	0.	0.	0.	0.
2.5119E-03	0.	0.	0.	0.	0.
3.9811E-03	0.	0.	0.	0.	0.
6.3096E-03	0.	0.	0.	0.	0.
10.0000E-03	0.	0.	0.	0.	0.
1.5849E-02	0.	0.	0.	0.	0.
2.5119E-02	0.	0.	0.	0.	0.
3.9811E-02	0.	0.	0.	0.	0.
6.3096E-02	0.	0.	0.	0.	0.
10.0000E-02	0.	0.	0.	0.	0.
1.5849E-01	0.	0.	0.	0.	0.
2.5119E-01	0.	0.	0.	4.7191E-04	0.
3.9811E-01	0.	4.3379E-06	0.	4.9149E-06	0.
6.3096E-01	0.	0.	0.	0.	0.
10.0000E-01	0.	0.	1.6741E 01	0.	0.
1.5849E 00	0.	0.	0.	0.	0.
2.5119E 00	0.	0.	0.	0.	0.
3.9811E 00	0.	0.	0.	0.	0.
6.3096E 00	0.	0.	0.	0.	0.
10.0000E 00	0.	0.	0.	0.	0.
1.5849E 01	0.	0.	0.	0.	0.
2.5119E 01	0.	0.	0.	0.	0.
3.9811E 01	0.	0.	0.	0.	0.
6.3096E 01	0.	0.	0.	0.	0.
10.0000E 01	0.	0.	0.	0.	0.
1.5849E 02	0.	0.	0.	0.	0.
2.5119E 02	0.	0.	0.	0.	0.
3.9811E 02	0.	0.	0.	0.	0.
6.3096E 02	0.	0.	0.	0.	0.
EJECTA VOLUME	0.	4.3379E-06	1.6741E 01	4.7683E-04	0.
EJECTA DEPTH	0.	2.4735E-11	8.6367E-05	2.2461E-09	0.

$E_p = 10^{12}$ ergs

LUNAR CRATER MODEL

CRATER EJECTA SIZE DISTRIBUTIONS

SCREEN SIZE	RING NO. 31 RAD. = 1.0000E 05	RING NO. 32 RAD. = 1.0000E 06	RING NO. 33 RAD. = 1.0000E 07	RING NO. 34 RAD. = 1.0000E 08	RING NO. 35 RAD. = 5.4664E 08
10.0000E-08	0.	0.	0.	0.	3.0452E-02
1.5849E-07	0.	0.	0.	0.	1.7509E-02
2.5119E-07	0.	0.	0.	0.	2.7317E-02
3.9811E-07	0.	0.	0.	0.	4.2267E-02
6.3096E-07	0.	0.	0.	2.3808E-03	6.2254E-02
10.0000E-07	0.	0.	0.	1.0377E-02	8.6942E-02
1.5849E-06	0.	0.	0.	2.7996E-02	1.1558E-01
2.5119E-06	0.	0.	0.	9.2340E-02	1.1575E-01
3.9811E-06	0.	0.	0.	2.2698E-01	6.7257E-02
6.3096E-06	0.	0.	6.1169E-03	3.8994E-01	1.7353E-02
10.0000E-06	0.	0.	4.0837E-02	5.3815E-01	0.
1.5849E-05	0.	0.	1.1765E-01	6.8521E-01	0.
2.5119E-05	0.	0.	3.5956E-01	7.4325E-01	0.
3.9811E-05	0.	0.	1.1576E 00	3.4753E-01	0.
6.3096E-05	0.	4.5198E-04	2.0212E 00	2.2662E-02	0.
10.0000E-05	0.	8.8802E-02	2.6458E 00	0.	0.
1.5849E-04	0.	3.6170E-01	3.2558E 00	0.	0.
2.5119E-04	0.	8.3783E-01	3.9379E 00	0.	0.
3.9811E-04	0.	3.0966E 00	3.1406E 00	0.	0.
6.3096E-04	0.	7.7202E 00	2.2623E-01	0.	0.
10.0000E-04	3.6792E-02	9.9771E 00	0.	0.	0.
1.5849E-03	6.6266E-01	1.2029E 01	0.	0.	0.
2.5119E-03	1.5533E 00	1.4244E 01	0.	0.	0.
3.9811E-03	3.7928E 00	1.4940E 01	0.	0.	0.
6.3096E-03	1.9418E 01	2.2232E 00	0.	0.	0.
10.0000E-03	2.5695E 01	0.	0.	0.	0.
1.5849E-02	3.0936E 01	0.	0.	0.	0.
2.5119E-02	3.4648E 01	0.	0.	0.	0.
3.9811E-02	3.4102E 01	0.	0.	0.	0.
6.3096E-02	3.0710E 01	0.	0.	0.	0.
10.0000E-02	3.0236E 01	0.	0.	0.	0.
1.5849E-01	3.5514E 01	0.	0.	0.	0.
2.5119E-01	4.1769E 01	0.	0.	0.	0.
3.9811E-01	4.2161E 01	0.	0.	0.	0.
6.3096E-01	3.2718E 01	0.	0.	0.	0.
10.0000E-01	0.	0.	0.	0.	0.
1.5849E 00	0.	0.	0.	0.	0.
2.5119E 00	0.	0.	0.	0.	0.
3.9811E 00	0.	0.	0.	0.	0.
6.3096E 00	0.	0.	0.	0.	0.
10.0000E 00	0.	0.	0.	0.	0.
1.5849E 01	0.	0.	0.	0.	0.
2.5119E 01	0.	0.	0.	0.	0.
3.9811E 01	0.	0.	0.	0.	0.
6.3096E 01	0.	0.	0.	0.	0.
10.0000E 01	0.	0.	0.	0.	0.
1.5849E 02	0.	0.	0.	0.	0.
2.5119E 02	0.	0.	0.	0.	0.
3.9811E 02	0.	0.	0.	0.	0.
6.3096E 02	0.	0.	0.	0.	0.
EJECTA VOLUME	3.6395E 02	6.5519E 01	1.6909E 01	3.0868E 00	5.8268E-01
EJECTA DEPTH	2.3172E-08	4.2132E-11	1.0877E-13	2.0411E-16	2.9873E-18

$E_p = 10^{14}$ ergs

LUNAR CRATER MODEL

CRATER EJECTA SIZE DISTRIBUTIONS

SCREEN SIZE	RING NO. 1 RAD. = 3.5580E 01	RING NO. 2 RAD. = 7.1161E 01	RING NO. 3 RAD. = 1.0674E 02	RING NO. 4 RAD. = 1.4232E 02	RING NO. 5 RAD. = 1.7790E 02
10.0000E-08	0.	0.	0.	0.	0.
1.5849E-07	0.	0.	0.	0.	0.
2.5119E-07	0.	0.	0.	0.	0.
3.9811E-07	0.	0.	0.	0.	0.
6.3096E-07	0.	0.	0.	0.	0.
10.0000E-07	0.	0.	0.	0.	0.
1.5849E-06	0.	0.	0.	0.	0.
2.5119E-06	0.	0.	0.	0.	0.
3.9811E-06	0.	0.	0.	0.	0.
6.3096E-06	0.	0.	0.	0.	0.
10.0000E-06	0.	0.	0.	0.	0.
1.5849E-05	0.	0.	0.	0.	0.
2.5119E-05	0.	0.	0.	0.	0.
3.9811E-05	0.	0.	0.	0.	0.
6.3096E-05	0.	0.	0.	0.	0.
10.0000E-05	0.	0.	0.	0.	0.
1.5849E-04	0.	0.	0.	0.	0.
2.5119E-04	0.	0.	0.	0.	0.
3.9811E-04	0.	0.	0.	0.	0.
6.3096E-04	0.	0.	0.	0.	0.
10.0000E-04	0.	0.	0.	0.	0.
1.5849E-03	0.	0.	0.	0.	0.
2.5119E-03	0.	0.	0.	0.	0.
3.9811E-03	0.	0.	0.	0.	0.
6.3096E-03	0.	0.	0.	0.	0.
10.0000E-03	0.	0.	0.	0.	0.
1.5849E-02	0.	0.	0.	0.	0.
2.5119E-02	0.	0.	0.	0.	0.
3.9811E-02	0.	0.	0.	0.	0.
6.3096E-02	0.	0.	0.	0.	0.
10.0000E-02	0.	0.	0.	0.	0.
1.5849E-01	0.	0.	0.	0.	0.
2.5119E-01	0.	0.	0.	0.	0.
3.9811E-01	0.	0.	0.	0.	0.
6.3096E-01	0.	0.	0.	0.	0.
10.0000E-01	0.	0.	0.	0.	0.
1.5849E 00	0.	0.	0.	0.	0.
2.5119E 00	0.	0.	0.	0.	0.
3.9811E 00	0.	0.	0.	0.	0.
6.3096E 00	0.	0.	0.	0.	7.3280E 01
10.0000E 00	0.	0.	0.	2.1245E 00	0.
1.5849E 01	0.	0.	5.6849E-03	0.	0.
2.5119E 01	0.	0.	0.	0.	0.
3.9811E 01	0.	0.	0.	0.	0.
6.3096E 01	0.	0.	0.	0.	0.
10.0000E 01	0.	0.	0.	0.	0.
1.5849E 02	0.	0.	0.	0.	0.
2.5119E 02	0.	0.	0.	0.	0.
3.9811E 02	0.	0.	0.	0.	0.
6.3096E 02	0.	0.	0.	0.	0.
EJECTA VOLUME	0.	0.	5.6849E-03	2.1245E 00	7.3280E 01
EJECTA DEPTH	0.	0.	5.7176E-07	1.5262E-04	4.0945E-03

LUNAR CRATER MODEL

$E_p = 10^{14}$ ergs

CRATER EJECTA SIZE DISTRIBUTIONS

SCREEN SIZE	RING NO. 6 RAD. = 2.1348E 02	RING NO. 7 RAD. = 2.4906E 02	RING NO. 8 RAD. = 2.8464E 02	RING NO. 9 RAD. = 3.2022E 02	RING NO. 10 RAD. = 3.5580E 02
10.0000E-08	0.	0.	0.	0.	0.
1.5849E-07	0.	0.	0.	0.	0.
2.5119E-07	0.	0.	0.	0.	0.
3.9811E-07	0.	0.	0.	0.	0.
6.3096E-07	0.	0.	0.	0.	0.
10.0000E-07	0.	0.	0.	0.	0.
1.5849E-06	0.	0.	0.	0.	0.
2.5119E-06	0.	0.	0.	0.	0.
3.9811E-06	0.	0.	0.	0.	0.
6.3096E-06	0.	0.	0.	0.	0.
10.0000E-06	0.	0.	0.	0.	0.
1.5849E-05	0.	0.	0.	0.	0.
2.5119E-05	0.	0.	0.	0.	0.
3.9811E-05	0.	0.	0.	0.	0.
6.3096E-05	0.	0.	0.	0.	0.
10.0000E-05	0.	0.	0.	0.	0.
1.5849E-04	0.	0.	0.	0.	0.
2.5119E-04	0.	0.	0.	0.	0.
3.9811E-04	0.	0.	0.	0.	0.
6.3096E-04	0.	0.	0.	0.	0.
10.0000E-04	0.	0.	0.	0.	0.
1.5849E-03	0.	0.	0.	0.	0.
2.5119E-03	0.	0.	0.	0.	0.
3.9811E-03	0.	0.	0.	0.	0.
6.3096E-03	0.	0.	0.	0.	0.
10.0000E-03	0.	0.	0.	0.	0.
1.5849E-02	0.	0.	0.	0.	0.
2.5119E-02	0.	0.	0.	0.	0.
3.9811E-02	0.	0.	0.	0.	0.
6.3096E-02	0.	0.	0.	0.	0.
10.0000E-02	0.	0.	0.	0.	0.
1.5849E-01	0.	0.	0.	0.	0.
2.5119E-01	0.	0.	0.	0.	0.
3.9811E-01	0.	0.	0.	0.	0.
6.3096E-01	0.	0.	0.	0.	0.
10.0000E-01	0.	0.	0.	0.	0.
1.5849E 00	0.	0.	0.	0.	0.
2.5119E 00	0.	0.	0.	0.	0.
3.9811E 00	0.	0.	5.9662E 02	0.	0.
6.3096E 00	0.	0.	0.	0.	0.
10.0000E 00	0.	0.	0.	0.	0.
1.5849E 01	0.	0.	0.	0.	0.
2.5119E 01	0.	0.	0.	0.	0.
3.9811E 01	0.	0.	0.	0.	0.
6.3096E 01	0.	0.	0.	0.	0.
10.0000E 01	0.	0.	0.	0.	0.
1.5849E 02	0.	0.	0.	0.	0.
2.5119E 02	0.	0.	0.	0.	0.
3.9811E 02	0.	0.	0.	0.	0.
6.3096E 02	0.	0.	0.	0.	0.
EJECTA VOLUME	0.	0.	5.9662E 02	0.	0.
EJECTA DEPTH	0.	0.	2.0002E-02	0.	0.

$E_p = 10^{14}$ ergs

LUNAR CRATER MODEL

CRATER EJECTA SIZE DISTRIBUTIONS

SCREEN SIZE	RING NO. 11 RAD. = 4.2697E 02	RING NO. 12 RAD. = 4.9813E 02	RING NO. 13 RAD. = 5.6929E 02	RING NO. 14 RAD. = 6.4045E 02	RING NO. 15 RAD. = 7.1161E 02
10.0000E-08	0.	0.	0.	0.	0.
1.5849E-07	0.	0.	0.	0.	0.
2.5119E-07	0.	0.	0.	0.	0.
3.9811E-07	0.	0.	0.	0.	0.
6.3096E-07	0.	0.	0.	0.	0.
10.0000E-07	0.	0.	0.	0.	0.
1.5849E-06	0.	0.	0.	0.	0.
2.5119E-06	0.	0.	0.	0.	0.
3.9811E-06	0.	0.	0.	0.	0.
6.3096E-06	0.	0.	0.	0.	0.
10.0000E-06	0.	0.	0.	0.	0.
1.5849E-05	0.	0.	0.	0.	0.
2.5119E-05	0.	0.	0.	0.	0.
3.9811E-05	0.	0.	0.	0.	0.
6.3096E-05	0.	0.	0.	0.	0.
10.0000E-05	0.	0.	0.	0.	0.
1.5849E-04	0.	0.	0.	0.	0.
2.5119E-04	0.	0.	0.	0.	0.
3.9811E-04	0.	0.	0.	0.	0.
6.3096E-04	0.	0.	0.	0.	0.
10.0000E-04	0.	0.	0.	0.	0.
1.5849E-03	0.	0.	0.	0.	0.
2.5119E-03	0.	0.	0.	0.	0.
3.9811E-03	0.	0.	0.	0.	0.
6.3096E-03	0.	0.	0.	0.	0.
10.0000E-03	0.	0.	0.	0.	0.
1.5849E-02	0.	0.	0.	0.	0.
2.5119E-02	0.	0.	0.	0.	0.
3.9811E-02	0.	0.	0.	0.	0.
6.3096E-02	0.	0.	0.	0.	0.
10.0000E-02	0.	0.	0.	0.	0.
1.5849E-01	0.	0.	0.	0.	0.
2.5119E-01	0.	0.	0.	0.	0.
3.9811E-01	0.	0.	0.	0.	0.
6.3096E-01	0.	2.6702E-03	0.	5.3356E-03	0.
10.0000E-01	0.	0.	0.	0.	0.
1.5849E 00	0.	0.	0.	3.4725E 03	0.
2.5119E 00	1.9363E 03	0.	0.	0.	0.
3.9811E 00	0.	0.	0.	0.	0.
6.3096E 00	0.	0.	0.	0.	0.
10.0000E 00	0.	0.	0.	0.	0.
1.5849E 01	0.	0.	0.	0.	0.
2.5119E 01	0.	0.	0.	0.	0.
3.9811E 01	0.	0.	0.	0.	0.
6.3096E 01	0.	0.	0.	0.	0.
10.0000E 01	0.	0.	0.	0.	0.
1.5849E 02	0.	0.	0.	0.	0.
2.5119E 02	0.	0.	0.	0.	0.
3.9811E 02	0.	0.	0.	0.	0.
6.3096E 02	0.	0.	0.	0.	0.
EJECTA VOLUME	1.9363E 03	2.6702E-03	0.	3.4725E 03	0.
EJECTA DEPTH	2.2130E-02	2.5822E-08	0.	2.5680E-02	0.

$E_p = 10^{14}$ ergs

LUNAR CRATER MODEL

CRATER EJECTA SIZE DISTRIBUTIONS

SCREEN SIZE	RING NO. 16 RAD. = 7.8277E 02	RING NO. 17 RAD. = 8.5393E 02	RING NO. 18 RAD. = 9.2509E 02	RING NO. 19 RAD. = 9.9625E 02	RING NO. 20 RAD. = 1.0674E 03
10.0000E-08	0.	0.	0.	0.	0.
1.5849E-07	0.	0.	0.	0.	0.
2.5119E-07	0.	0.	0.	0.	0.
3.9811E-07	0.	0.	0.	0.	0.
6.3096E-07	0.	0.	0.	0.	0.
10.0000E-07	0.	0.	0.	0.	0.
1.5849E-06	0.	0.	0.	0.	0.
2.5119E-06	0.	0.	0.	0.	0.
3.9811E-06	0.	0.	0.	0.	0.
6.3096E-06	0.	0.	0.	0.	0.
10.0000E-06	0.	0.	0.	0.	0.
1.5849E-05	0.	0.	0.	0.	0.
2.5119E-05	0.	0.	0.	0.	0.
3.9811E-05	0.	0.	0.	0.	0.
6.3096E-05	0.	0.	0.	0.	0.
10.0000E-05	0.	0.	0.	0.	0.
1.5849E-04	0.	0.	0.	0.	0.
2.5119E-04	0.	0.	0.	0.	0.
3.9811E-04	0.	0.	0.	0.	0.
6.3096E-04	0.	0.	0.	0.	0.
10.0000E-04	0.	0.	0.	0.	0.
1.5849E-03	0.	0.	0.	0.	0.
2.5119E-03	0.	0.	0.	0.	0.
3.9811E-03	0.	0.	0.	0.	0.
6.3096E-03	0.	0.	0.	0.	0.
10.0000E-03	0.	0.	0.	0.	0.
1.5849E-02	0.	0.	0.	0.	0.
2.5119E-02	0.	0.	0.	0.	0.
3.9811E-02	0.	0.	0.	0.	0.
6.3096E-02	0.	0.	0.	0.	0.
10.0000E-02	0.	0.	0.	0.	0.
1.5849E-01	0.	0.	0.	0.	0.
2.5119E-01	0.	0.	0.	0.	0.
3.9811E-01	2.2033E-01	0.	4.4028E-01	0.	0.
6.3096E-01	6.0453E-03	0.	6.7089E-03	7.3215E-03	0.
10.0000E-01	0.	0.	0.	4.2546E 03	0.
1.5849E 00	0.	0.	0.	0.	0.
2.5119E 00	0.	0.	0.	0.	0.
3.9811E 00	0.	0.	0.	0.	0.
6.3096E 00	0.	0.	0.	0.	0.
10.0000E 00	0.	0.	0.	0.	0.
1.5849E 01	0.	0.	0.	0.	0.
2.5119E 01	0.	0.	0.	0.	0.
3.9811E 01	0.	0.	0.	0.	0.
6.3096E 01	0.	0.	0.	0.	0.
10.0000E 01	0.	0.	0.	0.	0.
1.5849E 02	0.	0.	0.	0.	0.
2.5119E 02	0.	0.	0.	0.	0.
3.9811E 02	0.	0.	0.	0.	0.
6.3096E 02	0.	0.	0.	0.	0.
EJECTA VOLUME	2.2638E-01	0.	4.4699E-01	4.2546E 03	0.
EJECTA DEPTH	1.3552E-06	0.	2.2478E-06	1.9810E-02	0.

LUNAR CRATER MODEL

$E_p = 10^{14}$ ergs

CRATER EJECTA SIZE DISTRIBUTIONS

SCREEN SIZE	RING NO. 21 RAD. = 1.4232E 03	RING NO. 22 RAD. = 1.7790E 03	RING NO. 23 RAD. = 2.1348E 03	RING NO. 24 RAD. = 2.4906E 03	RING NO. 25 RAD. = 2.8464E 03
10.0000E-08	0.	0.	0	0.	0.
1.5849E-07	0.	0.	0.	0.	0.
2.5119E-07	0.	0.	0.	0.	0.
3.9811E-07	0.	0.	0.	0.	0.
6.3096E-07	0.	0.	0.	0.	0.
10.0000E-07	0.	0.	0.	0.	0.
1.5849E-06	0.	0.	0.	0.	0.
2.5119E-06	0.	0.	0.	0.	0.
3.9811E-06	0.	0.	0.	0.	0.
6.3096E-06	0.	0.	0.	0.	0.
10.0000E-06	0.	0.	0.	0.	0.
1.5849E-05	0.	0.	0.	0.	0.
2.5119E-05	0.	0.	0.	0.	0.
3.9811E-05	0.	0.	0.	0.	0.
6.3096E-05	0.	0.	0.	0.	0.
10.0000E-05	0.	0.	0.	0.	0.
1.5849E-04	0.	0.	0.	0.	0.
2.5119E-04	0.	0.	0.	0.	0.
3.9811E-04	0.	0.	0.	0.	0.
6.3096E-04	0.	0.	0.	0.	0.
10.0000E-04	0.	0.	0.	0.	0.
1.5849E-03	0.	0.	0.	0.	0.
2.5119E-03	0.	0.	0.	0.	0.
3.9811E-03	0.	0.	0.	0.	0.
6.3096E-03	0.	0.	0.	0.	0.
10.0000E-03	0.	0.	0.	0.	0.
1.5849E-02	0.	0.	0.	0.	0.
2.5119E-02	0.	0.	0.	0.	0.
3.9811E-02	0.	0.	0.	0.	0.
6.3096E-02	0.	0.	0.	0.	0.
10.0000E-02	0.	0.	0.	0.	3.4627E-04
1.5849E-01	0.	1.7249E 01	0.	0.	4.2151E 01
2.5119E-01	1.0157E 01	0.	7.6698E 00	3.4468E 01	3.9052E 01
3.9811E-01	1.0524E 00	1.9453E 00	4.6965E 00	1.7801E 01	3.3208E 01
6.3096E-01	7.3169E-02	4.0977E 03	0.	3.3651E 03	0.
10.0000E-01	0.	0.	0.	0.	0.
1.5849E 00	0.	0.	0.	0.	0.
2.5119E 00	0.	0.	0.	0.	0.
3.9811E 00	0.	0.	0.	0.	0.
6.3096E 00	0.	0.	0.	0.	0.
10.0000E 00	0.	0.	0.	0.	0.
1.5849E 01	0.	0.	0.	0.	0.
2.5119E 01	0.	0.	0.	0.	0.
3.9811E 01	0.	0.	0.	0.	0.
6.3096E 01	0.	0.	0.	0.	0.
10.0000E 01	0.	0.	0.	0.	0.
1.5849E 02	0.	0.	0.	0.	0.
2.5119E 02	0.	0.	0.	0.	0.
3.9811E 02	0.	0.	0.	0.	0.
6.3096E 02	0.	0.	0.	0.	0.
EJECTA VOLUME	1.1283E 01	4.1069E 03	1.2366E 01	3.4174E 03	1.1441E 02
EJECTA DEPTH	8.1054E-06	2.2947E-03	5.6533E-06	1.3219E-03	3.9356E-05

$E_p = 10^{14}$ ergs

LUNAR CRATER MODEL

CRATER EJECTA SIZE DISTRIBUTIONS

SCREEN SIZE	RING NO. 26 RAD. = 3.2022E 03	RING NO. 27 RAD. = 3.5580E 03	RING NO. 28 RAD. = 3.9139E 03	RING NO. 29 RAD. = 4.2697E 03	RING NO. 30 RAD. = 4.6255E 03
10.0000E-08	0.	0.	0.	0.	0.
1.5849E-07	0.	0.	0.	0.	0.
2.5119E-07	0.	0.	0.	0.	0.
3.9811E-07	0.	0.	0.	0.	0.
6.3096E-07	0.	0.	0.	0.	0.
10.0000E-07	0.	0.	0.	0.	0.
1.5849E-06	0.	0.	0.	0.	0.
2.5119E-06	0.	0.	0.	0.	0.
3.9811E-06	0.	0.	0.	0.	0.
6.3096E-06	0.	0.	0.	0.	0.
10.0000E-06	0.	0.	0.	0.	0.
1.5849E-05	0.	0.	0.	0.	0.
2.5119E-05	0.	0.	0.	0.	0.
3.9811E-05	0.	0.	0.	0.	0.
6.3096E-05	0.	0.	0.	0.	0.
10.0000E-05	0.	0.	0.	0.	0.
1.5849E-04	0.	0.	0.	0.	0.
2.5119E-04	0.	0.	0.	0.	0.
3.9811E-04	0.	0.	0.	0.	0.
6.3096E-04	0.	0.	0.	0.	0.
10.0000E-04	0.	0.	0.	0.	0.
1.5849E-03	0.	0.	0.	0.	0.
2.5119E-03	0.	0.	0.	0.	0.
3.9811E-03	0.	0.	0.	0.	0.
6.3096E-03	0.	0.	0.	0.	0.
10.0000E-03	0.	0.	0.	0.	0.
1.5849E-02	0.	0.	0.	0.	0.
2.5119E-02	0.	0.	0.	0.	0.
3.9811E-02	0.	0.	0.	2.9933E-02	2.9705E-02
6.3096E-02	1.4659E-05	1.5518E-04	0.	0.	6.3503E 01
10.0000E-02	0.	8.4228E 01	0.	0.	9.5431E 01
1.5849E-01	0.	4.3339E 01	4.7297E 01	5.0894E 01	4.2177E 02
2.5119E-01	5.9623E 01	0.	2.5120E 03	0.	0.
3.9811E-01	0.	0.	0.	0.	0.
6.3096E-01	0.	0.	0.	0.	0.
10.0000E-01	0.	0.	0.	0.	0.
1.5849E 00	0.	0.	0.	0.	0.
2.5119E 00	0.	0.	0.	0.	0.
3.9811E 00	0.	0.	0.	0.	0.
6.3096E 00	0.	0.	0.	0.	0.
10.0000E 00	0.	0.	0.	0.	0.
1.5849E 01	0.	0.	0.	0.	0.
2.5119E 01	0.	0.	0.	0.	0.
3.9811E 01	0.	0.	0.	0.	0.
6.3096E 01	0.	0.	0.	0.	0.
10.0000E 01	0.	0.	0.	0.	0.
1.5849E 02	0.	0.	0.	0.	0.
2.5119E 02	0.	0.	0.	0.	0.
3.9811E 02	0.	0.	0.	0.	0.
6.3096E 02	0.	0.	0.	0.	0.
EJECTA VOLUME	5.9623E 01	1.2757E 02	2.5593E 03	5.0924E 01	5.8074E 02
EJECTA DEPTH	1.7637E-05	3.3763E-05	6.1285E-04	1.1134E-05	1.1581E-04

$E_p = 10^{14}$ ergs

LUNAR CRATER MODEL

CRATER EJECTA SIZE DISTRIBUTIONS

SCREEN SIZE	RING NO. 31 RAD. = 1.0000E 05	RING NO. 32 RAD. = 1.0000E 06	RING NO. 33 RAD. = 1.0000E 07	RING NO. 34 RAD. = 1.0000E 08	RING NO. 35 RAD. = 5.4664E 08
10.0000E-08	0.	0.	0.	0.	2.4346E 00
1.5849E-07	0.	0.	0.	0.	1.4054E 00
2.5119E-07	0.	0.	0.	0.	2.2000E 00
3.9811E-07	0.	0.	0.	0.	3.4208E 00
6.3096E-07	0.	0.	0.	0.	5.2651E 00
10.0000E-07	0.	0.	0.	5.6142E-01	7.4246E 00
1.5849E-06	0.	0.	0.	1.7661E 00	1.0109E 01
2.5119E-06	0.	0.	0.	4.5785E 00	1.2873E 01
3.9811E-06	0.	0.	0.	1.5822E 01	8.5207E 00
6.3096E-06	0.	0.	0.	3.0914E 01	3.0400E 00
10.0000E-06	0.	0.	1.8952E 00	4.5018E 01	1.3336E-01
1.5849E-05	0.	0.	6.9503E 00	5.8022E 01	0.
2.5119E-05	0.	0.	1.9562E 01	6.8228E 01	0.
3.9811E-05	0.	0.	6.7095E 01	5.1420E 01	0.
6.3096E-05	0.	0.	1.5109E 02	8.7705E 00	0.
10.0000E-05	0.	2.0056E 00	2.0937E 02	0.	0.
1.5849E-04	0.	1.6151E 01	2.5986E 02	0.	0.
2.5119E-04	0.	5.1857E 01	3.0808E 02	0.	0.
3.9811E-04	0.	1.3636E 02	3.3290E 02	0.	0.
6.3096E-04	0.	5.0949E 02	8.6610E 01	0.	0.
10.0000E-04	1.9114E-04	7.3937E 02	0.	0.	0.
1.5849E-03	5.0852E 00	9.1775E 02	0.	0.	0.
2.5119E-03	9.7226E 01	1.0692E 03	0.	0.	0.
3.9811E-03	2.2423E 02	1.2029E 03	0.	0.	0.
6.3096E-03	8.7750E 02	7.6488E 02	0.	0.	0.
10.0000E-03	1.8519E 03	0.	0.	0.	0.
1.5849E-02	2.2025E 03	0.	0.	0.	0.
2.5119E-02	2.7214E 03	0.	0.	0.	0.
3.9811E-02	3.1564E 03	0.	0.	0.	0.
6.3096E-02	3.1272E 03	0.	0.	0.	0.
10.0000E-02	2.5657E 03	0.	0.	0.	0.
1.5849E-01	1.7625E 03	0.	0.	0.	0.
2.5119E-01	0.	0.	0.	0.	0.
3.9811E-01	0.	0.	0.	0.	0.
6.3096E-01	0.	0.	0.	0.	0.
10.0000E-01	0.	0.	0.	0.	0.
1.5849E 00	0.	0.	0.	0.	0.
2.5119E 00	0.	0.	0.	0.	0.
3.9811E 00	0.	0.	0.	0.	0.
6.3096E 00	0.	0.	0.	0.	0.
10.0000E 00	0.	0.	0.	0.	0.
1.5849E 01	0.	0.	0.	0.	0.
2.5119E 01	0.	0.	0.	0.	0.
3.9811E 01	0.	0.	0.	0.	0.
6.3096E 01	0.	0.	0.	0.	0.
10.0000E 01	0.	0.	0.	0.	0.
1.5849E 02	0.	0.	0.	0.	0.
2.5119E 02	0.	0.	0.	0.	0.
3.9811E 02	0.	0.	0.	0.	0.
6.3096E 02	0.	0.	0.	0.	0.
EJECTA VOLUME	1.8592E 04	5.4100E 03	1.4434E 03	2.8510E 02	5.6826E 01
EJECTA DEPTH	1.1861E-06	3.4789E-09	9.2844E-12	1.8852E-14	2.9134E-16

LUNAR CRATER MODEL

$E_p = 10^{16}$ ergs

CRATER EJECTA SIZE DISTRIBUTIONS

SCREEN SIZE	RING NO. 1 RAD. = 1.6515E 02	RING NO. 2 RAD. = 3.3030E 02	RING NO. 3 RAD. = 4.9545E 02	RING NO. 4 RAD. = 6.6060E 02	RING NO. 5 RAD. = 8.2575E 02
10.0000E-08	0.	0.	0.	0.	0.
1.5849E-07	0.	0.	0.	0.	0.
2.5119E-07	0.	0.	0.	0.	0.
3.9811E-07	0.	0.	0.	0.	0.
6.3096E-07	0.	0.	0.	0.	0.
10.0000E-07	0.	0.	0.	0.	0.
1.5849E-06	0.	0.	0.	0.	0.
2.5119E-06	0.	0.	0.	0.	0.
3.9811E-06	0.	0.	0.	0.	0.
6.3096E-06	0.	0.	0.	0.	0.
10.0000E-06	0.	0.	0.	0.	0.
1.5849E-05	0.	0.	0.	0.	0.
2.5119E-05	0.	0.	0.	0.	0.
3.9811E-05	0.	0.	0.	0.	0.
6.3096E-05	0.	0.	0.	0.	0.
10.0000E-05	0.	0.	0.	0.	0.
1.5849E-04	0.	0.	0.	0.	0.
2.5119E-04	0.	0.	0.	0.	0.
3.9811E-04	0.	0.	0.	0.	0.
6.3096E-04	0.	0.	0.	0.	0.
10.0000E-04	0.	0.	0.	0.	0.
1.5849E-03	0.	0.	0.	0.	0.
2.5119E-03	0.	0.	0.	0.	0.
3.9811E-03	0.	0.	0.	0.	0.
6.3096E-03	0.	0.	0.	0.	0.
10.0000E-03	0.	0.	0.	0.	0.
1.5849E-02	0.	0.	0.	0.	0.
2.5119E-02	0.	0.	0.	0.	0.
3.9811E-02	0.	0.	0.	0.	0.
6.3096E-02	0.	0.	0.	0.	0.
10.0000E-02	0.	0.	0.	0.	0.
1.5849E-01	0.	0.	0.	0.	0.
2.5119E-01	0.	0.	0.	0.	0.
3.9811E-01	0.	0.	0.	0.	0.
6.3096E-01	0.	0.	0.	7.2724E 01	1.4532E 02
10.0000E-01	0.	0.	5.4941E 00	4.1411E 00	9.6111E 00
1.5849E 00	0.	1.4877E-02	2.3701E-02	1.4958E-01	4.0065E 05
2.5119E 00	0.	0.	0.	4.2727E 05	0.
3.9811E 00	0.	0.	3.6279E 05	0.	0.
6.3096E 00	0.	2.1589E 05	0.	0.	0.
10.0000E 00	0.	7.4138E 04	0.	0.	0.
1.5849E 01	0.	1.0961E 04	0.	0.	0.
2.5119E 01	0.	4.4384E 02	0.	0.	0.
3.9811E 01	2.2929E 00	0.	0.	0.	0.
6.3096E 01	0.	0.	0.	0.	0.
10.0000E 01	0.	0.	0.	0.	0.
1.5849E 02	0.	0.	0.	0.	0.
2.5119E 02	0.	0.	0.	0.	0.
3.9811E 02	0.	0.	0.	0.	0.
6.3096E 02	0.	0.	0.	0.	0.
EJECTA VOLUME	2.2929E 00	3.0143E 05	3.6280E 05	4.2734E 05	4.0080E 05
EJECTA DEPTH	5.3519E-05	2.3452E 00	1.6936E 00	1.4250E 00	1.0395E 00

LUNAR CRATER MODEL

$E_p = 10^{16}$ ergs

CRATER EJECTA SIZE DISTRIBUTIONS

SCREEN SIZE	RING NO. 6 RAD. = 9.9090E 02	RING NO. 7 RAD. = 1.1560E 03	RING NO. 8 RAD. = 1.3212E 03	RING NO. 9 RAD. = 1.4863E 03	RING NO. 10 RAD. = 1.6515E 03
10.0000E-08	0.	0.	0.	0.	0.
1.5849E-07	0.	0.	0.	0.	0.
2.5119E-07	0.	0.	0.	0.	0.
3.9811E-07	0.	0.	0.	0.	0.
6.3096E-07	0.	0.	0.	0.	0.
10.0000E-07	0.	0.	0.	0.	0.
1.5849E-06	0.	0.	0.	0.	0.
2.5119E-06	0.	0.	0.	0.	0.
3.9811E-06	0.	0.	0.	0.	0.
6.3096E-06	0.	0.	0.	0.	0.
10.0000E-06	0.	0.	0.	0.	0.
1.5849E-05	0.	0.	0.	0.	0.
2.5119E-05	0.	0.	0.	0.	0.
3.9811E-05	0.	0.	0.	0.	0.
6.3096E-05	0.	0.	0.	0.	0.
10.0000E-05	0.	0.	0.	0.	0.
1.5849E-04	0.	0.	0.	0.	0.
2.5119E-04	0.	0.	0.	0.	0.
3.9811E-04	0.	0.	0.	0.	0.
6.3096E-04	0.	0.	0.	0.	0.
10.0000E-04	0.	0.	0.	0.	0.
1.5849E-03	0.	0.	0.	0.	0.
2.5119E-03	0.	0.	0.	0.	0.
3.9811E-03	0.	0.	0.	0.	0.
6.3096E-03	0.	0.	0.	0.	0.
10.0000E-03	0.	0.	0.	0.	0.
1.5849E-02	0.	0.	0.	0.	0.
2.5119E-02	0.	0.	0.	0.	0.
3.9811E-02	0.	0.	0.	0.	0.
6.3096E-02	0.	0.	0.	0.	0.
10.0000E-02	0.	0.	0.	0.	0.
1.5849E-01	0.	0.	0.	0.	0.
2.5119E-01	0.	0.	0.	2.5900E 03	0.
3.9811E-01	6.9599E 02	1.3908E 03	0.	1.5757E 03	1.7487E 03
6.3096E-01	1.6465E 02	1.8272E 02	4.1398E 02	1.7782E 03	0.
10.0000E-01	5.0122E 01	0.	3.2489E 05	0.	0.
1.5849E 00	0.	0.	0.	0.	0.
2.5119E 00	0.	0.	0.	0.	0.
3.9811E 00	0.	0.	0.	0.	0.
6.3096E 00	0.	0.	0.	0.	0.
10.0000E 00	0.	0.	0.	0.	0.
1.5849E 01	0.	0.	0.	0.	0.
2.5119E 01	0.	0.	0.	0.	0.
3.9811E 01	0.	0.	0.	0.	0.
6.3096E 01	0.	0.	0.	0.	0.
10.0000E 01	0.	0.	0.	0.	0.
1.5849E 02	0.	0.	0.	0.	0.
2.5119E 02	0.	0.	0.	0.	0.
3.9811E 02	0.	0.	0.	0.	0.
6.3096E 02	0.	0.	0.	0.	0.
EJECTA VOLUME	9.1076E 02	1.5735E 03	3.2531E 05	5.9439E 03	1.7487E 03
EJECTA DEPTH	1.9326E-03	2.9251E-03	5.0620E-01	8.1611E-03	2.1483E-03

LUNAR CRATER MODEL

$E_p = 10^{16}$ ergs

CRATER EJECTA SIZE DISTRIBUTIONS

SCREEN SIZE	RING NO. 11 RAD. = 1.9818E 03	RING NO. 12 RAD. = 2.3121E 03	RING NO. 13 RAD. = 2.6424E 03	RING NO. 14 RAD. = 2.9727E 03	RING NO. 15 RAD. = 3.3030E 03
10.0000E-08	0.	0.	0.	0.	0.
1.5849E-07	0.	0.	0.	0.	0.
2.5119E-07	0.	0.	0.	0.	0.
3.9811E-07	0.	0.	0.	0.	0.
6.3096E-07	0.	0.	0.	0.	0.
10.0000E-07	0.	0.	0.	0.	0.
1.5849E-06	0.	0.	0.	0.	0.
2.5119E-06	0.	0.	0.	0.	0.
3.9811E-06	0.	0.	0.	0.	0.
6.3096E-06	0.	0.	0.	0.	0.
10.0000E-06	0.	0.	0.	0.	0.
1.5849E-05	0.	0.	0.	0.	0.
2.5119E-05	0.	0.	0.	0.	0.
3.9811E-05	0.	0.	0.	0.	0.
6.3096E-05	0.	0.	0.	0.	0.
10.0000E-05	0.	0.	0.	0.	0.
1.5849E-04	0.	0.	0.	0.	0.
2.5119E-04	0.	0.	0.	0.	0.
3.9811E-04	0.	0.	0.	0.	0.
6.3096E-04	0.	0.	0.	0.	0.
10.0000E-04	0.	0.	0.	0.	0.
1.5849E-03	0.	0.	0.	0.	0.
2.5119E-03	0.	0.	0.	0.	0.
3.9811E-03	0.	0.	0.	0.	0.
6.3096E-03	0.	0.	0.	0.	0.
10.0000E-03	0.	0.	0.	0.	0.
1.5849E-02	0.	0.	0.	0.	0.
2.5119E-02	0.	0.	0.	0.	0.
3.9811E-02	0.	0.	0.	0.	0.
6.3096E-02	0.	0.	0.	0.	2.4111E 00
10.0000E-02	8.5399E-03	8.4749E-03	8.3454E-03	0.	8.8727E-03
1.5849E-01	0.	5.1474E 03	0.	1.0286E 04	0.
2.5119E-01	5.1754E 03	5.8637E 03	6.5074E 03	7.1016E 03	7.6417E 03
3.9811E-01	1.9084E 03	1.9072E 04	0.	1.6757E 05	0.
6.3096E-01	2.4025E 05	0.	0.	0.	0.
10.0000E-01	0.	0.	0.	0.	0.
1.5849E 00	0.	0.	0.	0.	0.
2.5119E 00	0.	0.	0.	0.	0.
3.9811E 00	0.	0.	0.	0.	0.
6.3096E 00	0.	0.	0.	0.	0.
10.0000E 00	0.	0.	0.	0.	0.
1.5849E 01	0.	0.	0.	0.	0.
2.5119E 01	0.	0.	0.	0.	0.
3.9811E 01	0.	0.	0.	0.	0.
6.3096E 01	0.	0.	0.	0.	0.
10.0000E 01	0.	0.	0.	0.	0.
1.5849E 02	0.	0.	0.	0.	0.
2.5119E 02	0.	0.	0.	0.	0.
3.9811E 02	0.	0.	0.	0.	0.
6.3096E 02	0.	0.	0.	0.	0.
EJECTA VOLUME	2.4733E 05	3.0083E 04	6.5074E 03	1.8496E 05	7.6441E 03
EJECTA DEPTH	1.3120E-01	1.3503E-02	2.5315E-03	6.3488E-02	2.3477E-03

LUNAR CRATER MODEL

$E_p = 10^{16}$ ergs

CRATER EJECTA SIZE DISTRIBUTIONS

[illegible]EN SIZE	RING NO. 16 RAD. = 3.6333E 03	RING NO. 17 RAD. = 3.9636E 03	RING NO. 18 RAD. = 4.2939E 03	RING NO. 19 RAD. = 4.6242E 03	RING NO. 20 RAD. = 4.9545E 03
[illegible]00E-08	0.	0.	0.	0.	0.
[illegible]9E-07	0.	0.	0.	0.	0.
[illegible]0E-07	0.	0.	0.	0.	0.
[illegible]E-07	0.	0.	0.	0.	0.
[illegible]6E-07	0.	0.	0.	0.	0.
[illegible]00E-07	0.	0.	0.	0.	0.
1.5849E-06	0.	0.	0.	0.	0.
2.5119E-06	0.	0.	0.	0.	0.
3.9811E-06	0.	0.	0.	0.	0.
[illegible]04E-06	0.	0.	0.	0.	0.
[illegible]00E-06	0.	0.	0.	0.	0.
[illegible]49E-05	0.	0.	0.	0.	0.
[illegible]19E-05	0.	0.	0.	0.	0.
[illegible]11E-05	0.	0.	0.	0.	0.
[illegible]49E-05	0.	0.	0.	0.	0.
[illegible]00E-05	0.	0.	0.	0.	0.
[illegible]4E-04	0.	0.	0.	0.	0.
2.5119E-04	0.	0.	0.	0.	0.
3.9811E-04	0.	0.	0.	0.	0.
[illegible]96E-04	0.	0.	0.	0.	0.
[illegible]00E-04	0.	0.	0.	0.	0.
[illegible]49E-03	0.	0.	0.	0.	0.
[illegible]19E-03	0.	0.	0.	0.	0.
[illegible]11E-03	0.	0.	0.	0.	0.
[illegible]49E-03	0.	0.	0.	0.	0.
10.0000E-03	0.	0.	0.	0.	0.
[illegible]00E-02	0.	0.	0.	0.	0.
[illegible]19E-02	0.	0.	0.	0.	0.
3.9811E-02	0.	0.	0.	0.	5.6795E 01
6.3096E-02	1.4247E 00	1.6239E-01	1.7190E 00	0.	0.
[illegible]00E-02	6.7791E 03	0.	1.3546E 04	0.	1.1156E-02
[illegible]49E-01	1.1654E 04	0.	1.2933E 04	1.4114E 04	0.
[illegible]19E-01	6.3330E 04	0.	0.	1.1204E 05	0.
[illegible]11E-01	0.	0.	0.	0.	0.
[illegible]96E-01	0.	0.	0.	0.	0.
10.0000E-01	0.	0.	0.	0.	0.
1.5849E 00	0.	0.	0.	0.	0.
2.5119E 00	0.	0.	0.	0.	0.
[illegible]11E 00	0.	0.	0.	0.	0.
[illegible]96E 00	0.	0.	0.	0.	0.
[illegible]00E 00	0.	0.	0.	0.	0.
[illegible]49E 01	0.	0.	0.	0.	0.
[illegible]19E 01	0.	0.	0.	0.	0.
[illegible]11E 01	0.	0.	0.	0.	0.
[illegible]96E 01	0.	0.	0.	0.	0.
[illegible]00E 01	0.	0.	0.	0.	0.
[illegible]49E 02	0.	0.	0.	0.	0.
[illegible]19E 02	0.	0.	0.	0.	0.
[illegible]11E 02	0.	0.	0.	0.	0.
[illegible]96E 02	0.	0.	0.	0.	0.
[illegible]E	8.1764E 04	1.6239E-01	2.6481E 04	1.2576E 05	5.6807E 01
[illegible]	2.2720E-02	4.1190E-08	6.1810E-03	2.7395E-02	1.1430E-05

LUNAR CRATER MODEL

$E_p = 10^{16}$ ergs

CRATER EJECTA SIZE DISTRIBUTIONS

SCREEN SIZE	RING NO. 21 RAD. = 6.6060E 03	RING NO. 22 RAD. = 8.2575E 03	RING NO. 23 RAD. = 9.9090E 03	RING NO. 24 RAD. = 1.1560E 04	RING NO. 25 RAD. = 1.3212E 04
10.0000E-08	0.	0.	0.	0.	0.
1.5849E-07	0.	0.	0.	0.	0.
2.5119E-07	0.	0.	0.	0.	0.
3.9811E-07	0.	0.	0.	0.	0.
6.3096E-07	0.	0.	0.	0.	0.
10.0000E-07	0.	0.	0.	0.	0.
1.5849E-06	0.	0.	0.	0.	0.
2.5119E-06	0.	0.	0.	0.	0.
3.9811E-06	0.	0.	0.	0.	0.
6.3096E-06	0.	0.	0.	0.	0.
10.0000E-06	0.	0.	0.	0.	0.
1.5849E-05	0.	0.	0.	0.	0.
2.5119E-05	0.	0.	0.	0.	0.
3.9811E-05	0.	0.	0.	0.	0.
6.3096E-05	0.	0.	0.	0.	0.
10.0000E-05	0.	0.	0.	0.	0.
1.5849E-04	0.	0.	0.	0.	0.
2.5119E-04	0.	0.	0.	0.	0.
3.9811E-04	0.	0.	0.	0.	0.
6.3096E-04	0.	0.	0.	0.	0.
10.0000E-04	0.	0.	0.	0.	0.
1.5849E-03	0.	0.	0.	0.	0.
2.5119E-03	0.	0.	0.	0.	0.
3.9811E-03	0.	0.	0.	0.	0.
6.3096E-03	0.	0.	0.	0.	0.
10.0000E-03	0.	0.	0.	0.	0.
1.5849E-02	0.	0.	0.	0.	2.9150E 03
2.5119E-02	0.	5.6014E 02	3.6869E 02	3.9935E 02	4.8956E 03
3.9811E-02	1.1187E 02	5.9009E 01	5.8112E 03	1.1679E 04	1.3231E 04
6.3096E-02	2.0503E 04	2.5151E 00	1.5485E 04	3.5950E 04	6.7021E 04
10.0000E-02	3.2381E 04	3.8590E 04	1.6576E 05	4.7866E 04	0.
1.5849E-01	1.4105E 05	7.3978E 04	0.	0.	0.
2.5119E-01	0.	0.	0.	0.	0.
3.9811E-01	0.	0.	0.	0.	0.
6.3096E-01	0.	0.	0.	0.	0.
10.0000E-01	0.	0.	0.	0.	0.
1.5849E 00	0.	0.	0.	0.	0.
2.5119E 00	0.	0.	0.	0.	0.
3.9811E 00	0.	0.	0.	0.	0.
6.3096E 00	0.	0.	0.	0.	0.
10.0000E 00	0.	0.	0.	0.	0.
1.5849E 01	0.	0.	0.	0.	0.
2.5119E 01	0.	0.	0.	0.	0.
3.9811E 01	0.	0.	0.	0.	0.
6.3096E 01	0.	0.	0.	0.	0.
10.0000E 01	0.	0.	0.	0.	0.
1.5849E 02	0.	0.	0.	0.	0.
2.5119E 02	0.	0.	0.	0.	0.
3.9811E 02	0.	0.	0.	0.	0.
6.3096E 02	0.	0.	0.	0.	0.
EJECTA VOLUME	1.9405E 05	1.1319E 05	1.8743E 05	9.5895E 04	8.8062E 04
EJECTA DEPTH	6.4705E-03	2.9355E-03	3.9771E-03	1.7218E-03	1.3703E-03

LUNAR CRATER MODEL

$E_p = 10^{16}$ ergs

CRATER EJECTA SIZE DISTRIBUTIONS

SCREEN SIZE	RING NO. 26 RAD. = 1.4863E 04	RING NO. 27 RAD. = 1.6515E 04	RING NO. 28 RAD. = 1.8166E 04	RING NO. 29 RAD. = 1.9818E 04	RING NO. 30 RAD. = 2.1469E 04
10.0000E-08	0.	0.	0.	0.	0.
1.5849E-07	0.	0.	0.	0.	0.
2.5119E-07	0.	0.	0.	0.	0.
3.9811E-07	0.	0.	0.	0.	0.
6.3096E-07	0.	0.	0.	0.	0.
10.0000E-07	0.	0.	0.	0.	0.
1.5849E-06	0.	0.	0.	0.	0.
2.5119E-06	0.	0.	0.	0.	0.
3.9811E-06	0.	0.	0.	0.	0.
6.3096E-06	0.	0.	0.	0.	0.
10.0000E-06	0.	0.	0.	0.	0.
1.5849E-05	0.	0.	0.	0.	0.
2.5119E-05	0.	0.	0.	0.	0.
3.9811E-05	0.	0.	0.	0.	0.
6.3096E-05	0.	0.	0.	0.	0.
10.0000E-05	0.	0.	0.	0.	0.
1.5849E-04	0.	0.	0.	0.	0.
2.5119E-04	0.	0.	0.	0.	0.
3.9811E-04	0.	0.	0.	0.	0.
6.3096E-04	0.	0.	0.	0.	0.
10.0000E-04	0.	0.	0.	0.	0.
1.5849E-03	0.	0.	0.	0.	0.
2.5119E-03	0.	0.	0.	0.	0.
3.9811E-03	0.	0.	0.	0.	0.
6.3096E-03	0.	0.	0.	0.	0.
10.0000E-03	6.3225E-03	6.2744E-03	0.	2.6706E 03	2.6503E 03
1.5849E-02	0.	1.4297E 03	0.	0.	4.6689E 03
2.5119E-02	0.	5.2649E 02	8.8540E 03	5.8429E 02	1.0032E 04
3.9811E-02	8.0971E 01	1.5410E 04	0.	3.3080E 04	1.4209E 05
6.3096E-02	1.2033E 05	0.	3.0687E 04	0.	0.
10.0000E-02	0.	0.	0.	0.	0.
1.5849E-01	0.	0.	0.	0.	0.
2.5119E-01	0.	0.	0.	0.	0.
3.9811E-01	0.	0.	0.	0.	0.
6.3096E-01	0.	0.	0.	0.	0.
10.0000E-01	0.	0.	0.	0.	0.
1.5849E 00	0.	0.	0.	0.	0.
2.5119E 00	0.	0.	0.	0.	0.
3.9811E 00	0.	0.	0.	0.	0.
6.3096E 00	0.	0.	0.	0.	0.
10.0000E 00	0.	0.	0.	0.	0.
1.5849E 01	0.	0.	0.	0.	0.
2.5119E 01	0.	0.	0.	0.	0.
3.9811E 01	0.	0.	0.	0.	0.
6.3096E 01	0.	0.	0.	0.	0.
10.0000E 01	0.	0.	0.	0.	0.
1.5849E 02	0.	0.	0.	0.	0.
2.5119E 02	0.	0.	0.	0.	0.
3.9811E 02	0.	0.	0.	0.	0.
6.3096E 02	0.	0.	0.	0.	0.
EJECTA VOLUME	1.2041E 05	1.7366E 04	3.9541E 04	3.6335E 04	1.5944E 05
EJECTA DEPTH	1.6533E-03	2.1334E-04	4.3949E-04	3.6974E-04	1.4987E-03

$E_p = 10^{16}$ ergs

LUNAR CRATER MODEL

CRATER EJECTA SIZE DISTRIBUTIONS

SCREEN SIZE	RING NO. 31 RAD. = 1.0000E 05	RING NO. 32 RAD. = 1.0000E 06	RING NO. 33 RAD. = 1.0000E 07	RING NO. 34 RAD. = 1.0000E 08	RING NO. 35 RAD. = 5.4664E 08
10.0000E-08	0.	0.	0.	0.	1.9769E 02
1.5849E-07	0.	0.	0.	0.	1.1435E 02
2.5119E-07	0.	0.	0.	0.	1.7934E 02
3.9811E-07	0.	0.	0.	0.	2.7965E 02
6.3096E-07	0.	0.	0.	0.	4.3221E 02
10.0000E-07	0.	0.	0.	2.4821E 01	6.3458E 02
1.5849E-06	0.	0.	0.	1.2006E 02	8.6783E 02
2.5119E-06	0.	0.	0.	2.9256E 02	1.1531E 03
3.9811E-06	0.	0.	0.	1.2963E 03	8.0672E 02
6.3096E-06	0.	0.	0.	2.6291E 03	2.2365E 02
10.0000E-06	0.	0.	5.9272E 01	3.8063E 03	5.6960E 01
1.5849E-05	0.	0.	5.7460E 02	4.9118E 03	0.
2.5119E-05	0.	0.	1.4243E 03	5.7236E 03	0.
3.9811E-05	0.	0.	4.0229E 03	5.5155E 03	0.
6.3096E-05	0.	0.	1.0878E 04	1.8999E 03	0.
10.0000E-05	0.	1.4153E 00	1.6962E 04	4.9977E 01	0.
1.5849E-04	0.	9.5712E 02	2.0754E 04	0.	0.
2.5119E-04	0.	3.9222E 03	2.4039E 04	0.	0.
3.9811E-04	0.	8.4152E 03	2.7821E 04	0.	0.
6.3096E-04	0.	2.8864E 04	1.7570E 04	0.	0.
10.0000E-04	0.	5.6438E 04	4.9058E 02	0.	0.
1.5849E-03	4.1879E 02	6.8898E 04	0.	0.	0.
2.5119E-03	6.1735E 03	8.0495E 04	0.	0.	0.
3.9811E-03	1.4066E 04	9.5264E 04	0.	0.	0.
6.3096E-03	4.2576E 04	8.8298E 04	0.	0.	0.
10.0000E-03	1.3512E 05	4.9764E 03	0.	0.	0.
1.5849E-02	1.5068E 05	0.	0.	0.	0.
2.5119E-02	1.6413E 05	0.	0.	0.	0.
3.9811E-02	1.9568E 04	0.	0.	0.	0.
6.3096E-02	0.	0.	0.	0.	0.
10.0000E-02	0.	0.	0.	0.	0.
1.5849E-01	0.	0.	0.	0.	0.
2.5119E-01	0.	0.	0.	0.	0.
3.9811E-01	0.	0.	0.	0.	0.
6.3096E-01	0.	0.	0.	0.	0.
10.0000E-01	0.	0.	0.	0.	0.
1.5849E 00	0.	0.	0.	0.	0.
2.5119E 00	0.	0.	0.	0.	0.
3.9811E 00	0.	0.	0.	0.	0.
6.3096E 00	0.	0.	0.	0.	0.
10.0000E 00	0.	0.	0.	0.	0.
1.5849E 01	0.	0.	0.	0.	0.
2.5119E 01	0.	0.	0.	0.	0.
3.9811E 01	0.	0.	0.	0.	0.
6.3096E 01	0.	0.	0.	0.	0.
10.0000E 01	0.	0.	0.	0.	0.
1.5849E 02	0.	0.	0.	0.	0.
2.5119E 02	0.	0.	0.	0.	0.
3.9811E 02	0.	0.	0.	0.	0.
6.3096E 02	0.	0.	0.	0.	0.
EJECTA VOLUME	5.3273E 05	4.3654E 05	1.2460E 05	2.6270E 04	4.9461E 03
EJECTA DEPTH	3.5553E-05	2.8072E-07	8.0149E-10	1.7370E-12	2.5358E-14

LUNAR CRATER MODEL

$E_p = 10^{18}$ ergs

CRATER EJECTA SIZE DISTRIBUTIONS

SCREEN SIZE	RING NO. 1 RAD. = 7.6656E 02	RING NO. 2 RAD. = 1.5331E 03	RING NO. 3 RAD. = 2.2997E 03	RING NO. 4 RAD. = 3.0662E 03	RING NO. 5 RAD. = 3.8328E 03
10.0000E-08	0.	0.	0.	0.	0.
1.5849E-07	0.	0.	0.	0.	0.
2.5119E-07	0.	0.	0.	0.	0.
3.9811E-07	0.	0.	0.	0.	0.
6.3096E-07	0.	0.	0.	0.	0.
10.0000E-07	0.	0.	0.	0.	0.
1.5849E-06	0.	0.	0.	0.	0.
2.5119E-06	0.	0.	0.	0.	0.
3.9811E-06	0.	0.	0.	0.	0.
6.3096E-06	0.	0.	0.	0.	0.
10.0000E-06	0.	0.	0.	0.	0.
1.5849E-05	0.	0.	0.	0.	0.
2.5119E-05	0.	0.	0.	0.	0.
3.9811E-05	0.	0.	0.	0.	0.
6.3096E-05	0.	0.	0.	0.	0.
10.0000E-05	0.	0.	0.	0.	0.
1.5849E-04	0.	0.	0.	0.	0.
2.5119E-04	0.	0.	0.	0.	0.
3.9811E-04	0.	0.	0.	0.	0.
6.3096E-04	0.	0.	0.	0.	0.
10.0000E-04	0.	0.	0.	0.	0.
1.5849E-03	0.	0.	0.	0.	0.
2.5119E-03	0.	0.	0.	0.	0.
3.9811E-03	0.	0.	0.	0.	0.
6.3096E-03	0.	0.	0.	0.	0.
10.0000E-03	0.	0.	0.	0.	0.
1.5849E-02	0.	0.	0.	0.	0.
2.5119E-02	0.	0.	0.	0.	0.
3.9811E-02	0.	0.	0.	0.	0.
6.3096E-02	0.	0.	0.	0.	5.1692E 03
10.0000E-02	0.	0.	1.1530E 02	2.2710E 02	1.1980E 02
1.5849E-01	0.	4.6909E-01	6.4320E-01	6.9700E 05	1.3928E 06
2.5119E-01	0.	0.	1.7716E 06	1.3378E 06	3.1048E 06
3.9811E-01	0.	1.0562E 06	1.6826E 06	1.0619E 07	7.0264E 06
6.3096E-01	0.	9.5237E 05	3.6925E 06	1.0722E 07	0.
10.0000E-01	5.6564E 04	6.5881E 05	1.6002E 07	0.	0.
1.5849E 00	6.6461E 03	2.3087E 07	0.	0.	0.
2.5119E 00	1.8265E 02	3.1442E 07	0.	0.	0.
3.9811E 00	0.	3.9283E 07	0.	0.	0.
6.3096E 00	0.	4.2775E 07	0.	0.	0.
10.0000E 00	3.7550E 07	0.	0.	0.	0.
1.5849E 01	2.3571E 07	0.	0.	0.	0.
2.5119E 01	8.8227E 06	0.	0.	0.	0.
3.9811E 01	1.5012E 06	0.	0.	0.	0.
6.3096E 01	7.7072E 04	0.	0.	0.	0.
10.0000E 01	6.1587E 02	0.	0.	0.	0.
1.5849E 02	0.	0.	0.	0.	0.
2.5119E 02	0.	0.	0.	0.	0.
3.9811E 02	0.	0.	0.	0.	0.
6.3096E 02	0.	0.	0.	0.	0.
EJECTA VOLUME	7.1586E 07	1.3925E 08	2.3149E 07	2.3375E 07	1.1529E 07
EJECTA DEPTH	7.7556E 01	5.0290E 01	5.0160E 00	3.6179E 00	1.3879E 00

LUNAR CRATER MODEL

$E_p = 10^{18}$ ergs

CRATER EJECTA SIZE DISTRIBUTIONS

SCREEN SIZE	RING NO. 6 RAD. = 4.5993E 03	RING NO. 7 RAD. = 5.3659E 03	RING NO. 8 RAD. = 6.1325E 03	RING NO. 9 RAD. = 6.9990E 03	RING NO. 10 RAD. = 7.6656E 03
10.0000E-08	0.	0.	0.	0.	0.
1.5849E-07	0.	0.	0.	0.	0.
2.5119E-07	0.	0.	0.	0.	0.
3.9811E-07	0.	0.	0.	0.	0.
6.3096E-07	0.	0.	0.	0.	0.
10.0000E-07	0.	0.	0.	0.	0.
1.5849E-06	0.	0.	0.	0.	0.
2.5119E-06	0.	0.	0.	0.	0.
3.9811E-06	0.	0.	0.	0.	0.
6.3096E-06	0.	0.	0.	0.	0.
10.0000E-06	0.	0.	0.	0.	0.
1.5849E-05	0.	0.	0.	0.	0.
2.5119E-05	0.	0.	0.	0.	0.
3.9811E-05	0.	0.	0.	0.	0.
6.3096E-05	0.	0.	0.	0.	0.
10.0000E-05	0.	0.	0.	0.	0.
1.5849E-04	0.	0.	0.	0.	0.
2.5119E-04	0.	0.	0.	0.	0.
3.9811E-04	0.	0.	0.	0.	0.
6.3096E-04	0.	0.	0.	0.	0.
10.0000E-04	0.	0.	0.	0.	0.
1.5849E-03	0.	0.	0.	0.	0.
2.5119E-03	0.	0.	0.	0.	0.
3.9811E-03	0.	0.	0.	0.	0.
6.3096E-03	0.	0.	0.	0.	0.
10.0000E-03	0.	0.	0.	0.	0.
1.5849E-02	0.	0.	0.	0.	0.
2.5119E-02	0.	0.	0.	0.	0.
3.9811E-02	0.	0.	7.3696E 04	3.1199E 03	3.3027E 04
6.3096E-02	3.4024E 03	3.6953E 03	5.3643E 05	0.	1.0[illegible]E 06
10.0000E-02	6.5539E 05	1.3098E 06	1.5063E 02	1.4840E 06	1.6[illegible]E 06
1.5849E-01	1.5780E 06	1.7512E 06	3.9676E 06	1.7043E 07	0.
2.5119E-01	1.6192E 07	0.	4.5411E 06	0.	0.
3.9811E-01	0.	0.	0.	0.	0.
6.3096E-01	0.	0.	0.	0.	0.
10.0000E-01	0.	0.	0.	0.	0.
1.5849E 00	0.	0.	0.	0.	0.
2.5119E 00	0.	0.	0.	0.	0.
3.9811E 00	0.	0.	0.	0.	0.
6.3096E 00	0.	0.	0.	0.	0.
10.0000E 00	0.	0.	0.	0.	0.
1.5849E 01	0.	0.	0.	0.	0.
2.5119E 01	0.	0.	0.	0.	0.
3.9811E 01	0.	0.	0.	0.	0.
6.3096E 01	0.	0.	0.	0.	0.
10.0000E 01	0.	0.	0.	0.	0.
1.5849E 02	0.	0.	0.	0.	0.
2.5119E 02	0.	0.	0.	0.	0.
3.9811E 02	0.	0.	0.	0.	0.
6.3096E 02	0.	0.	0.	0.	0.
EJECTA VOLUME	1.8428E 07	3.0647E 06	9.1190E 06	1.8530E 07	2.7495E 06
EJECTA DEPTH	1.8150E 00	2.5541E-01	6.5964E-01	1.1909E 00	1.5578E-01

LUNAR CRATER MODEL

$E_p = 10^{18}$ ergs

CRATER EJECTA SIZE DISTRIBUTIONS

SCREEN SIZE	RING NO. 11 RAD. = 9.1987E 03	RING NO. 12 RAD. = 1.0732E 04	RING NO. 13 RAD. = 1.2265E 04	RING NO. 14 RAD. = 1.3798E 04	RING NO. 15 RAD. = 1.5331E 04
10.0000E-08	0.	0.	0.	0.	0.
1.5849E-07	0.	0.	0.	0.	0.
2.5119E-07	0.	0.	0.	0.	0.
3.9811E-07	0.	0.	0.	0.	0.
6.3096E-07	0.	0.	0.	0.	0.
10.0000E-07	0.	0.	0.	0.	0.
1.5849E-06	0.	0.	0.	0.	0.
2.5119E-06	0.	0.	0.	0.	0.
3.9811E-06	0.	0.	0.	0.	0.
6.3096E-06	0.	0.	0.	0.	0.
10.0000E-06	0.	0.	0.	0.	0.
1.5849E-05	0.	0.	0.	0.	0.
2.5119E-05	0.	0.	0.	0.	0.
3.9811E-05	0.	0.	0.	0.	0.
6.3096E-05	0.	0.	0.	0.	0.
10.0000E-05	0.	0.	0.	0.	0.
1.5849E-04	0.	0.	0.	0.	0.
2.5119E-04	0.	0.	0.	0.	0.
3.9811E-04	0.	0.	0.	0.	0.
6.3096E-04	0.	0.	0.	0.	0.
10.0000E-04	0.	0.	0.	0.	0.
1.5849E-03	0.	0.	0.	0.	0.
2.5119E-03	0.	0.	0.	0.	0.
3.9811E-03	0.	0.	0.	0.	0.
6.3096E-03	0.	0.	0.	0.	0.
10.0000E-03	0.	0.	0.	0.	0.
1.5849E-02	0.	3.0107E-02	2.9878E-02	2.5433E 05	2.5239E 05
2.5119E-02	1.3163E 05	1.3063E 05	1.2863E 05	0.	4.1184E 05
3.9811E-02	0.	4.3245E 05	8.3088E 05	0.	9.4038E 05
6.3096E-02	5.3920E 03	1.2106E 06	1.3958E 06	1.4591E 06	6.9718E 06
10.0000E-02	1.7970E 06	1.7959E 07	0.	1.8529E 06	0.
1.5849E-01	2.9105E 06	0.	0.	0.	0.
2.5119E-01	0.	0.	0.	0.	0.
3.9811E-01	0.	0.	0.	0.	0.
6.3096E-01	0.	0.	0.	0.	0.
10.0000E-01	0.	0.	0.	0.	0.
1.5849E 00	0.	0.	0.	0.	0.
2.5119E 00	0.	0.	0.	0.	0.
3.9811E 00	0.	0.	0.	0.	0.
6.3096E 00	0.	0.	0.	0.	0.
10.0000E 00	0.	0.	0.	0.	0.
1.5849E 01	0.	0.	0.	0.	0.
2.5119E 01	0.	0.	0.	0.	0.
3.9811E 01	0.	0.	0.	0.	0.
6.3096E 01	0.	0.	0.	0.	0.
10.0000E 01	0.	0.	0.	0.	0.
1.5849E 02	0.	0.	0.	0.	0.
2.5119E 02	0.	0.	0.	0.	0.
3.9811E 02	0.	0.	0.	0.	0.
6.3096E 02	0.	0.	0.	0.	0.
EJECTA VOLUME	4.8446E 06	1.9733E 07	2.3553E 06	3.5663E 06	8.5764E 06
EJECTA DEPTH	1.1929E-01	4.1113E-01	4.2530E-02	5.6820E-02	1.2226E-01

LUNAR CRATER MODEL

$E_p = 10^{18}$ ergs

CRATER EJECTA SIZE DISTRIBUTIONS

SCREEN SIZE	RING NO. 16 RAD. = 1.6864E 04	RING NO. 17 RAD. = 1.9397E 04	RING NO. 18 RAD. = 1.9931E 04	RING NO. 19 RAD. = 2.1464E 04	RING NO. 20 RAD. = 2.2997E 04
10.0000E-08	0.	0.	0.	0.	0.
1.5849E-07	0.	0.	0.	0.	0.
2.5119E-07	0.	0.	0.	0.	0.
3.9811E-07	0.	0.	0.	0.	0.
6.3096E-07	0.	0.	0.	0.	0.
10.0000E-07	0.	0.	0.	0.	0.
1.5849E-06	0.	0.	0.	0.	0.
2.5119E-06	0.	0.	0.	0.	0.
3.9811E-06	0.	0.	0.	0.	0.
6.3096E-06	0.	0.	0.	0.	0.
10.0000E-06	0.	0.	0.	0.	0.
1.5849E-05	0.	0.	0.	0.	0.
2.5119E-05	0.	0.	0.	0.	0.
3.9811E-05	0.	0.	0.	0.	0.
6.3096E-05	0.	0.	0.	0.	0.
10.0000E-05	0.	0.	0.	0.	0.
1.5849E-04	0.	0.	0.	0.	0.
2.5119E-04	0.	0.	0.	0.	0.
3.9811E-04	0.	0.	0.	0.	0.
6.3096E-04	0.	0.	0.	0.	0.
10.0000E-04	0.	0.	0.	0.	0.
1.5849E-03	0.	0.	0.	0.	0.
2.5119E-03	0.	0.	0.	0.	0.
3.9811E-03	0.	0.	0.	0.	0.
6.3096E-03	0.	0.	0.	0.	0.
10.0000E-03	1.4591E 01	3.5826E 00	1.0797E 01	1.2307E 00	3.3052E 05
1.5849E-02	0.	2.4854E 05	0.	0.	3.5441E-02
2.5119E-02	0.	0.	7.0463E 05	0.	1.7196E 05
3.9811E-02	5.2734E 04	1.1071E 06	4.0994E 05	1.0804E 06	1.1626E 06
6.3096E-02	7.6101E 06	0.	1.1762E 06	0.	0.
10.0000E-02	0.	0.	0.	0.	0.
1.5849E-01	0.	0.	0.	0.	0.
2.5119E-01	0.	0.	0.	0.	0.
3.9811E-01	0.	0.	0.	0.	0.
6.3096E-01	0.	0.	0.	0.	0.
10.0000E-01	0.	0.	0.	0.	0.
1.5849E 00	0.	0.	0.	0.	0.
2.5119E 00	0.	0.	0.	0.	0.
3.9811E 00	0.	0.	0.	0.	0.
6.3096E 00	0.	0.	0.	0.	0.
10.0000E 00	0.	0.	0.	0.	0.
1.5849E 01	0.	0.	0.	0.	0.
2.5119E 01	0.	0.	0.	0.	0.
3.9811E 01	0.	0.	0.	0.	0.
6.3096E 01	0.	0.	0.	0.	0.
10.0000E 01	0.	0.	0.	0.	0.
1.5849E 02	0.	0.	0.	0.	0.
2.5119E 02	0.	0.	0.	0.	0.
3.9811E 02	0.	0.	0.	0.	0.
6.3096E 02	0.	0.	0.	0.	0.
EJECTA VOLUME	7.6628E 06	1.3556E 06	2.2907E 06	1.0804E 06	1.6650E 06
EJECTA DEPTH	9.8833E-02	1.5964E-02	2.4918E-02	1.0838E-02	1.5551E-02

LUNAR CRATER MODEL

$E_p = 10^{18}$ ergs

CRATER EJECTA SIZE DISTRIBUTIONS

SCREEN SIZE	RING NO. 21 RAD. = 3.0662E 04	RING NO. 22 RAD. = 3.9328E 04	RING NO. 23 RAD. = 4.5093E 04	RING NO. 24 RAD. = 5.3659E 04	RING NO. 25 RAD. = 6.1325E 04
10.0000E-08	0.	0.	0.	0.	0.
1.5849E-07	0.	0.	0.	0.	0.
2.5119E-07	0.	0.	0.	0.	0.
3.9811E-07	0.	0.	0.	0.	0.
6.3096E-07	0.	0.	0.	0.	0.
10.0000E-07	0.	0.	0.	0.	0.
1.5849E-06	0.	0.	0.	0.	0.
2.5119E-06	0.	0.	0.	0.	0.
3.9811E-06	0.	0.	0.	0.	0.
6.3096E-06	0.	0.	0.	0.	0.
10.0000E-06	0.	0.	0.	0.	0.
1.5849E-05	0.	0.	0.	0.	0.
2.5119E-05	0.	0.	0.	0.	0.
3.9811E-05	0.	0.	0.	0.	0.
6.3096E-05	0.	0.	0.	0.	0.
10.0000E-05	0.	0.	0.	0.	0.
1.5849E-04	0.	0.	0.	0.	0.
2.5119E-04	0.	0.	0.	0.	0.
3.9811E-04	0.	0.	0.	0.	0.
6.3096E-04	0.	0.	0.	0.	0.
10.0000E-04	0.	0.	0.	0.	0.
1.5849E-03	0.	0.	0.	0.	0.
2.5119E-03	0.	0.	0.	0.	0.
3.9811E-03	0.	0.	7.1480E 03	7.6965E 03	5.5864E 05
6.3096E-03	1.3445E 03	6.5527E 05	3.2177E 05	0.	4.2083E 05
10.0000E-03	6.5098E 05	4.6495E 05	1.9061E 01	6.3197E 05	7.0717E 05
1.5849E-02	1.1184E 06	7.5115E 05	1.6324E 06	3.3260E 06	5.0701E 06
2.5119E-02	3.3771E 06	8.2922E 06	0.	4.7115E 05	0.
3.9811E-02	9.8148E 06	5.6460E 05	0.	0.	0.
6.3096E-02	0.	0.	0.	0.	0.
10.0000E-02	0.	0.	0.	0.	0.
1.5849E-01	0.	0.	0.	0.	0.
2.5119E-01	0.	0.	0.	0.	0.
3.9811E-01	0.	0.	0.	0.	0.
6.3096E-01	0.	0.	0.	0.	0.
10.0000E-01	0.	0.	0.	0.	0.
1.5849E 00	0.	0.	0.	0.	0.
2.5119E 00	0.	0.	0.	0.	0.
3.9811E 00	0.	0.	0.	0.	0.
6.3096E 00	0.	0.	0.	0.	0.
10.0000E 00	0.	0.	0.	0.	0.
1.5849E 01	0.	0.	0.	0.	0.
2.5119E 01	0.	0.	0.	0.	0.
3.9811E 01	0.	0.	0.	0.	0.
6.3096E 01	0.	0.	0.	0.	0.
10.0000E 01	0.	0.	0.	0.	0.
1.5849E 02	0.	0.	0.	0.	0.
2.5119E 02	0.	0.	0.	0.	0.
3.9811E 02	0.	0.	0.	0.	0.
6.3096E 02	0.	0.	0.	0.	0.
EJECTA VOLUME	1.4963E 07	1.0728E 07	1.9614E 06	4.4368E 06	6.7568E 06
EJECTA DEPTH	2.3158E-02	1.2914E-02	1.9318E-03	3.6976E-03	4.8802E-03

LUNAR CRATER MODEL

$E_p = 10^{18}$ ergs

CRATER EJECTA SIZE DISTRIBUTIONS

SCREEN SIZE	RING NO. 26 RAD. = 6.8990E 04	RING NO. 27 RAD. = 7.6656E 04	RING NO. 28 RAD. = 8.4321E 04	RING NO. 29 RAD. = 9.1987E 04	RING NO. 30 RAD. = 9.9653E 04
10.0000E-08	0.	0.	0.	0.	0.
1.5849E-07	0.	0.	0.	0.	0.
2.5119E-07	0.	0.	0.	0.	0.
3.9811E-07	0.	0.	0.	0.	0.
6.3096E-07	0.	0.	0.	0.	0.
10.0000E-07	0.	0.	0.	0.	0.
1.5849E-06	0.	0.	0.	0.	0.
2.5119E-06	0.	0.	0.	0.	0.
3.9811E-06	0.	0.	0.	0.	0.
6.3096E-06	0.	0.	0.	0.	0.
10.0000E-06	0.	0.	0.	0.	0.
1.5849E-05	0.	0.	0.	0.	0.
2.5119E-05	0.	0.	0.	0.	0.
3.9811E-05	0.	0.	0.	0.	0.
6.3096E-05	0.	0.	0.	0.	0.
10.0000E-05	0.	0.	0.	0.	0.
1.5849E-04	0.	0.	0.	0.	0.
2.5119E-04	0.	0.	0.	0.	0.
3.9811E-04	0.	0.	0.	0.	0.
6.3096E-04	0.	0.	0.	0.	0.
10.0000E-04	0.	0.	0.	0.	0.
1.5849E-03	0.	0.	4.4335E-01	4.3998E-01	0.
2.5119E-03	2.8340E 04	2.8124E 04	2.3904E 03	2.3553E 05	2.0863E 05
3.9811E-03	2.3379E 04	2.5492E 05	0.	2.9640E 05	5.0446E 04
6.3096E-03	8.8159E 02	5.4397E 05	9.6208E 02	4.3883E 05	1.7812E 05
10.0000E-03	4.7119E 05	5.0143E 06	3.3329E 05	3.5864E 05	2.9722E 06
1.5849E-02	0.	7.2072E 04	2.2565E 05	0.	0.
2.5119E-02	0.	0.	0.	0.	0.
3.9811E-02	0.	0.	0.	0.	0.
6.3096E-02	0.	0.	0.	0.	0.
10.0000E-02	0.	0.	0.	0.	0.
1.5849E-01	0.	0.	0.	0.	0.
2.5119E-01	0.	0.	0.	0.	0.
3.9811E-01	0.	0.	0.	0.	0.
6.3096E-01	0.	0.	0.	0.	0.
10.0000E-01	0.	0.	0.	0.	0.
1.5849E 00	0.	0.	0.	0.	0.
2.5119E 00	0.	0.	0.	0.	0.
3.9811E 00	0.	0.	0.	0.	0.
6.3096E 00	0.	0.	0.	0.	0.
10.0000E 00	0.	0.	0.	0.	0.
1.5849E 01	0.	0.	0.	0.	0.
2.5119E 01	0.	0.	0.	0.	0.
3.9811E 01	0.	0.	0.	0.	0.
6.3096E 01	0.	0.	0.	0.	0.
10.0000E 01	0.	0.	0.	0.	0.
1.5849E 02	0.	0.	0.	0.	0.
2.5119E 02	0.	0.	0.	0.	0.
3.9811E 02	0.	0.	0.	0.	0.
6.3096E 02	0.	0.	0.	0.	0.
EJECTA VOLUME	5.2379E 05	5.9134E 06	5.6230E 05	1.3294E 06	3.4094E 06
EJECTA DEPTH	3.3381E-04	3.3719E-03	2.9009E-04	6.2621E-04	1.4773E-03

LUNAR CRATER MODEL

$E_p = 10^{18}$ ergs

CRATER EJECTA SIZE DISTRIBUTIONS

SCREEN SIZE	RING NO. 31 RAD. = 1.0000E 05	RING NO. 32 RAD. = 1.0000E 06	RING NO. 33 RAD. = 1.0000E 07	RING NO. 34 RAD. = 1.0000E 08	RING NO. 35 RAD. = 5.4664E 08
10.0000E-08	0.	0.	0.	0.	1.6370E 04
1.5849E-07	0.	0.	0.	0.	9.4821E 03
2.5119E-07	0.	0.	0.	0.	1.4891E 04
3.9811E-07	0.	0.	0.	0.	2.3266E 04
6.3096E-07	0.	0.	0.	0.	3.6067E 04
10.0000E-07	0.	0.	0.	1.2691E 03	5.3992E 04
1.5849E-06	0.	0.	0.	9.0672E 03	7.4195E 04
2.5119E-06	0.	0.	0.	2.5490E 04	9.7172E 04
3.9811E-06	0.	0.	0.	8.9136E 04	1.0536E 05
6.3096E-06	0.	0.	0.	1.9905E 05	3.8854E 04
10.0000E-06	0.	0.	4.9077E 02	3.2277E 05	3.7572E 03
1.5849E-05	0.	0.	3.6869E 04	4.4911E 05	0.
2.5119E-05	0.	0.	9.5205E 04	4.9189E 05	0.
3.9811E-05	0.	0.	2.6342E 05	5.2144E 05	0.
6.3096E-05	0.	0.	9.0069E 05	1.4064E 05	0.
10.0000E-05	0.	0.	1.4273E 06	1.8833E 03	0.
1.5849E-04	0.	3.4849E 04	1.7041E 06	0.	0.
2.5119E-04	0.	2.5553E 05	1.9601E 06	0.	0.
3.9811E-04	0.	5.8611E 05	2.2695E 06	0.	0.
6.3096E-04	0.	2.3829E 06	1.3276E 06	0.	0.
10.0000E-04	0.	4.5336E 06	1.8831E 04	0.	0.
1.5849E-03	0.	5.4145E 06	0.	0.	0.
2.5119E-03	0.	6.0515E 06	0.	0.	0.
3.9811E-03	0.	7.0915E 06	0.	0.	0.
6.3096E-03	0.	7.8375E 06	0.	0.	0.
10.0000E-03	0.	1.8803E 05	0.	0.	0.
1.5849E-02	0.	0.	0.	0.	0.
2.5119E-02	0.	0.	0.	0.	0.
3.9811E-02	0.	0.	0.	0.	0.
6.3096E-02	0.	0.	0.	0.	0.
10.0000E-02	0.	0.	0.	0.	0.
1.5849E-01	0.	0.	0.	0.	0.
2.5119E-01	0.	0.	0.	0.	0.
3.9811E-01	0.	0.	0.	0.	0.
6.3096E-01	0.	0.	0.	0.	0.
10.0000E-01	0.	0.	0.	0.	0.
1.5849E 00	0.	0.	0.	0.	0.
2.5119E 00	0.	0.	0.	0.	0.
3.9811E 00	0.	0.	0.	0.	0.
6.3096E 00	0.	0.	0.	0.	0.
10.0000E 00	0.	0.	0.	0.	0.
1.5849E 01	0.	0.	0.	0.	0.
2.5119E 01	0.	0.	0.	0.	0.
3.9811E 01	0.	0.	0.	0.	0.
6.3096E 01	0.	0.	0.	0.	0.
10.0000E 01	0.	0.	0.	0.	0.
1.5849E 02	0.	0.	0.	0.	0.
2.5119E 02	0.	0.	0.	0.	0.
3.9811E 02	0.	0.	0.	0.	0.
6.3096E 02	0.	0.	0.	0.	0.
EJECTA VOLUME	0.	3.4386E 07	1.0004E 07	2.2517E 06	4.7341E 05
EJECTA DEPTH	0.	2.2112E-05	6.4349E-08	1.4489E-10	2.4271E-12